To the Graduate Council:

I am submitting herewith a dissertation written by Allen Fort Gwinn, Jr. entitled "A Finite Element Model Updating Technique for Adjustment of Parameters Near Boundaries." I have examined the final copy of this dissertation for form and content and recommend that it be accepted in partial fulfillment of the requirements for the degree of Doctor of Philosophy, with a major in Engineering Science.

R. Engels

Dr. Remi C. Engels, Major Professor

We have read this dissertation and recommend its acceptance:

KC Reddy

Dr. K. C. Reddy

John E. Caruthers

Dr. John E. Caruthers

Louis R. Deken

Dr. Louis R. Deken

Charles C Limbaugh

Dr. Charles Limbaugh

Accepted by the Council:

Carl Minkel

Associate Vice Chancellor and
Dean of the Graduate School

A Finite Element Model UpdatingTechnique for Adjustment of Parameters Near Boundaries

A Dissertation

Presented for the

Doctor of Philosophy

Degree

The University of Tennessee, Knoxville

Allen Fort Gwinn, Jr.

December 1998

DEDICATION

This work is dedicated to the memory of my father Allen Fort Gwinn, Sr. (b. Jan. 8, 1921, d. Feb. 16, 1991), who taught me the value of knowledge. It is also dedicated to the memory of Sue Collin Dorris (b. Feb. 18, 1915, d. Feb. 24,1997). "Aunt Sue" was a dedicated educator throughout her long life. It is only through her generous gift that this work was made possible. I think they both would approve of this investment.

ACKNOWLEDGMENTS

There are many people that helped to make this work possible. The list of those who deserve credit includes my advisor, Dr. Remi Engels, who remained patient with me throughout the long struggle; my wife, Elizabeth, who has always been supportive; my children, Trey and Susan, whom I adore; and Aunt Sue, whose generous gift has made this all possible. I also want to thank Tom Hartvigsen for his support during the testing phase, and Kurt Nichol for providing the test article. But most of all, I want to thank my Lord and Savior, Jesus Christ, who gives both knowledge and wisdom.

ABSTRACT

Even though there have been many advances in research related to methods of updating finite element models based on measured normal mode vibration characteristics, there is yet to be a widely accepted method that works reliably with a wide range of problems. This dissertation focuses on the specific class of problems having to do with changes in stiffness near the clamped boundary of plate structures. This class of problems is especially important as it relates to the performance of turbine engine blades, where a change in stiffness at the base of the blade can be indicative of structural damage.

The method that is presented herein is a new technique for resolving the differences between the physical structure and the finite element model. It is a semi-iterative technique that incorporates a "physical expansion" of the measured eigenvectors along with appropriate scaling of these expanded eigenvectors into an iterative loop that uses the Engels' model modification method to then calculate adjusted stiffness parameters for the finite element model.

Three example problems are presented that use eigenvalues and mass normalized eigenvectors that have been calculated from experimentally obtained accelerometer readings. The test articles that were used were all thin plates with one edge fully clamped. They each had a cantilevered length of 8.5 inches and a width of 4 inches. The three plates differed from one another in thickness from 0.100 inches to 0.188 inches. These dimensions were selected in order to approximate a gas turbine engine blade.

The semi-iterative modification technique is shown to do an excellent job of

calculating the necessary adjustments to the finite element model so that the analytically determined eigenvalues and eigenvectors for the adjusted model match the corresponding values from the experimental data with good agreement. Furthermore, the semi-iterative method is quite robust. For the examples presented here, the method consistently converged to a stable solution and did not exhibit sensitivity to minor errors in the measured mode shapes.

TABLE OF CONTENTS

PAGE

1. INTRODUCTION 1

2. BACKGROUND 4

Direct Updating Techniques 7

Indirect Updating Techniques 9

Common Problems 11

3. THE ENGELS MODIFICATION METHOD 14

Basic Assumptions 14

General Description of the Method 15

4. IMPROVED SEMI-ITERATIVE TECHNIQUE 31

Expansion Method 31

Eigenvector Scaling 34

Analytical Validation of the Semi-Iterative Technique 37

Discussion of Results 41

5. EXPERIMENTAL VALIDATION OF THE SEMI-ITERATIVE METHOD 53

Test Objectives and Procedure 53

Description of Test Articles 56

Example 1, Test Article P8540188 62

Example 2, Test Article P8540100 70

Example 3, Test Article P8540100M 78

6. CONCLUSIONS 88

Discussion of Results 88

Areas of Further Study 89

LIST OF REFERENCES 92

APPENDICES 94

APPENDIX 1. TEST PLAN 95

APPENDIX 2. TEST DATA SUMMARY 100

APPENDIX 3. IMPACT HAMMER CALIBRATION CERTIFICATE 130

APPENDIX 4. EIGENVECTORS CALCULATED FROM MEASURED DATA . . 132

VITA 135

LIST OF TABLES

TABLE PAGE

1. Comparison of Uncorrected Frequencies, Pseudo-Experimental Case 39

2. Comparison of Corrected Frequencies, Pseudo-Experimental Case 48

3. Comparison of Corrected Mode Shapes, Pseudo-Experimental Case 48

4. Test Article Configurations 56

5. Comparison of Measured and Analytical Natural Frequencies, Example 1 62

6. Measured versus Adjusted Frequencies, Example 1 64

7. Comparison of Measured and Analytical Natural Frequencies, Example 2 70

8. Measured versus Adjusted Frequencies, Example 2 72

9. Measured versus Adjusted Frequencies, Example 3 81

10. Measured versus Unadjusted Frequencies, Example 3 86

A4-1. Raw Tabulated Eigenvectors as Calculated from Measured Data 133

A4-2. Processed Eigenvectors for P8540188 134

A4-3 Processed Eigenvectors for P8540100 134

A4-4 Processed Eigenvectors for P8540100M 134

LIST OF FIGURES

FIGURE PAGE

1. Flow Diagram Summarizing FE Model Updating Techniques 5
2. Flow Diagram for Direct Technique in Dynamic Model Updating 8
3. Flow Diagram for Indirect Technique in Dynamic Model Updating 10
4. Flow Diagram Illustrating the Semi-Iterative XMOD Solution 32
5. Unperturbed Finite Element Model Used as Input to XMOD 38
6. Finite Element Model Used to Generate the Pseudo-Experimental Data 40
7. Distribution of Stiffness Values Across the Plate Width 42
8. Convergence for Eigenvector Scaling = 1.0, Pseudo-Experimental Case 43
9. Convergence for Eigenvector Scaling = 0.8, Pseudo-Experimental Case 44
10. Convergence for Eigenvector Scaling = 0.6, Pseudo-Experimental Case 45
11. Convergence for Eigenvector Scaling = 0.4, Pseudo-Experimental Case 46
12. Convergence for Eigenvector Scaling = 0.2, Pseudo-Experimental Case 47
13. Comparison of Eigenvectors for Mode 1, Pseudo-Experimental Case 49
14. Comparison of Eigenvectors for Mode 2, Pseudo-Experimental Case 50
15. Comparison of Eigenvectors for Mode 3, Pseudo-Experimental Case 51
16. Comparison of Eigenvectors for Mode 4, Pseudo-Experimental Case 52
17. Schematic Representation of Experimental Set-up 54
18. Cantilevered Plate Test Configuration 55

19. Light Weight Accelerometer, Shown Mounted on Test Article 57

20. Instrumented Mini-Hammer (Shown with Standard Hammer) 58

21. Test Article P8540188 59

22. Test Article P8540100 60

23. Test Article P8540100M 61

24. General Arrangement of Mounting Fixture and Test Article 63

25. Convergence for Example 1, Eigenvector Scaling = 0.4 65

26. Comparison of Eigenvectors for Mode 1, Example 1 66

27. Comparison of Eigenvectors for Mode 2, Example 1 67

28. Comparison of Eigenvectors for Mode 3, Example 1 68

29. Comparison of Eigenvectors for Mode 4, Example 1 69

30. Nodes Corresponding to Measurement Data Points Used, Example 2 71

31. Convergence for Example 2, Eigenvector Scaling = 0.5 73

32. Comparison of Eigenvectors for Mode 1, Example 2 74

33. Comparison of Eigenvectors for Mode 2, Example 2 75

34. Comparison of Eigenvectors for Mode 3, Example 2 76

35. Comparison of Eigenvectors for Mode 4, Example 2 77

36. Comparison of Eigenvectors for Mode 2 with Scaled Data, Example 2 79

37. Convergence for Example 3, Eigenvector Scaling = 1.0 80

38. Comparison of Eigenvectors for Mode 1, Example 3 82

39. Comparison of Eigenvectors for Mode 2, Example 3 83

40. Comparison of Eigenvectors for Mode 3, Example 3 84

41. Comparison of Eigenvectors for Mode 4, Example 3 85

42. Comparison of Eigenvectors for Mode 2 with Scaled Data, Example 3 87

A1-1 Data Point Locations 97

A2-1 Test Article P8540188, Frequency Response Plots 103

A2-2 Test Article P8540100, Frequency Response Plots 111

A2-3 Test Article P8540100M, Frequency Response Plots 119

A2-4 Mode Shapes for P8540188 as Generated From Test Data by the I-DEAS Software 127

A2-5 Mode Shapes for P8540100 as Generated From Test Data by the I-DEAS Software 128

A2-6 Mode Shapes for P8540100M as Generated From Test Data by the I-DEAS Software 129

1. INTRODUCTION

Although it is often sufficiently accurate and convenient to make the assumption that an engineering system is static in nature, no system is absolutely unchanging with respect to time. Aircraft structures undergo variations in geometry and aerodynamic loading that can result in unstable flight characteristics. Rotating machinery produce self-exciting load variations resulting from inherent imbalance of shaft components. Even building structures are subject to seismic forces and fluctuating wind loads, as well as the harmonic excitation resulting from vortex shedding that can result in destructive resonance.

By ignoring these effects the engineer may be unintentionally placing lives and property at serious risk. This is especially true in the present socio-economic environment where market forces are driving the designer to produce better performing products with a smaller investment in material.

Fortunately, experimental and computational techniques for measuring and predicting the response of a structure to dynamic loads have kept pace with the need to reduce weight and increase performance. Experimental methods advanced significantly in the late 1960's and early 1970's due to the emergence of economical accelerometers and the development of the Fast Fourier Transform (FFT) into an efficient algorithm for converting time-domain data into frequency-domain data [1]. About the same time, large main frame computers made the Finite Element Method (FEM) a practical means of

solving complex static and dynamic problems in solid mechanics. Then, in the mid-1980's the development of the micro-processor gave an increased impetous to both experimental and analytical methods of analysis.

Until recent years, the experimenter and the analyst tended to work independently of each other, rarely trying to resolve the often large discrepancies in the measured versus the calculated vibration characteristics of a structure. Again, the confluence of developments is making it more desirable and practical to identify and resolve these discrepancies. It is now recognized that, by having a valid analytical model that accurately predicts the dynamic response of the system under consideration, one can investigate the effects of modifications, correct unforeseen deficiencies, and detect developing structural damage. Since the measured and calculated dynamic characteristics of a structure are usually significantly different, it becomes critical that the analyst be able to identify the reasons for these discrepancies and then define a rationale for modifying the computational model so that it more closely agrees with the observed dynamic characteristics of the structure.

Many different methods of identifying and correcting the errors (usually assumed to be in the finite element model) have emerged, several of which will be discussed in the next chapter. For the most part, these methods involve the use of the natural frequencies and normalized mode shapes as test data. The use of mode shapes requires the matching of data at specific spatial locations in the system. Since the spatial density of data associated with the finite element model is usually much higher than that of the experimental data it becomes necessary to either expand the experimental data to yield

data at the corresponding finite element model degrees of freedom or to reduce the finite element degrees of freedom to those corresponding to the experimental spatial locations. This procedure is complicated by the fact that the experimental data usually is limited to the three translational degrees of freedom at each data location.

The objective of this dissertation is to present an improved method of resolving the discrepancies between the experimentally obtained modal characteristics of a structural system and its analytically determined characteristics. This approach is based on the Engels model modification method [2] which uses a perturbed finite element formulation to isolate the parameters that are candidates for adjustment. This dissertation presents a refinement of the Engels model modification method with specific application to the case where the parameters to be changed are near the clamped boundary of cantilevered thin plate structures.

2. BACKGROUND

The field of model updating using modal characteristics can be broken up into two very broad categories; time-domain methods and frequency-domain methods [3] [4]. Although there have been many significant contributions to our knowledge of finite element model updating via time-domain methods, the practical implementation of these methods remains beyond the reach of most engineers. The availability of more economical signal analysis hardware and software has driven most of the interest in this area toward frequency-domain methods. Frequency-domain methods can be further subdivided into two very broad categories; direct updating techniques and indirect updating techniques [4]. This is illustrated in Figure 1.

From the literature, it can be seen that, for both direct and indirect methods, the emphasis in this field of study has been on matching the eigenvector at each degree of freedom in the system, point for point. Although this approach seems quite reasonable, the resulting solution is often very sensitive to small variations in the data due to computational round-off and measurement uncertainty. These variations are present in both the analytically and experimentally obtained modal characteristics .

A comparison of experimental errors shows that, while the natural frequencies can be obtained to an accuracy of ±1% the corresponding eigenvectors are no better than ±10% [4]. Conversely, the computational model is only as good as the assumptions necessary to discretize the structure. The boundary conditions, mass and stiffness distri-

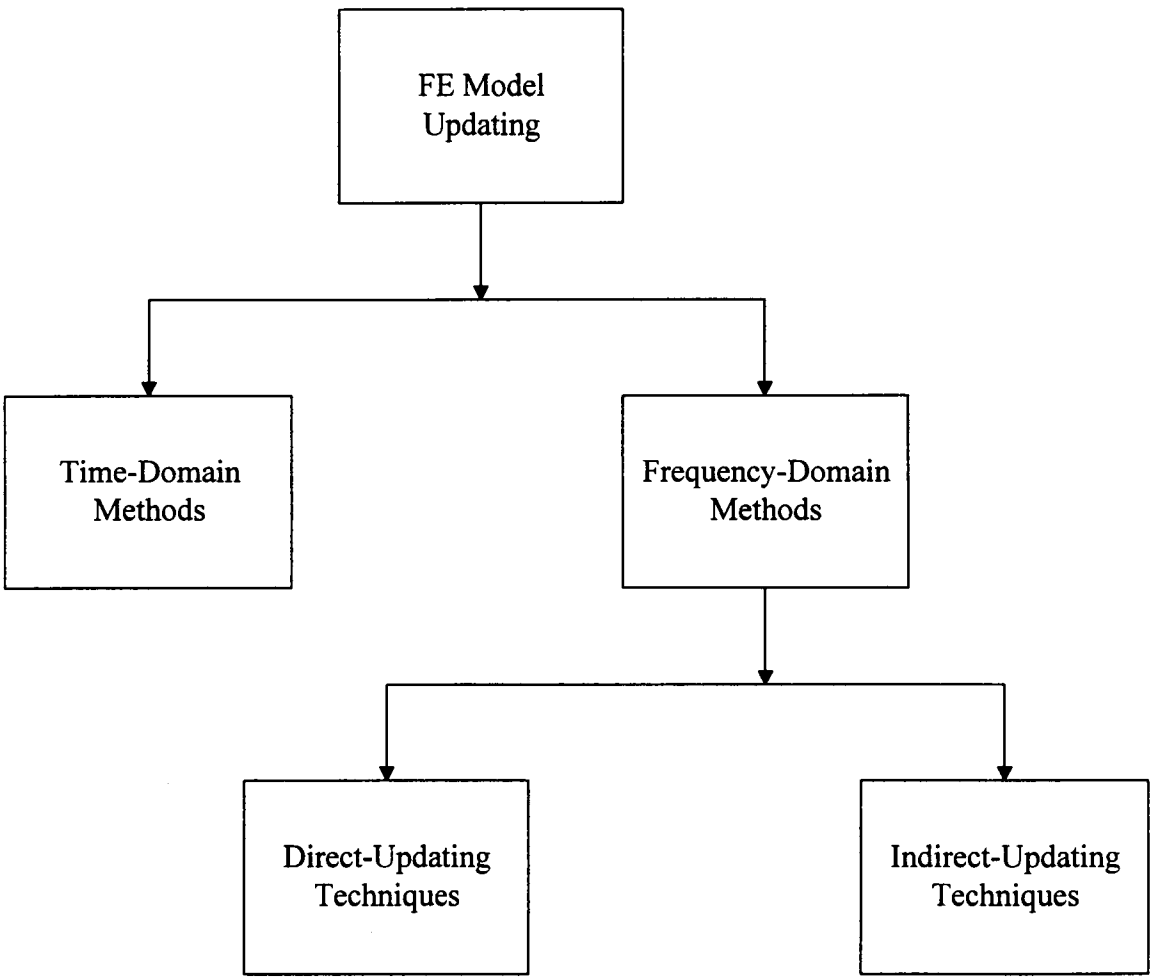


Figure 1. Flow Diagram Summarizing FE Model Updating Techniques

butions, and element formulations used throughout the finite element model will have a direct bearing on the quality of the computational solution. These discretization assumptions are usually taken as more uncertain since they are not normally taken from actual measurements of the test article. Therefore, the experimentally obtained eigenvalues and eigenvectors are normally taken as an "accurate" representation of the modal characteristics.

Another discrepancy results from the fact that the number of finite element model degrees of freedom is usually much larger than the number of tested degrees of freedoms. Also, the finite element data may contain degrees of freedom that cannot be obtained experimentally, such as rotations at a point. This leaves us with the paradox that although the computational model is taken as the more imperfect representation, it yields a smoother, more plentiful continuum of information. The analyst must now decide whether to condense the finite element data to match the number and types of experimental degrees of freedom using such techniques as proposed by Guyan [6] or Paz [7], or to expand the experimental data to match the number of degrees of freedom of the finite element model using methods developed by Kidder [8], Lieven and Ewins [9], or Lipkens and Vandeurzen [10] . Unfortunately, even with the latter approach, it is sometimes necessary to discard degrees of freedom from the finite element model that cannot be measured experimentally. Clearly, such an approach is not likely to yield a unique solution.

Direct Updating Techniques

The general procedure followed in direct updating techniques is illustrated in Figure 2. These methods are characterized by the fact that modifications are made directly on the system matrices based on enforcing the orthogonality condition as in the following approach developed by To, Lin, and Ewins [11] and illustrated in the following set of equations.

$$M_e = M_a + \Delta M \tag{1}$$

$$K_e = K_a + \Delta K \tag{2}$$

$$\Delta M = M_a(\Phi_e \Phi_e^T - \Phi_a \Phi_a^T) M_a \tag{3}$$

$$\Delta K = K_a \left(\frac{\Phi_e \Phi_e^T}{\omega_{e_i}^2} - \frac{\Phi_a \Phi_a^T}{\omega_{a_i}^2} \right) K_a \tag{4}$$

where M_a and K_a represent the analytically determined mass and stiffness matrices and M_e and K_e represent the experimentally determined mass and stiffness matrices. Similarly, Φ_a and Φ_e represent the analytical and experimental mass normalized mode shapes and ω_{ai} and ω_{ei} represent the ith analytical and experimental natural frequencies.

Direct methods are very attractive due to the fact that the values of ΔM and ΔK can be determined in a single pass, thus greatly reducing the amount of computational effort required. However, they suffer from some serious deficiencies also. The updated

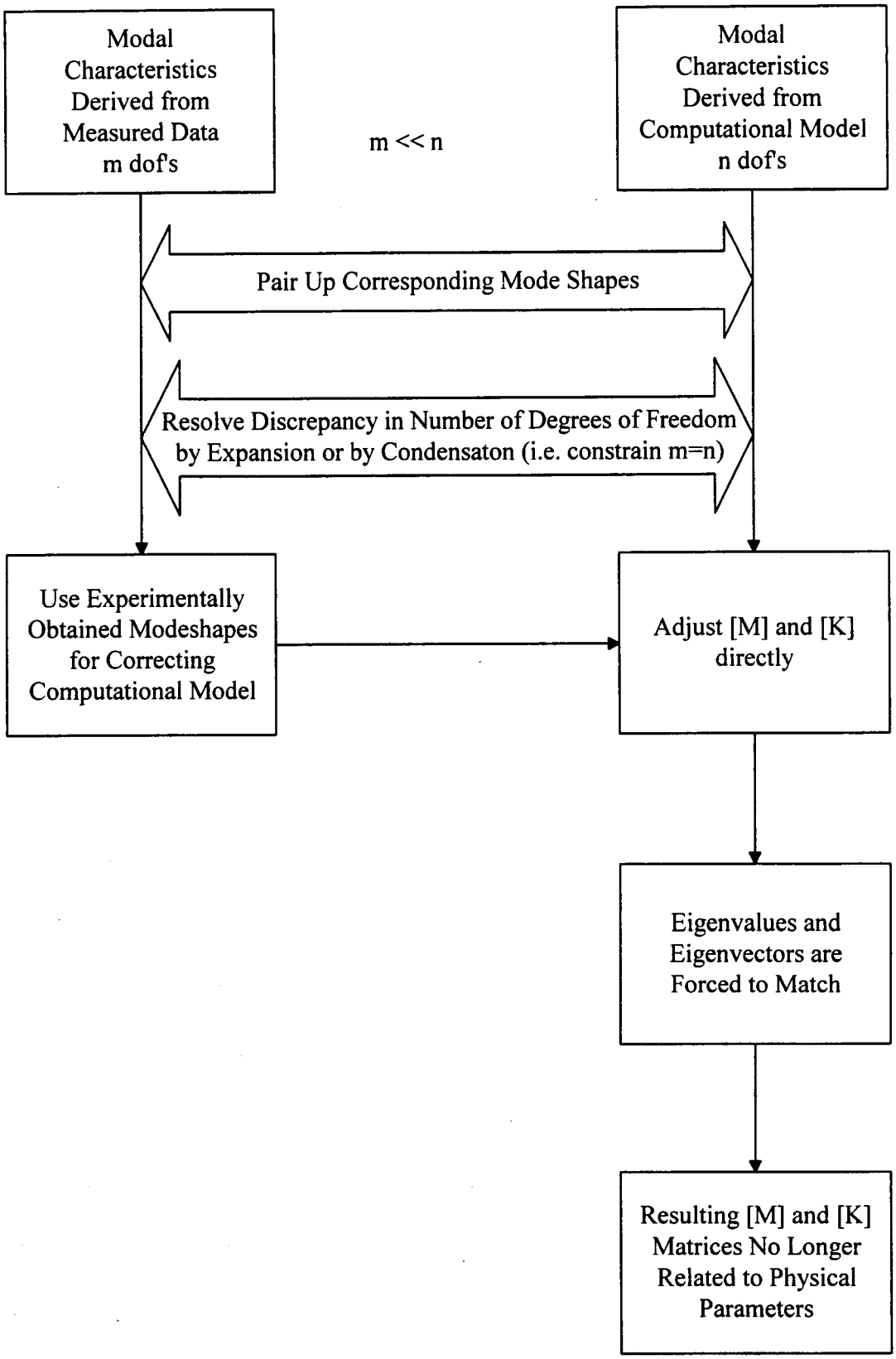


Figure 2, Flow Diagram for Direct Techniques in Dynamic Model Updating

matrices no longer maintain any of the physical significance, thus losing direct access to the system parameters. This creates serious difficulties when computing, for example, stresses and strains. Also, the updated mass and stiffness matrices are no longer banded. Furthermore, these methods do not allow for the pre-selection of the most suspect system parameters.

Indirect Updating Techniques

Indirect updating techniques allow for identification and correction of parameters that have physical significance. Examples of such parameters are: Young's modulus, mass density, cross-sectional area, moment of inertia, plate thickness, damage factors, and Poisson's ratio. Because the geometry of a structure is usually well known, geometric parameters are rarely independently targeted for change. However, they do often occur in combinations with other material parameters.

Indirect updating techniques fall into two broad categories, iterative and constrained least-squares methods. The most widely used iterative technique is the "Sensitivity-Based Element-by-Element Updating Procedure" [12] or SB-EBE method (see Figure 3). This method is based on using eigenvalue and eigenvector derivatives [13] (also referred to as sensitivities) to locate parameters within the system that have the most influence on the natural frequencies and mode shapes. These derivatives are then used to predict the amount of change required in each parameter to correct the analytical model. The model is then updated and the eigenvalue problem is again solved and the modal results are compared with their experimental counterparts. The solution is iterated until a

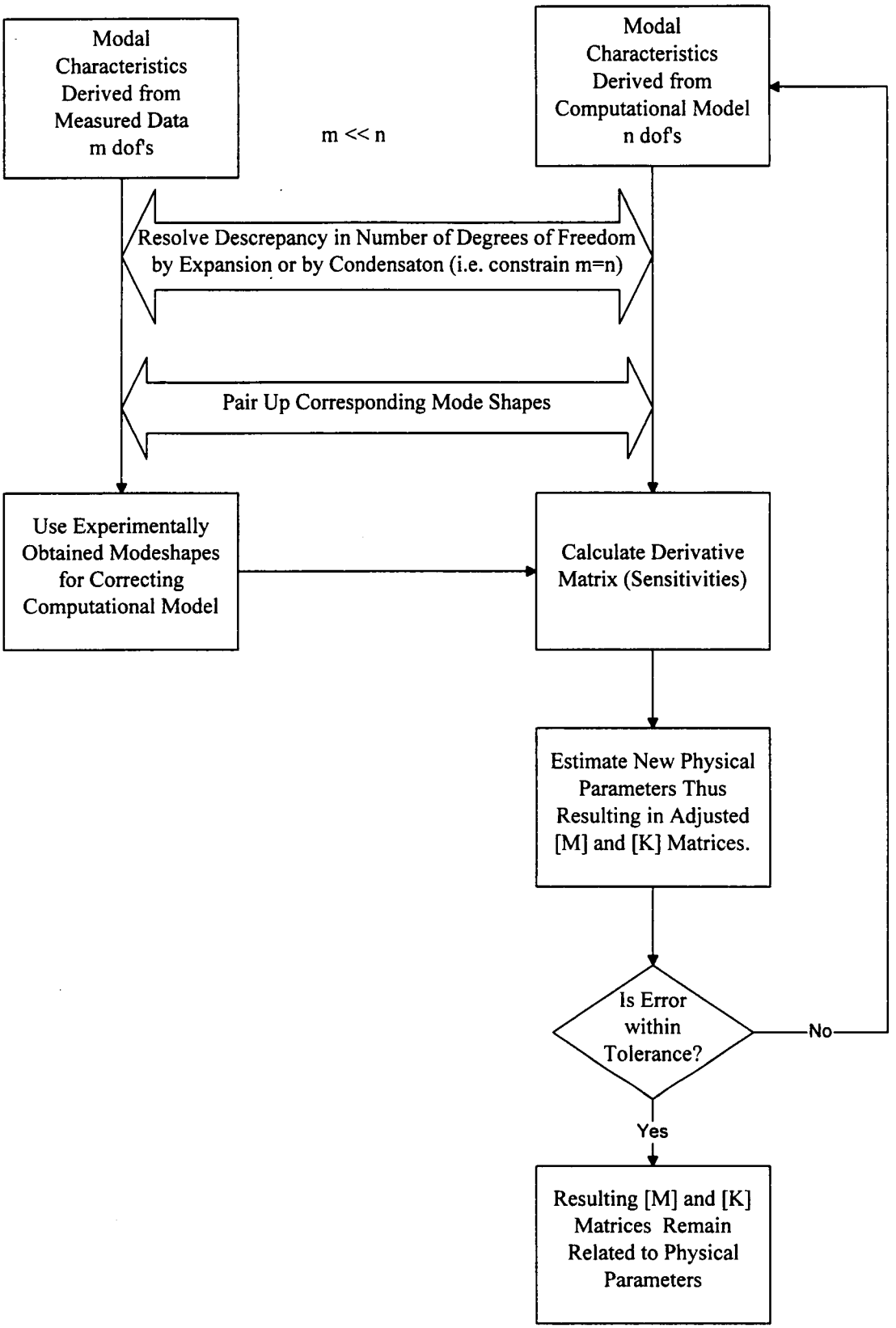


Figure 3, Flow Diagram for Indirect Techniques for Dynamic Model Updating

specified convergence criterion is satisfied.

The constrained least-squares approach as implemented by Nash [14] involves minimization of a function in the form:

$$F_{\min} = \sum_{i=1}^{r} \alpha_i \frac{(\omega_{iE}^{\ 2} - \omega_{ia}^{\ 2})^2}{\omega_{iE}^{\ 4}} + \sum_{i=1}^{r} \beta_i \frac{\{\phi_{iE} - \phi_{ia}\}^T D \{\phi_{iE} - \phi_{ia}\}}{\phi_{iE}^{\ T} D \phi_{iE}} \qquad (5)$$

where α_i and β_i are weighting factors and D is a weighting matrix. The derivatives of the eigenvalues and eigenvectors with respect to selected physical parameters are used in the minimization, thus allowing the analyst to pre-select the parameters of interest.

Common Problems

Model modification is still plagued with many difficulties and a workable approach has not yet emerged. Ibrahim [15] lists a summary of problems, issues, and difficulties that he feels are common to all model updating techniques. His list includes:

1. Criteria for finite element models' correctibility need to be developed.

2. Guidelines for acceptable discrepancies between analysis and test and confidence indicators for one or the other or both need to be established.

3. The size of the analytical finite element model is very large compared to that of the test.

4. Model reduction or condensation techniques are not fully developed, understood or justified.

5. Modal identification algorithms identify a limited number of modes at a limited number of coordinates.

6. Test coordinates and degrees of freedom are incomplete and are different from those of the analytical model.

7. The normal mode approach is frequently used even for structures that have highly complex modes (e.g. non-proportional damping).

8. Damping modeling and correction need to be addressed in future updating techniques.

9. There is no established scientific criteria for designating or selecting the elements of the analytical model to be changed.

10. The algorithms to use modal test data to improve analytical models are not sufficiently rigorous and lack physical justification or meaning.

11. The updated model, in some cases, is no more than a group of numbers and lacks physical significance.

12. There is no established and acceptable criteria to judge the soundness or accuracy of the updated model as far as input/output or stresses and strains are concerned. The ability of the improved model to reproduce the same set of modes, that were used for updating, is insufficient and redundant.

13. Effects of linear assumptions of analysis and test on the process of updating remain to be considered and investigated.

14. More considerations must be given to the non-modal approach.

It can be seen from the previous list that although significant advances have been made during the last two decades, many areas in the field of model updating are yet to be fully addressed. There has not arisen a single, universal method that works for all or even most cases. Each modification technique addresses only certain classes of problems more or less effectively, so that it is often advisable to apply multiple methods in order to develop confidence in the solution. The method that is presented here is applied

specifically to the boundary condition problem where the stiffness parameters near the physical boundaries are suspect and are targeted for change.

3. THE ENGELS MODIFICATION METHOD

The proposed finite element model modification technique is based on a method developed by Engels and implemented in the computer program MODMOD [2]. Engels' method makes use of a perturbed finite element formulation that extracts the physical parameters from the element matrices in such a way as to allow for a single step minimum norm solution of the unknown parameter changes. The method employs standard finite element (FE) procedures and does not require exact duplication of the test data. It allows for large parameter changes and is not iterative.

Basic Assumptions

The Engels method relies on three basic assumptions:

I. All obvious testing and modeling errors have been eliminated.

II. The structure's geometry is known.

III. All parameters needing change have been identified.

The implications of these assumptions is immediately apparent. Assumption I implies that both the test data and the computational model are of high fidelity. Assumption II states that the differences between the two sets of data is not due to changes in geometry. The consequence of these assumptions taken together is two fold.

First, the measured data must accurately represent the behavior of the physical system. Secondly, the computational model must be an accurate portrayal of the structure to the best of the analyst's knowledge.

Assumption III states that the analyst has prior knowledge of which parameters require modification. Localization of errors is a critical step in the overall model modification process which has been addressed by numerous researchers [5], [11], [15]. The implication of this assumption is to say that the error localization process has been previously carried out by other means.

General Description of the Method

The discrepancies between analysis and test data belong in one of two categories. The first category contains the discrepancies caused by the limitations of the measuring devices and the standard modeling approximations . The second category includes the discrepancies due to such things as poorly known material properties and inaccurate idealizations of boundary conditions. It is this second category of discrepancies that model modification methods aims to minimize by changing a selected set of system parameters.

Any model modification method yields meaningful parameter changes only if the first category of discrepancies does not overwhelm the second. This can be assured by, first, choosing optimum test locations on the structure that produce maximum second category discrepancies and then minimizing first category discrepancies by carefully monitoring the testing and modeling procedures so that gross errors can be detected and

corrected as implied by Assumption I. The resulting test data now accurately reflect the behavior of the real structure and the analytical data do the same for the model. At this stage then, more credence must be given to the test data because they now reflect the structure's real behavior. Thus, the problem becomes one of modifying the model's parameters so that the analytical results agree reasonably well with their given test counterparts.

As with any finite element formulation, the elements of the structure's mass and stiffness matrices are functions of specific combinations of geometric properties, such as length, area, and moment of inertia, and material properties, such as Young's modulus, Poisson's ratio, and mass density. These parameters can be brought outside of the elemental stiffness and mass matrices as constants. Some care in selecting the parameter combinations is necessary to insure that the mass parameters and stiffness parameters are uncoupled from one another. These parameters will be referred to as p_{ei}^{m} and p_{ei}^{k}, where the superscripts m and k are used to differentiate between mass and stiffness parameters, respectively. The subscript i is an index that ranges from 1 to I_e^m and 1 to I_e^k, respectively, where I_e^m is the number of mass parameters for element e and I_e^k is the number of stiffness parameters for element e.

In general, there will be a single mass parameter, p_{el}^{m}, per element that is a combination of mass density and various geometric properties. Also, there are often multiple stiffness parameters, p_{ei}^{k}, that are combined in a linear fashion in order to generalize the element stiffness matrix. The p_{ei}^{k} 's represent coefficients that are combinations of Young's modulus and Poisson's ratio with the geometric properties that

are associated with the formation of the stiffness matrix.

For example, the response of an axial bar, e, is governed by the property combinations $p_{el}^{k} = EA/L$ and $p_{el}^{m} = \rho AL/6$ where E is Young's modulus, A is the cross sectional area, L is the length, and ρ is the mass density of the bar. Parameters such as p_{el}^{k} and p_{el}^{m} are collected as elements of the system parameter vector $\mathbf{p}$. Now, according to Assumption III, the vector $\mathbf{p}$ can be partitioned into a vector $\mathbf{p}_1$ of parameters targeted for change and a vector $\mathbf{p}_2$ of unchanged parameters

$$\mathbf{p} \triangleq \begin{Bmatrix} \mathbf{p}_1 \\ \mathbf{p}_2 \end{Bmatrix} \triangleq \begin{Bmatrix} \mathbf{p}_1^0 + \Delta \mathbf{p}_1 \\ \mathbf{p}_2^0 \end{Bmatrix} \tag{6}$$

$$\mathbf{p}^0 \triangleq \begin{Bmatrix} \mathbf{p}_1^0 \\ \mathbf{p}_2^0 \end{Bmatrix} \tag{7}$$

where $\mathbf{p}^0$ is the known unperturbed parameter vector and $\Delta\mathbf{p}_1$ contains the unknown parameter changes. In general, $\Delta\mathbf{p}_1$ contains a relatively small number of parameters. The symbol $\triangleq$ means "stands for" or "is defined as".

At the same time, $\mathbf{p}$ can also be partitioned according to mass and stiffness parameters.

$$\mathbf{p} \triangleq \begin{Bmatrix} \mathbf{p}_m \\ \mathbf{p}_k \end{Bmatrix}$$

$$\mathbf{p}_m \triangleq \begin{Bmatrix} \mathbf{p}_{m1} \\ \mathbf{p}_{m2} \end{Bmatrix}, \quad \mathbf{p}_k \triangleq \begin{Bmatrix} \mathbf{p}_{k1} \\ \mathbf{p}_{k2} \end{Bmatrix}$$

$$\mathbf{p}_1 \triangleq \begin{Bmatrix} \mathbf{p}_{m1} \\ \mathbf{p}_{k1} \end{Bmatrix}, \quad \mathbf{p}_2 \triangleq \begin{Bmatrix} \mathbf{p}_{m2} \\ \mathbf{p}_{k2} \end{Bmatrix}$$

The vectors $\mathbf{p}_{mi}$ and $\mathbf{p}_{ki}$ (i = 1, 2) correspond to mass and stiffness parameters, respectively. It is further assumed that only modal test data (i.e., natural frequencies and mode shapes) are to be used to estimate these changes in parameters.

The Engels method begins with the basic eigenvalue problem equations for a linear elastic system, which can be stated as

$$K\Phi = M\Phi\Lambda \tag{8}$$

where K is the system stiffness matrix of size n×n , M is the system mass matrix of size n×n , Φ is the n×n matrix containing the complete set of eigenvectors, and Λ is a n×n diagonal matrix containing the eigenvalues. The solution to the structural eigenproblem also results in the following orthonormality conditions

$$\Phi^T M \Phi = I \tag{9}$$

$$\Phi^T K \Phi = \Lambda \tag{10}$$

The Engels model modification method then is a means of solving the inverse eigenproblem and consists of finding a set of parameter changes, $\Delta \mathbf{p}_1$, such that equation (8) and the corresponding orthonormality conditions in equations (9) and (10) are satisfied for a set of experimentally determined eigenvalues and eigenvectors.

The first step is to redefine M and K to be

$$M \triangleq M^0 + \Delta M$$

$$K \triangleq K^0 + \Delta K$$

so that M and K are the structure's corrected mass and stiffness matrices. Λ then becomes the diagonal test eigenvalue matrix, and Φ becomes the test mode matrix. M^0 and K^0 represent the known unperturbed analytical mass and stiffness matrices. The parameter changes $\Delta \mathbf{p}_1$ cause the change ΔM and ΔK in the mass and stiffness matrices necessary to minimize the discrepancies between analysis and test.

Next, consider a typical column of equation (8) such that

$$(K - \lambda M)\phi = 0 \tag{11}$$

where λ and ϕ are a test pair. This equation will now be written as an explicit function of $\mathbf{p}_1$.

Assumption II implies zero changes in the geometric parameters. The element mass and stiffness matrices then can be written as linear functions of certain parameter combinations. Assumption II is often reasonable and, in many cases, can be relaxed if needed. As an example, consider again the consistent finite element (FE) mass and stiffness matrices m and k of an axial bar

$$m = \frac{\rho AL}{6}\begin{bmatrix} 2 & 1 \\ 1 & 2 \end{bmatrix}, \qquad k = \frac{EA}{L}\begin{bmatrix} 1 & -1 \\ -1 & 1 \end{bmatrix} \tag{12}$$

where $p_{el}^{m} = \rho AL/6$ and $p_{ei}^{k} = EA/L$ are the appropriate parameter combinations that make m and k a linear functions of p_{el}^{m} and p_{el}^{k} Assumption II is not needed. In contrast, the consistent mass and stiffness matrices for a beam are linear in $p_{el}^{m} = \rho AL/420$ and $p_{el}^{k} = EI/L^{3}$ (where I is the area moment of inertia for the bar) only if Assumption II is invoked.

In general, let m_e and k_e be the mass and stiffness matrices of a typical finite element e. Based on Assumption II the element mass and stiffness matrices can be written as

$$m_e = \sum_{i=1}^{I_e^m} m_{ei} p_{ei}^m, \qquad k_e = \sum_{i=1}^{I_e^k} k_{ei} p_{ei}^k \tag{13}$$

where m_{ei} and k_{ei} are known matrices, while I_e^m and I_e^k are the number of parameters associated with m_e and k_e. Thus, for the axial bar $I_e^m = I_e^k = 1$ and

$$m_{e1} = \begin{bmatrix} 2 & 1 \\ 1 & 2 \end{bmatrix}, \quad k_{e1} = \begin{bmatrix} 1 & -1 \\ -1 & 1 \end{bmatrix}, \quad p_{e1}^m = \frac{\rho AL}{6}, \quad p_{e1}^k = \frac{EA}{L} \tag{14}$$

For the eight noded brick element used in this study there is only one mass parameter, p_{e1}^m, and two stiffness parameters, p_{e1}^k and p_{e2}^k, defined as

$$p_{e1}^m = \rho \tag{15}$$

$$p_{e1}^k = \frac{E}{(1+\nu)(1-2\nu)} \tag{16}$$

$$p_{e2}^k = \frac{E\nu}{(1+\nu)(1-2\nu)} \tag{17}$$

where ν is Poisson's ratio, ρ is the mass density, and E is Young's modulus. The matrices corresponding to p_{e1}^m, p_{e1}^k, and p_{e2}^k are

$$m_{el} = \left[\frac{1}{8} \delta_{ij} \int_{-1}^{1} \int_{-1}^{1} \int_{-1}^{1} |\det J| \, d\xi \, d\eta \, d\zeta \right] \tag{18}$$

$$k_{ei} = \int_{-1}^{1} B^T C_i B \, |\det J| \, d\xi \, d\eta \, d\zeta, \quad i = 1,2 \tag{19}$$

where ξ, η, and ζ are natural coordinates and $|\det J|$ is the Jacobian determinant. Also,

$$C_1 = \begin{bmatrix} 1 & 0 & 0 & 0 & 0 & 0 \\ 0 & 1 & 0 & 0 & 0 & 0 \\ 0 & 0 & 1 & 0 & 0 & 0 \\ 0 & 0 & 0 & 0.5 & 0 & 0 \\ 0 & 0 & 0 & 0 & 0.5 & 0 \\ 0 & 0 & 0 & 0 & 0 & 0.5 \end{bmatrix}$$

$$C_2 = \begin{bmatrix} -1 & 1 & 1 & 0 & 0 & 0 \\ 1 & -1 & 1 & 0 & 0 & 0 \\ 1 & 1 & -1 & 0 & 0 & 0 \\ 0 & 0 & 0 & -1 & 0 & 0 \\ 0 & 0 & 0 & 0 & -1 & 0 \\ 0 & 0 & 0 & 0 & 0 & -1 \end{bmatrix}$$

The mass and stiffness matrices M and K of a structure then have the form

$$M = \sum_e Q_e^T T_e^T \left(\sum_{i=1}^{I_e^m} m_{ei} p_{ei}^m \right) T_e Q_e \tag{20}$$

$$K = \sum_e Q_e^T T_e^T \left(\sum_{i=1}^{I_e^k} k_{ei} p_{ei}^k \right) T_e Q_e \tag{21}$$

where T_e is the local to global coordinate transformation for an element and Q_e locates an element vector in the system vector.

Substituting equations (20) and (21) into equation (11) yields

$$(K - \lambda M)\phi = \sum_e Q_e^T \left[\sum_{i=1}^{I_e^k} \mathbf{k}_{ei} p_{ei}^k - \lambda \sum_{i=1}^{I_e^m} \mathbf{m}_{ei} p_{ei}^m \right] = 0 \tag{22}$$

where the symbol, $\sum_e$, means "the sum over all elements" and

$$\mathbf{m}_{ei} \triangleq T_e^T m_{ei} T_e \varphi_e \tag{23a}$$

$$\mathbf{k}_{ei} \triangleq T_e^T k_{ei} T_e \varphi_e \tag{23b}$$

$$\varphi_e \triangleq Q_e \phi \tag{23c}$$

So that φ_e contains the elements of ϕ corresponding to the element degrees of freedom.

Next, let

$$\mu_e \triangleq \left[\mathbf{m}_{e1} \cdots \mathbf{m}_{I_e^m}\right], \qquad \kappa_e \triangleq \left[\mathbf{k}_{e1} \cdots \mathbf{k}_{I_e^k}\right] \tag{24}$$

so that equation (22) can be written as

$$[K-\lambda M]\phi = \sum_e Q_e^T [\kappa_e P_e^k \mathbf{p}_k - \lambda \mu_e P_e^m \mathbf{p}_m] = 0 \tag{25}$$

where

$$\mathbf{p}_e^m \triangleq \begin{Bmatrix} p_{e1}^m \\ \cdots \\ p_{I_e^m}^m \end{Bmatrix}, \qquad \mathbf{p}_e^k \triangleq \begin{Bmatrix} p_{e1}^k \\ \cdots \\ p_{I_e^k}^k \end{Bmatrix}$$

and

$$\mathbf{p}_e^m \triangleq P_e^m \mathbf{p}_m$$

$$\mathbf{p}_e^k \triangleq P_e^k \mathbf{p}_k$$

where P_e^k and P_e^m are locator matrices that place the element mass and stiffness parameter vectors $\mathbf{p}_e^k$ and $\mathbf{p}_e^m$ into the system vectors $\mathbf{p}_m$ and $\mathbf{p}_k$. Equation (25) can now be written in the form

$$\left[\sum_e Q_e^T \kappa_e P_e^k\right] \mathbf{p}_k - \lambda \left[\sum_e Q_e^T \mu_e P_e^m\right] \mathbf{p}_m = 0 \tag{26}$$

Then, considering equations (20) through (26), the left side of equation (11) can be written as

$$(K - \lambda M)\,\phi \triangleq D\,\mathbf{p} \tag{27}$$

where

$$D \triangleq \begin{bmatrix} -\lambda d_m & d_k \end{bmatrix}$$

and

$$d_m \triangleq \sum_e Q_e^T \mu_e P_e^m, \qquad d_k \triangleq \sum_e Q_e^T \kappa_e P_e^k, \tag{28}$$

Next, partition d_m and d_k according to changed and unchanged parameters

$$d_m \triangleq \begin{bmatrix} d_{m11} & d_{m12} \\ d_{m21} & d_{m22} \end{bmatrix}, \quad d_k \triangleq \begin{bmatrix} d_{k11} & d_{k12} \\ d_{k21} & d_{k22} \end{bmatrix} \tag{29}$$

From this, it can be seen that d_{m11} and d_{k11} follow from equation (28) where the summation is taken over the $\mathbf{p}_1$ elements only. Similarly, d_{m22} and d_{k22} are given by equation (28) with the summation over the $\mathbf{p}_2$ elements only. The matrices d_{m12} and d_{k12} correspond to elements that have $\mathbf{p}_2$ parameters but have degrees of freedom in common

with one or more $\mathbf{p}_1$ elements. Also, d_{m2l} and d_{k2l} are zero because elements with $\mathbf{p}_2$ parameters clearly have no degrees of freedom in common with elements containing $\mathbf{p}_1$ parameters even if they have degrees of freedom in common with $\mathbf{p}_1$ elements. Equation (11) can then be written as

$$\begin{bmatrix} -\lambda d_{m11} & d_{k11} \\ 0 & 0 \end{bmatrix} \begin{Bmatrix} p_{m1} \\ p_{k1} \end{Bmatrix} = -\begin{bmatrix} -\lambda d_{m12} & d_{k12} \\ -\lambda d_{m22} & d_{k22} \end{bmatrix} \begin{Bmatrix} p^o_{m2} \\ p^o_{k2} \end{Bmatrix} \tag{30}$$

The second partition in equation (30) represents a set of constraints

$$\mathbf{0} = [-\lambda d_{m22} \quad d_{k22}] \begin{Bmatrix} p^0_{m2} \\ p^0_{k2} \end{Bmatrix} \tag{31}$$

If these constraints are not satisfied then the set of targeted parameters $\mathbf{p}_1$ is not sufficient to characterize the discrepancies between analysis and test. The set $\mathbf{p}_1$ must be expanded or the test data must be reviewed (i.e. Assumption I is not satisfied). If the constraints are reasonably well satisfied then $\mathbf{p}_1$ contains at least a sufficient number of parameters and the model modification procedure may continue.

Next consider typical columns of the orthonormality conditions as expressed in equations (9) and (10)

$$\Phi^T M\phi = e \tag{32}$$

$$\Phi^T K\phi = \lambda e \tag{33}$$

where e is a vector that consists of all zeroes except for the element in the position corresponding to the mode number of ϕ, which has a value of one.

These can now be written as

$$\Phi^T d_m p_m = e \tag{34}$$

$$\Phi^T d_k p_k = \lambda e \tag{35}$$

Letting $\Phi^T \triangleq [\Phi_1{}^T \quad \Phi_2{}^T]^T$ and using equation (29) yields

$$\Phi^T d_{m11} p_{m1} = e - [\Phi_1^T d_{m12} + \Phi_2^T d_{m22}] p_{m2}^0 \tag{36}$$

$$\Phi^T d_{k11} p_{k1} = \lambda e - [\Phi_1^T d_{k12} + \Phi_2^T d_{k22}] p_{k2}^0 \tag{37}$$

The first partition of equation (30) and equations (36) and (37) can be combined in one equation

$$\begin{bmatrix} -\lambda d_{m11} & d_{k11} \\ \Phi_1^T d_{m11} & 0 \\ 0 & \Phi_1^T d_{k11} \end{bmatrix} \begin{Bmatrix} p_{m1} \\ p_{k1} \end{Bmatrix} = \begin{Bmatrix} 0 \\ e \\ \lambda e \end{Bmatrix} + \begin{bmatrix} -\lambda d_{m12} & d_{k12} \\ -\Phi_1^T d_{m12} - \Phi_2^T d_{m22} & 0 \\ 0 & -\Phi_1^T d_{k21} - \Phi_2^T d_{k22} \end{bmatrix} \begin{Bmatrix} p_{m2}^0 \\ p_{k2}^0 \end{Bmatrix} \quad \textbf{(38)}$$

with constraint equation (31)

$$-\lambda d_{m22} p_{m2}^0 + d_{k22} p_{k2}^0 = \mathbf{0} \quad \textbf{(39)}$$

There exists a set of equations (38) and (39) for each test pair (λ, ϕ). All these equations can be combined into

$$D p_1 = d \quad \textbf{(40)}$$

with

$$D \triangleq \begin{bmatrix} \cdots & \cdots \\ -\lambda_i d_{m11}^i & d_{k11}^i \\ \Phi^T d_{m11}^i & 0 \\ 0 & \Phi^T d_{k11}^i \\ \cdots & \cdots \end{bmatrix}, \qquad i=1,2,\ldots,L \quad \textbf{(41)}$$

and

$$d \triangleq \begin{Bmatrix} \cdots \\ 0 \\ e_i \\ \lambda_i e_i \\ \cdots \end{Bmatrix} + \begin{bmatrix} \cdots & \cdots \\ \lambda_i d^i_{m12} & -d^i_{k12} \\ -\Phi_1^T d^i_{m12} - \Phi_2^T d^i_{m22} & 0 \\ 0 & -\Phi_1^T d^i_{k12} - \Phi_2^T d^i_{k22} \\ \cdots & \cdots \end{bmatrix} \begin{Bmatrix} p^0_{m2} \\ p^0_{k2} \end{Bmatrix}, \quad i=1,2,...,L \qquad (42)$$

where L is the number of test pairs used. Furthermore, the first term on the right hand side of equation (42) can be eliminated by dividing through by λ_i and eliminating the diagonal components of the orthogonality constraints. D is a matrix of size $r \times s$, such that

$$r = L \times (n_1 + 2)$$

where n_1 is the number of degrees of freedom associated with the $\boldsymbol{p}_1$ elements. The dimension s is equal to the total number of parameters to be changed in all elements. The vector $\boldsymbol{d}$ is also of length r. The vector $\boldsymbol{p}_1$ is of length s.

Substituting $\boldsymbol{p}_1 = \boldsymbol{p}_1^o + \Delta\boldsymbol{p}_1$ from equation (6) into equation (40) results in

$$D\Delta p_1 = \boldsymbol{d} - D\boldsymbol{p}_1^o \qquad (43)$$

which can then be solved for $\Delta\boldsymbol{p}_1$ via the least squares method. The normal equations are then expressed as

$$(D^T D)\Delta p_1 = D^T(d - Dp_1^o) \tag{44}$$

and then

$$\Delta p_1 = [D^T D]^{-1} D^T(d - Dp_1^o) \tag{45}$$

Before solving for Δp_1 in equation (45), it is necessary to determine the eigenvalues of $D^T D$ in order to check for singularities or ill-conditioning. Only when $D^T D$ is well-behaved is it possible to proceed with the solution. If $D^T D$ is not well-behaved, the choice of p_1 paramaeters or the quality of the test data may be suspect. Once assured of a valid set of equations, equation (45) can be solved for the required changes to the pre-selected element parameters necessary to correct the finite element model in order to achieve the best fit of the experimental modes and frequencies.

4. IMPROVED SEMI-ITERATIVE TECHNIQUE

While the Engels' method has been shown to go directly to the correct solution in a single step for analytically precise data that has a one-to-one spatial correspondence with the finite element model to be modified, it becomes unstable when the eigenvector at a single node in the region near the boundary deviates from the analytically precise eigenvector by an amount as small as 0.01%. Not only does this impose an unreasonable requirement on the test measurement, it also means that the expansion technique to be employed must result in a set of expanded eigenvectors that are consistent with the analytically precise solution. The improved semi-iterative approach, presented in this chapter and implemented in the computer program XMOD, overcomes the inherent difficulties that are present in the direct solution technique.

There are two critical elements that are necessary for the success of the improved semi-iterative approach. The first of these is the incorporation of a data expansion technique that is consistent with the physical problem into an iterative loop that updates the modified parameters in the finite element model. The second key is the application of an appropriate weighting factor to the experimentally measured eigenvectors. A flow diagram illustrating the new method is shown in figure 4.

Expansion Method

Various expansion techniques were evaluated based on the need for a resulting set

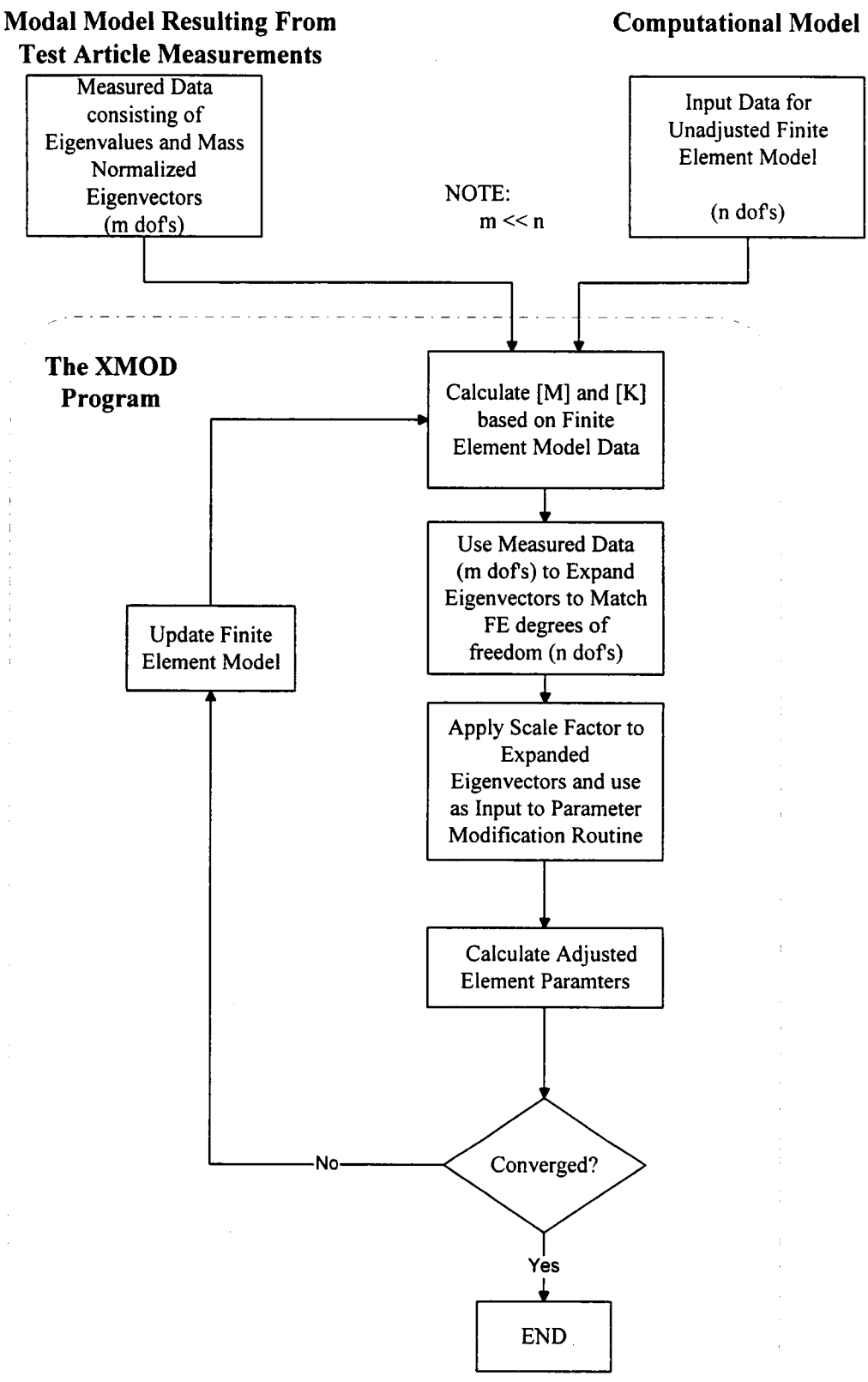


Figure 4, Flow Diagram Illustrating the Semi-Iterative XMOD Solution

of values that maintain a high degree of physical compatibility with the initial finite element model. The method that was selected based on this requirement is a variation of the "physical expansion" technique suggested by Kidder [8]. This technique is derived from an inverse Guyan reduction formulation starting with the basic eigenproblem equation

$$(K - \lambda_m M)\phi_x = \{ 0 \}$$

where K is the unperturbed finite element stiffness matrix, M is the unperturbed finite element mass matrix, λ_m is a measured eigenvalue, and ϕ_x is the fully expanded mode shape based on measured data.

Partitioning the matrices into known and unknown parts yields

$$\left(\begin{bmatrix} K_{11} & K_{12} \\ K_{21} & K_{22} \end{bmatrix} - \lambda_m \begin{bmatrix} M_{11} & M_{12} \\ M_{21} & M_{22} \end{bmatrix} \right) \begin{Bmatrix} \phi_1 \\ \phi_2 \end{Bmatrix}_x = \{ 0 \}$$

where $\{\phi_1\}_x$ are the degrees of freedom from ϕ_x that have been measured experimentally and $\{\phi_2\}_x$ are the unmeasured degrees of freedom of ϕ_x that are to be calculated. Now solving for $\{\phi_2\}_x$ results in

$$\{ \phi_2 \}_x = \left([K_{22}] - \lambda_m [M_{22}] \right)^{-1} \left([K_{21}] - \lambda_m [M_{21}] \right) \{ \phi_1 \}_x$$

This expansion technique has the advantage that by using the unperturbed finite element stiffness and mass matrices, the physical connectivity properties are imposed directly. But since the original matrices are used, the accuracy of the expanded eigenvectors depends on the validity of the model at the previous computational step. Fortunately, this is a relatively small penalty for the case where the modifications are near the boundary.

Eigenvector Scaling

The second critical element in the successful implementation of the method was the application of a scaling multiplier to the expanded experimentally derived eigenvectors. Under certain conditions the semi-iterative technique tends to over adjust the stiffness parameters resulting in negative values for Poisson's ratio that are not physically possible. By applying a scale factor to the set of expanded experimental eigenvectors, ϕ_x, the rate of change in stiffness parameters is slowed so that Poisson's ratio remains close to the initial values allowing the technique to converge to corresponding realistic values for Young's modulus. Thus, eigenvector scaling effectively damps the solution so that reliable convergence to a stable solution is possible.

As can be seen in equations (16) and (17) p_1^k and p_2^k are related by Poisson's Ratio, ν. The resulting relationships between Δp_1^k, Δp_2^k, E, and ν are:

$$\nu_{i+1} = \frac{[1+(\Delta p_2^k)_i]}{[1+(\Delta p_1^k)_i]}\nu_i \qquad (46)$$

$$E_{i+1} = D_i[1+(\Delta p_1^k)_i](1+\nu_{i+1})(1-2\nu_{i+1}) \qquad (47)$$

where the subscript *i* indicates values for the ith iteration and:

$$D_i = \frac{E_i}{(1+\nu_i)(1-2\nu_i)}$$

From equations (46) and (47) above, it can be seen that in order for Poisson's ratio to remain within the theoretical limitations of 0.0 to 0.5 and Young's modulus greater than zero, the following conditions must be met:

$$-1 < (\Delta p_1^k)_I$$

$$-1 < (\Delta p_2^k)_I$$

and

$$\frac{1+(\Delta p_1^k)_i}{1+(\Delta p_2^k)_i} > 2\nu_i$$

Furthermore, if a nearly constant Poisson's ratio is desired, then the following additional condition is also necessary

$$(\Delta p_1^k)_1 \approx (\Delta p_2^k)_1.$$

By discarding the diagonal members of the orthogonality condition, the Engels' method avoids the need to maintain the absolute magnitudes of the measured and adjusted eigenvectors, thus relying more heavily on the orthogonal nature of the eigenproblem. This characteristic of the Engels' method also allows the equations to be scaled resulting in scaled parameters Δp_1^k and Δp_2^k.

The application of scaling was found to be especially useful for those instances where the calculated values for Δp_1^k are negative. This happens for the case where the unperturbed initial value for Young's modulus is higher than the adjusted value resulting from the measured frequencies and mode shapes (e.g. the measured natural frequency is lower than the natural frequency of the initial unperturbed model). Conversely, it was found that the application of scaling to the case where Δp_1^k is always a positive value (e.g. the measured natural frequency is higher than that of the initial unperturbed model) resulted in very little effect on stability.

The use of eigenvector scaling in conjunction with the "physical expansion" technique proves to be highly effective in solving the boundary condition problem when incorporated into the Engels' method. The following chapters present example problems using both analytically generated test data and measured test data. These examples show

that the solution reliably converges to a stable solution within very few steps. The only penalty being the rather costly inversion of the stiffness matrix term. This cost can, however, be minimized through the application of the proper numerical techniques.

Analytical Validation of Semi-iterative Technique

A two step approach has been employed to validate the semi-iterative model modification technique. The first step was to use precise "test" data that was analytically determined (pseudo-experimental data) using the same finite element formulation that is used in the XMOD program. The second step was to use actual experimentally determined frequencies and mode shapes to demonstrate the method in a practical application.

The general layout for the initially unperturbed finite element model used in the analytical validation process is shown in figure 5. The total thickness of the plate was taken as 0.188 inches in order to match one of the test articles used during the experimental validation process. The model is made up of 240 nodes and 120 elements. The model is two elements deep through the plate thickness. The initially unperturbed model assumes that the eight elements adjacent to the clamped boundary have a modulus of elasticity equal to 30 million pounds per square inch. The remainder of the plate is assumed to be homogeneous aluminum with a modulus of elasticity of 10.6 million pounds per square inch (see figure 5).

The analytically generated pseudo-experimental data comes from another finite element model with identical geometry. It differs in that the modulus of elasticity is

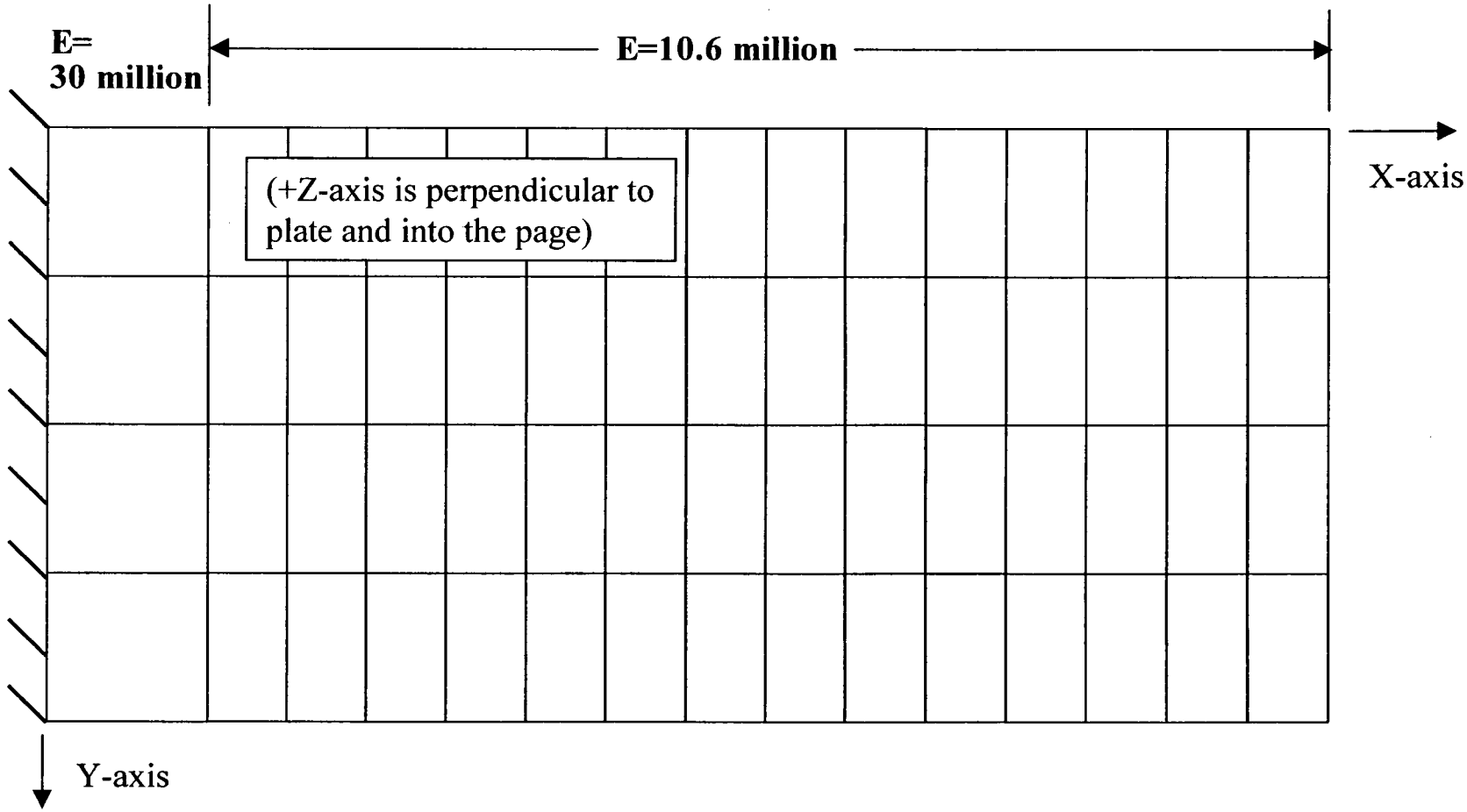


Figure 5, Unperturbed Finite Element Model Used as Input to XMOD

equal to 10.6 million pounds per square inch for all elements as shown in figure 6. The six data points that were selected correspond to nodes 122, 124, 152, 154, 212, and 214. The four lowest eigenvalues and the z-components of the analytical eigenvector at these six locations were used as the test data. These six locations were chosen based on a cursory review of the vectors resulting from the measured data and are the same points used in the experimental validation of the technique for the corresponding plate.

The unmodified natural frequencies of the two different models is summarized in the following table. The theoretical values that are presented in this table are based on the work of Gorman [16]. The difference in stiffness near the boundary for the two models was chosen based on producing a measurable difference in modal characteristics. As can be seen in this table the differences in frequency between the two models varies from 6.88 % to 16.0 %.

Table 1, Comparison of Uncorrected Frequencies, Pseudo-Experimental Case

Mode Number	Characteristic Shape	Pseudo-Experimental Data		Unperturbed XMOD model Results (Iteration=0)	Difference FEA vs. Unperturbed (per cent)
		Theory (Gorman)	Finite Element		
1	Bending	89.68 hz	90.09 hz	104.51 hz	16.0%
2	Twisting	404.5 hz	386.6 hz	413.2 hz	6.88%
3	Bending	558.8 hz	558.9 hz	631.0 hz	12.9%
4	Twisting	1313. hz	1264. hz	1354. hz	7.12%

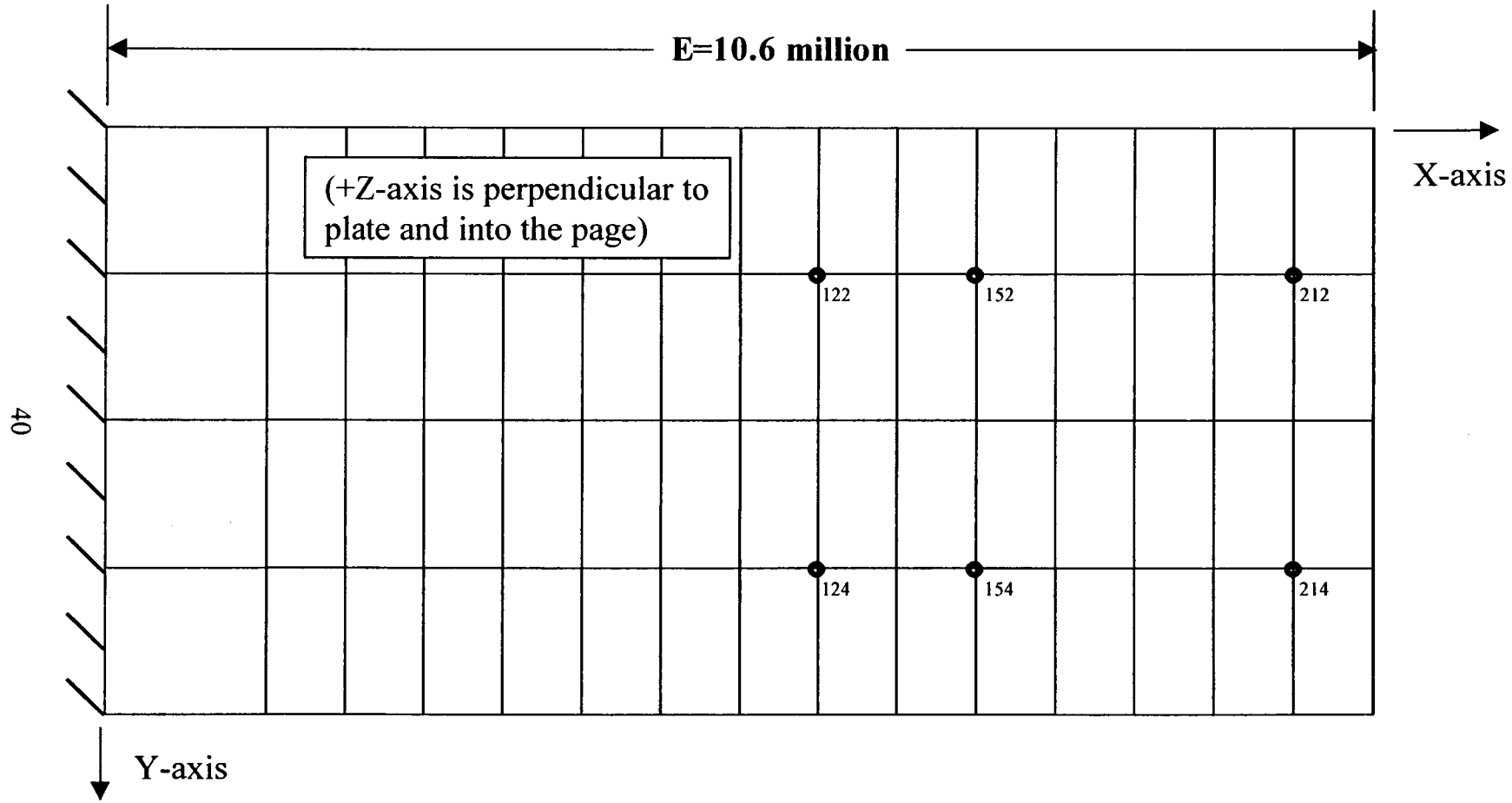


Figure 6, Finite Element Model Used to Generate the Pseudo-Experimental Data

Discussion of Results

It was found that after only a few iterations the solution would converge to a stable solution. It was also found that the resulting solution was not uniform across the plate, but varied across the width of the plate in a symmetric fashion. For this particular example the four elements that were adjacent to the free edges of the plate (referred to as exterior elements) converge to a value of Young's modulus equal to 12.5 million pounds per square inch, while the four interior elements approach a value of 9.1 million pounds per square inch. This represents errors of 17.9% and -14.2% respectively. However, when viewed in terms of a mean value of 10.8 million pounds per square inch the error is only 1.88%. The distribution of stiffness values as a function of plate width is illustrated in figure 7.

The convergence of the technique proved to be very stable and predictable. The method required four to ten iterations to obtain a stable solution depending on the amount of scaling applied to the measured eigenvectors. Figures 8, 9, 10, 11, and 12 show the convergence characteristics for eigenvector scale factors of 1.0, 0.8, 0.6, 0.4, and 0.2.

In order to better assess the validity of the solution, it is necessary to substitute the estimated values for Young's modulus and Poisson's ratio back into the finite element model and compare the resulting frequencies and mode shapes with the pseudo-experimental data that was used as input to XMOD. The values that were chosen for comparison come from the eighth iteration with the measured eigenvector scaled by 40%. As can be seen in table 2, the natural frequencies are very close, varying from the pseudo-experimental finite element model by much less than 0.4% for all frequencies.

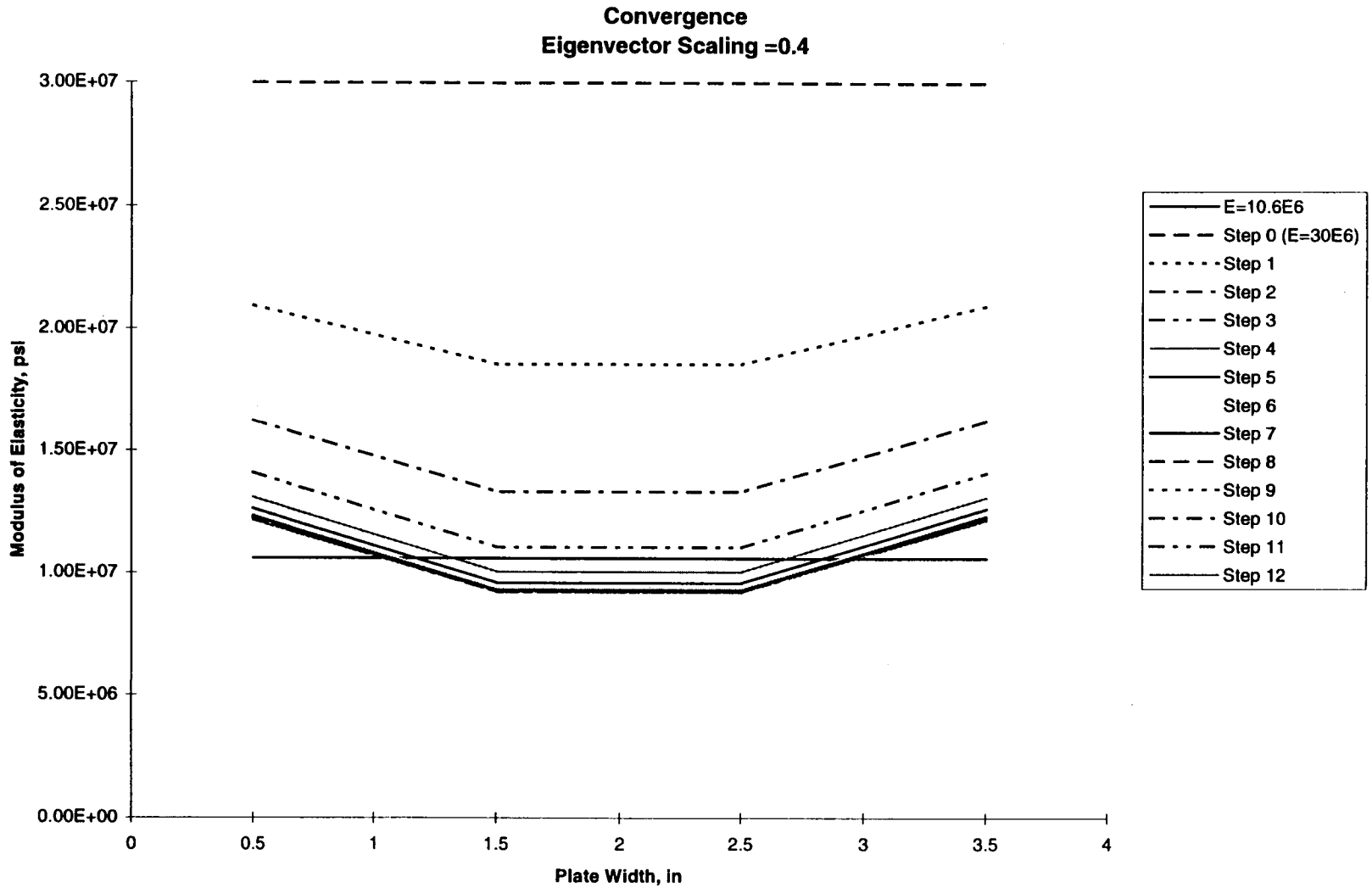


Figure 7, Distribution of Stiffness Values Across the Plate Width

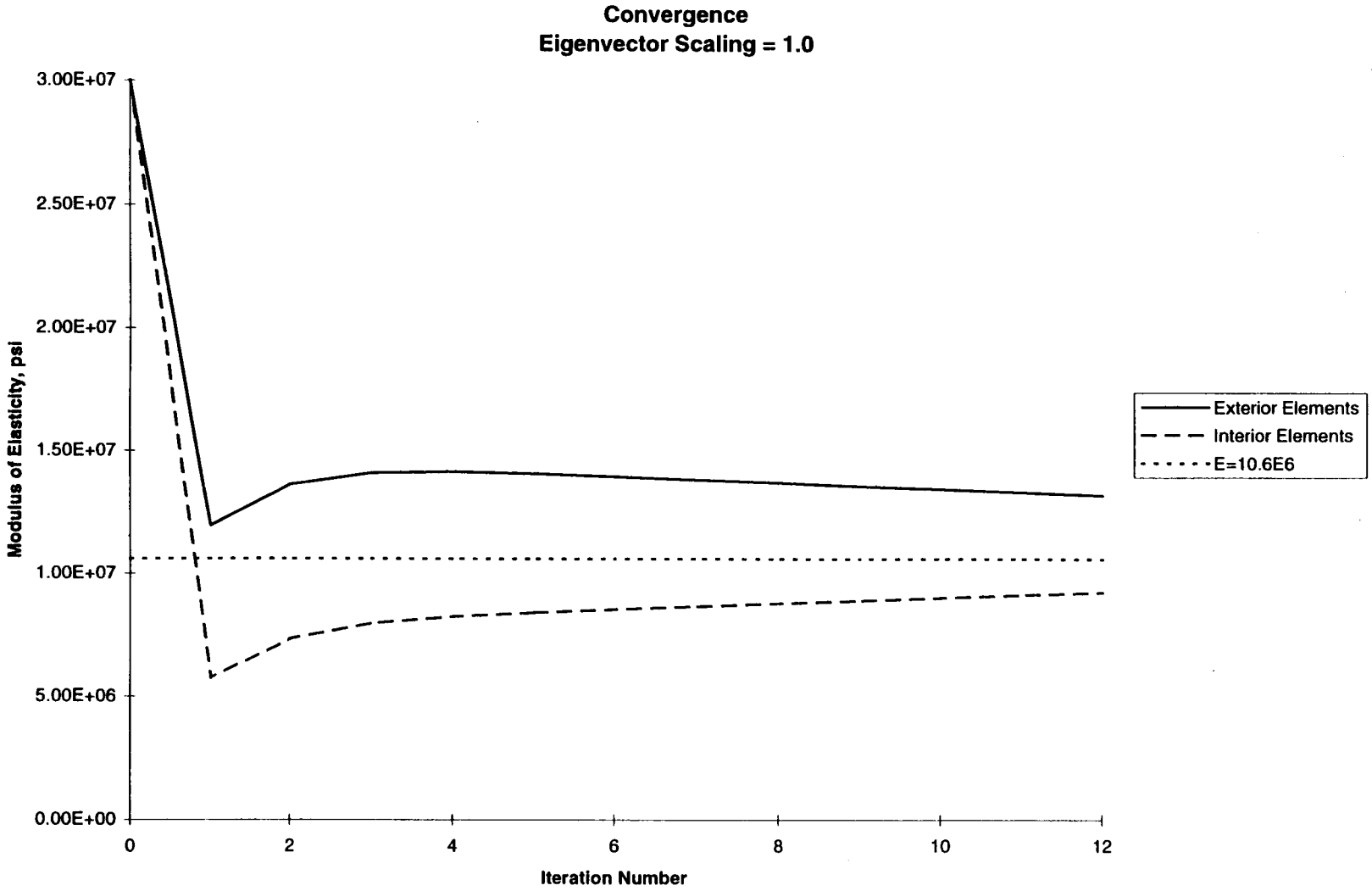


Figure 8, Convergence for Eigenvector Scaling = 1.0, Pseudo-Experimental Case

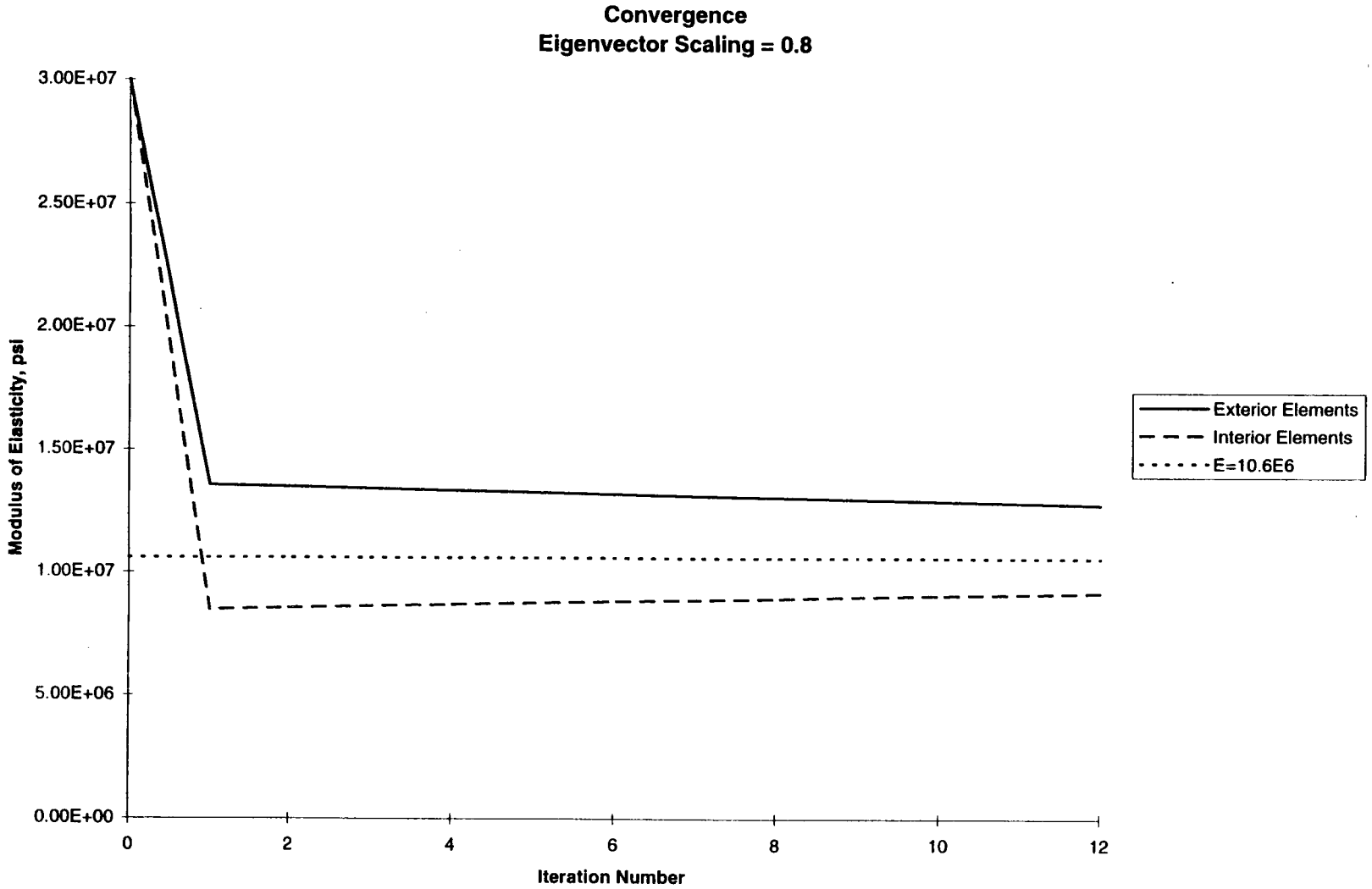


Figure 9, Convergence for Eigenvector Scaling = 0.8, Pseudo-Experimental Case

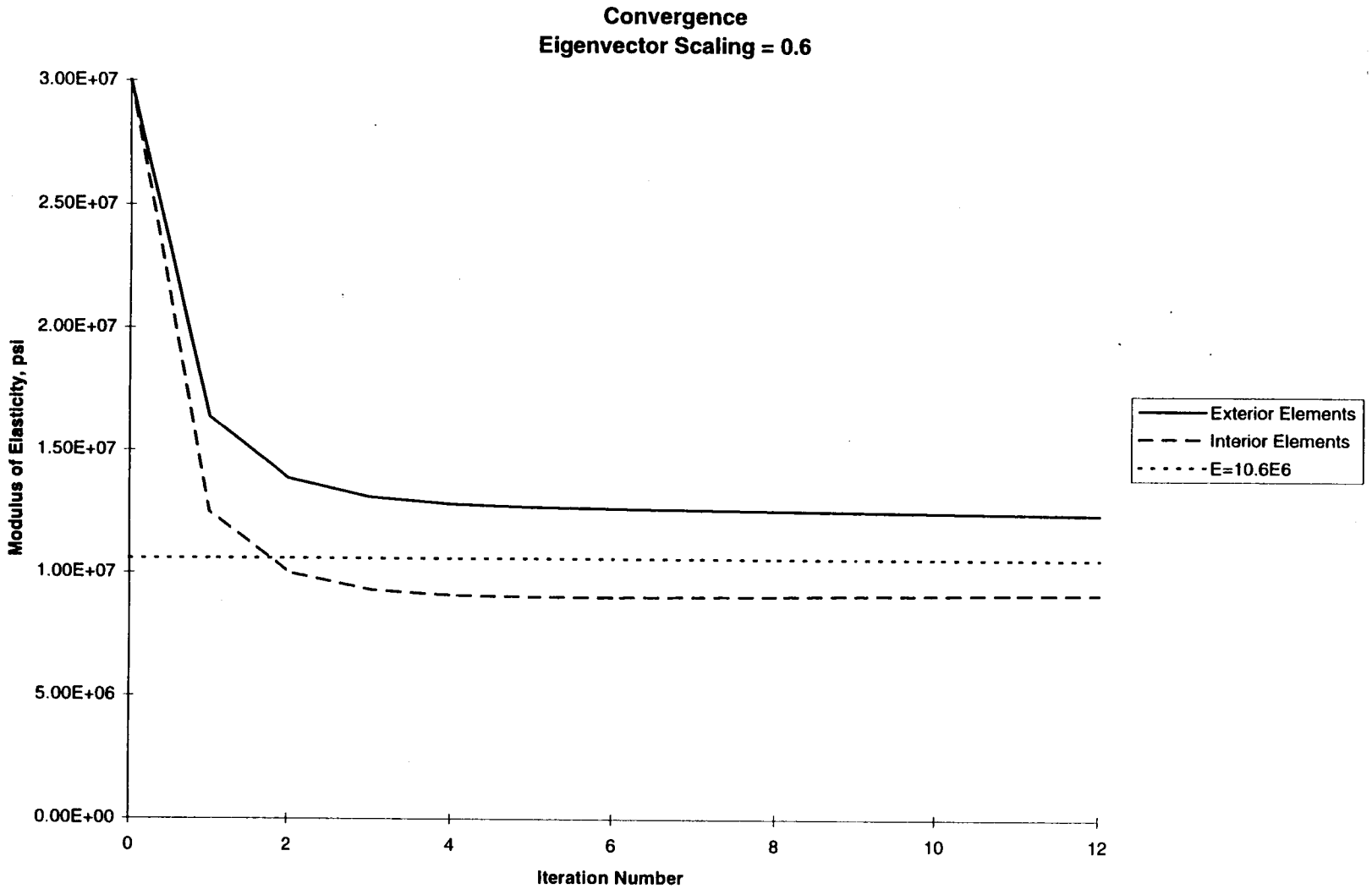


Figure 10, Convergence for Eigenvector Scaling = 0.6, Pseudo-Experimental Case

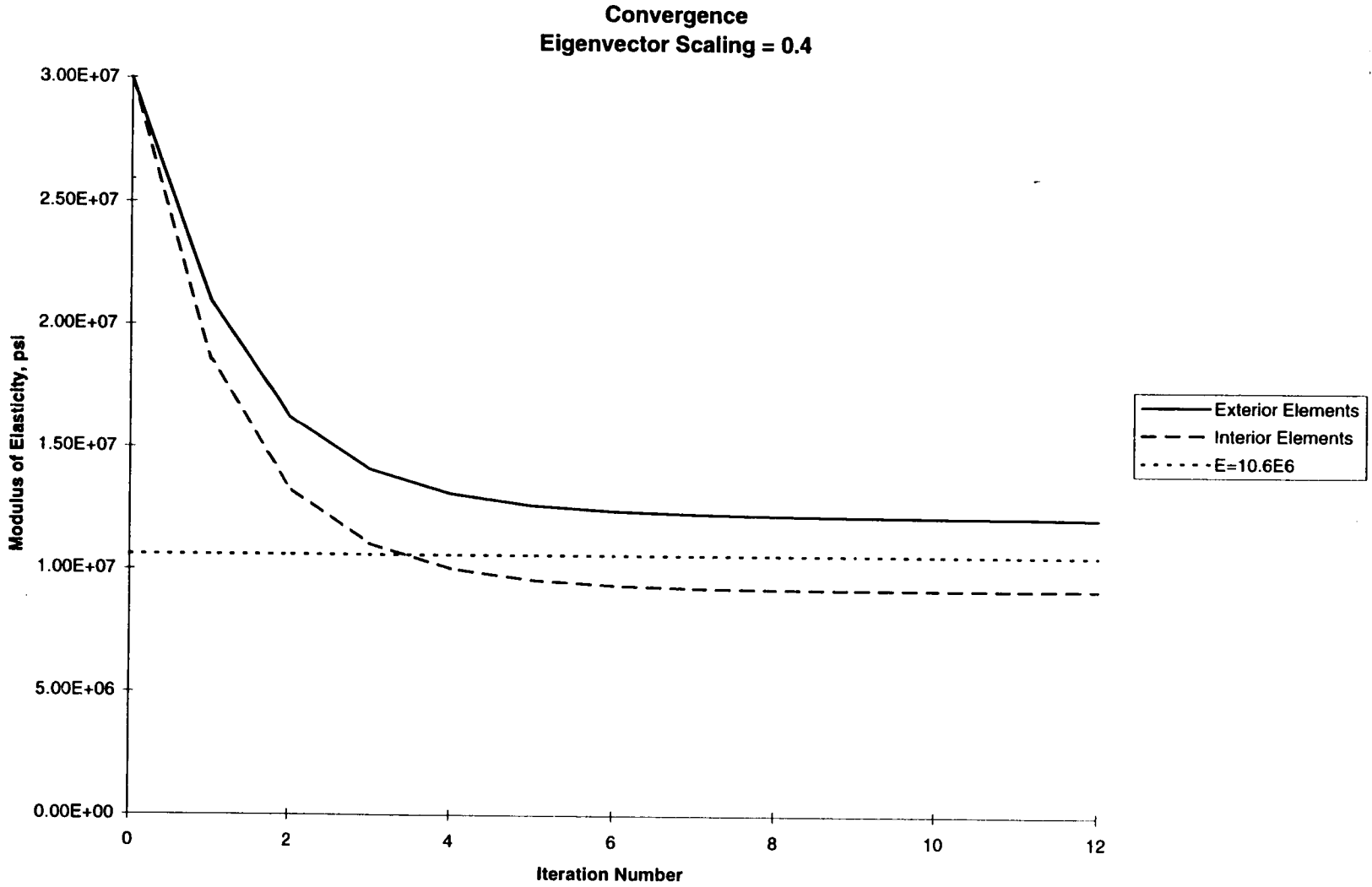


Figure 11, Convergence for Eigenvector Scaling = 0.4, Pseudo-Experimental Case

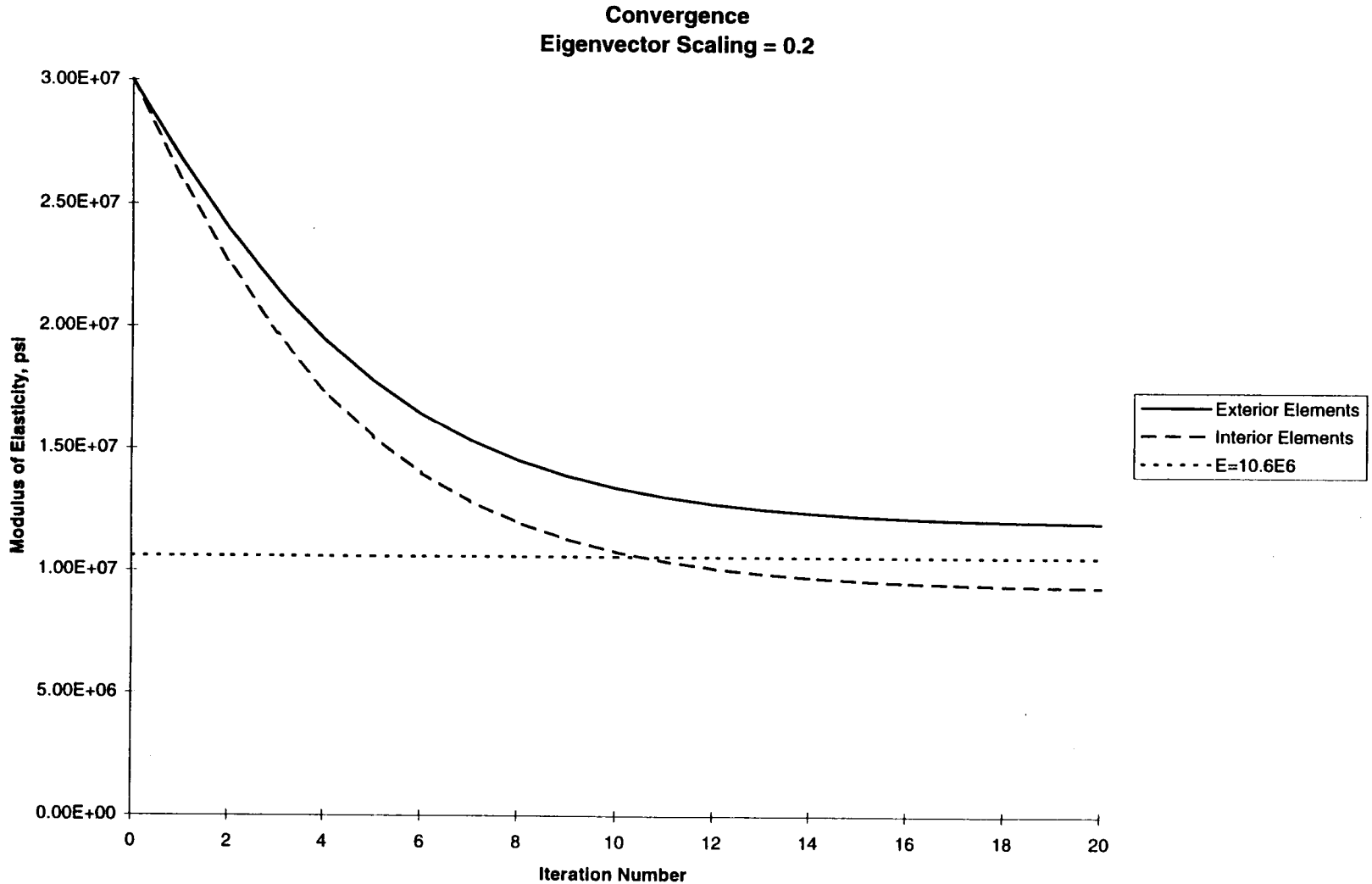


Figure 12, Convergence for Eigenvector Scaling = 0.2, Pseudo-Experimental Case

Table 2, Comparison of Corrected Frequencies, Pseudo-Experimental Case

Mode Number	FEA Pseudo-Experimental (hz)	FEA Resulting Eighth Iteration (hz)	Error (per cent)
1	90.09	90.05	0.05%
2	386.6	388.0	-0.36%
3	558.9	559.5	-0.11%
4	1264.	1269.	-0.40%

The mode shapes also show excellent agreement with a maximum deviation from the pseudo-experimental values of less than 3% in the fourth mode shape as shown in table 3. Figures 13, 14, 15, and 16 show the comparison between the mass normalized mode shapes for the unperturbed model (iteration = 0) and the mass normalized mode shapes for the eighth iteration with the pseudo-experimental data points superimposed on the plots. Since the results are symmetric, the data is plotted along a line passing through nodes 122, 152, and 212 parallel to the X-axis. As can be seen from the resulting data, XMOD predicts the required modifications to the finite element model to a magnitude well within the limits of measurement accuracy.

Table 3, Comparison of Corrected Mode Shapes, Pseudo-Experimental Case

Node Number	Mode 1 (% difference)	Mode 2 (% difference)	Mode 3 (% difference)	Mode 4 (% difference)
122	-0.006%	-0.13%	0.06%	0.77%
152	-0.001%	0.03%	0.13%	2.99%
212	0.004%	0.18%	0.04%	0.07%

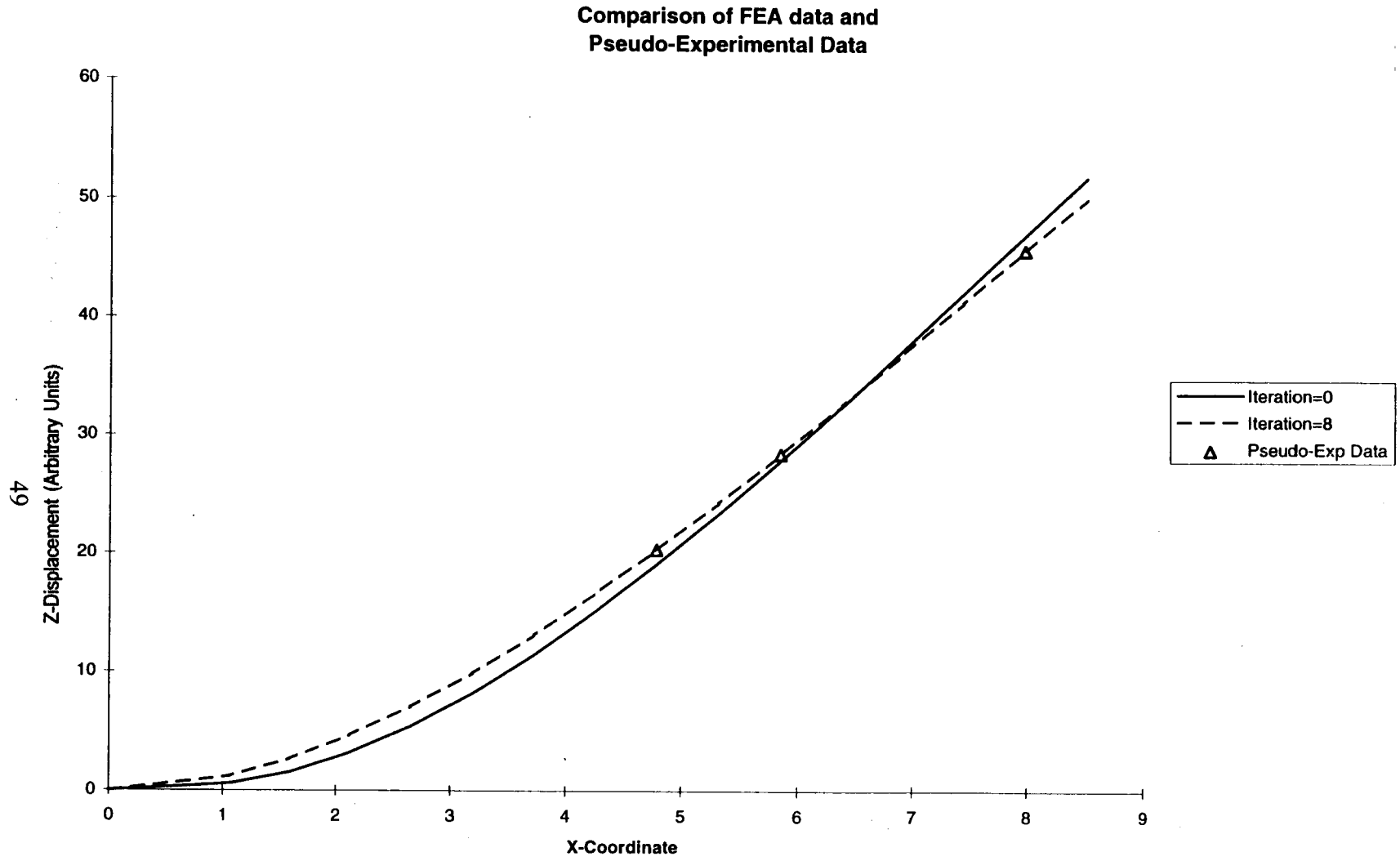


Figure 13, Comparison of Eigenvector for Mode 1, Pseudo-Experimental Case

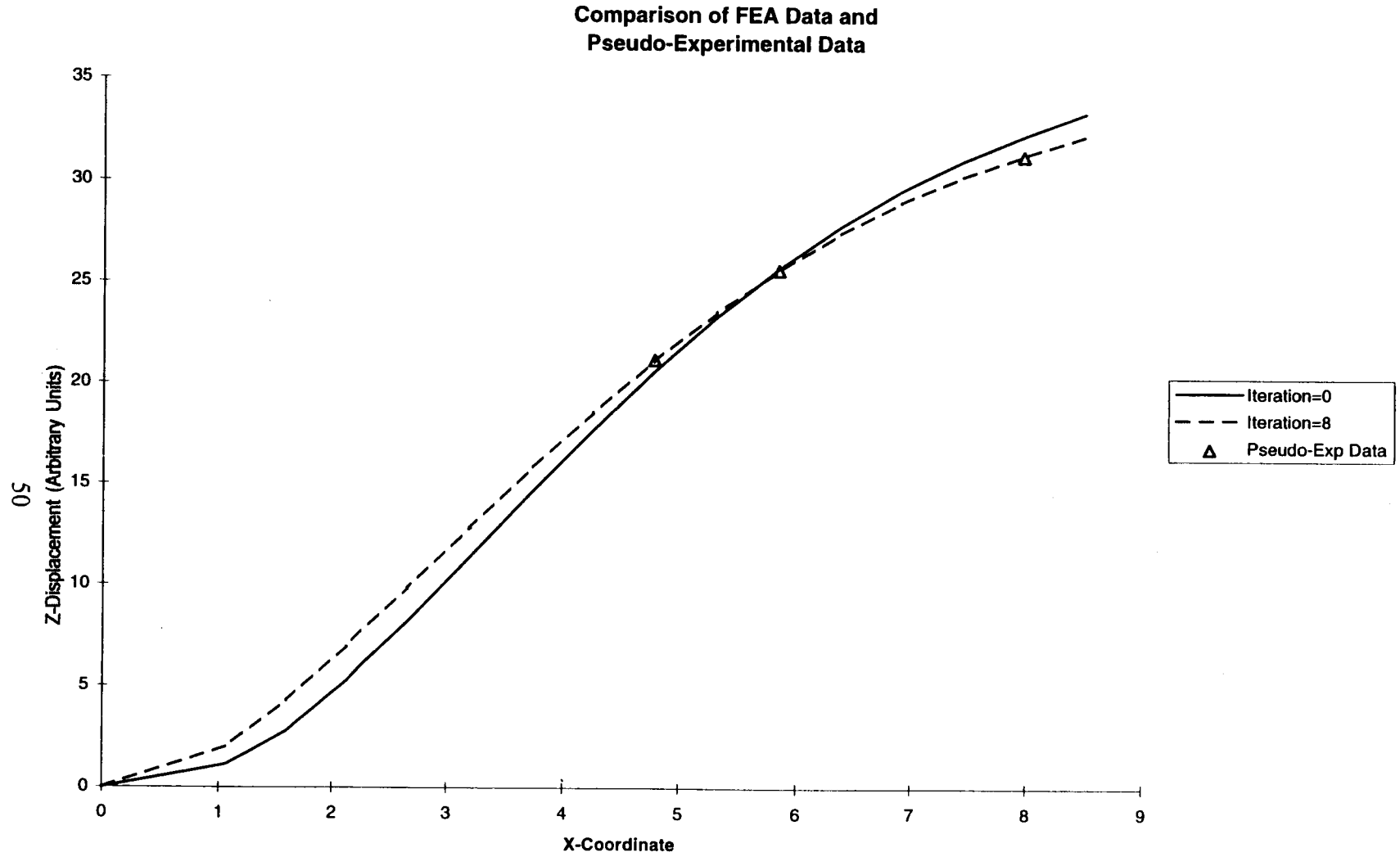


Figure 14, Comparison of Eigenvector for Mode 2, Pseudo-Experimental Case

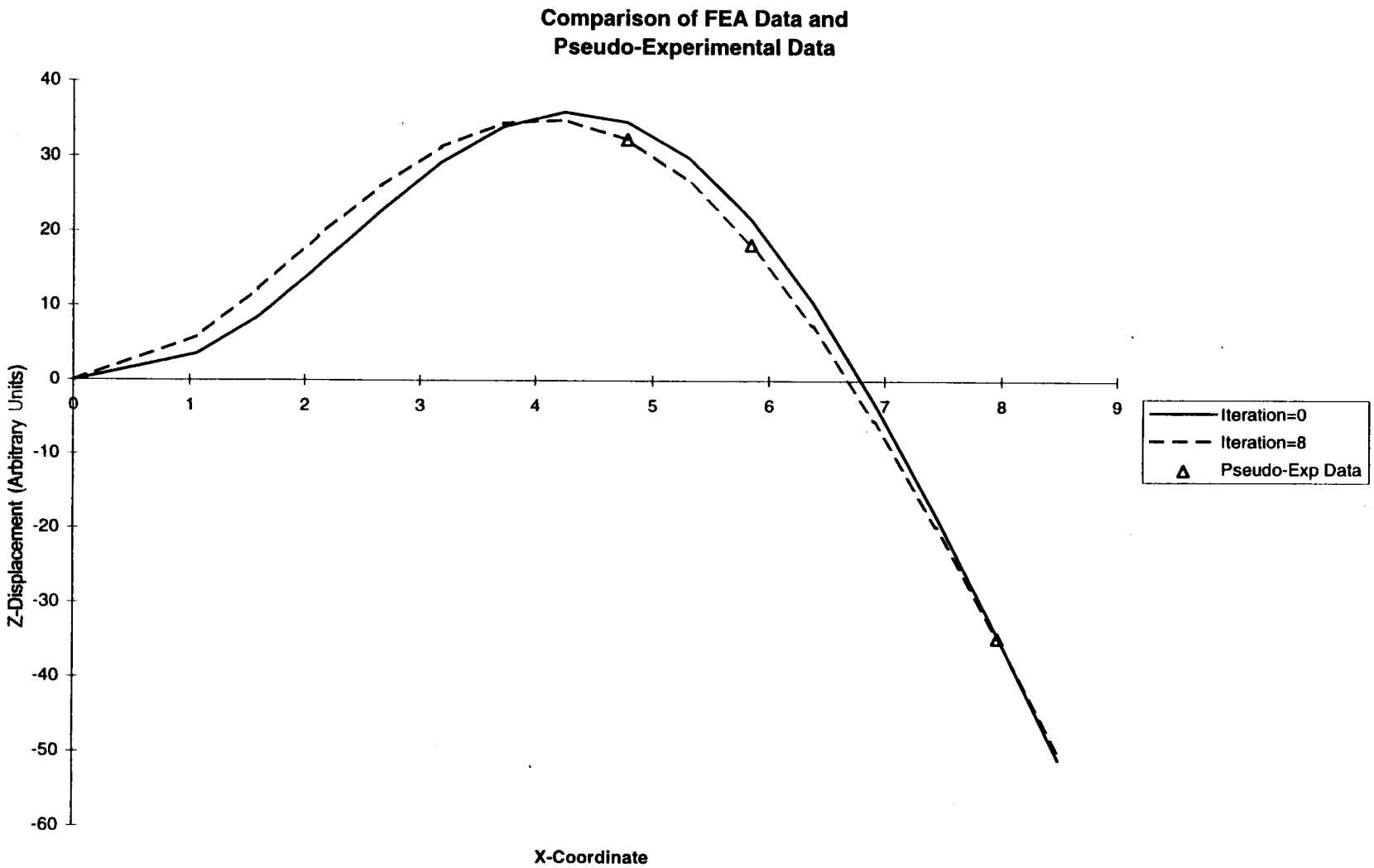


Figure 15, Comparison of Eigenvector for Mode 3, Pseudo-Experimental Case

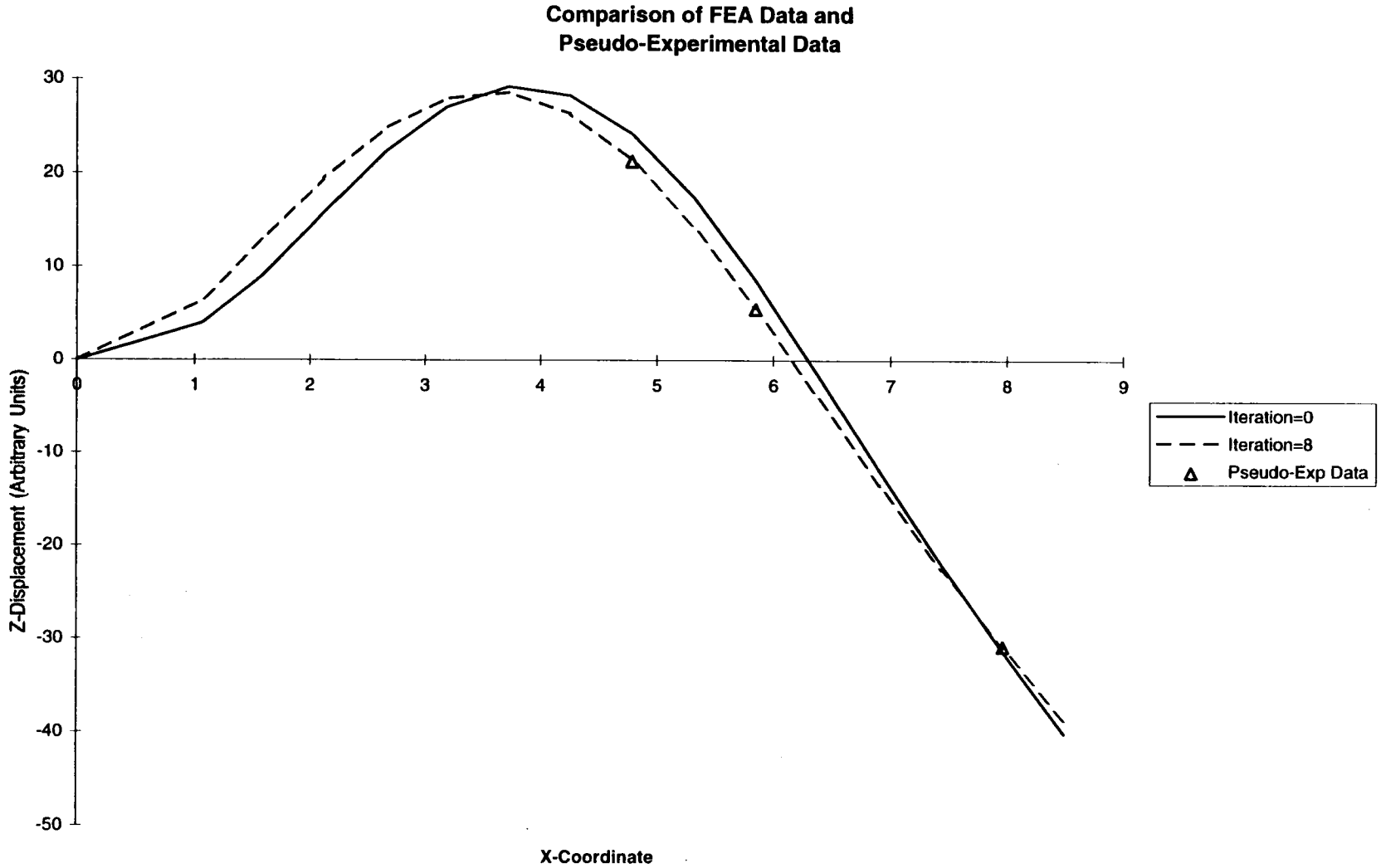


Figure 16, Comparison of Eigenvector for Mode 4, Pseudo-Experimental Case

5. EXPERIMENTAL VALIDATION OF SEMI-ITERATIVE TECHNIQUE

The next step in the validation of the semi-iterative modification technique is to apply the method to measured data from a physical model. The results that are presented in this section are from three different test articles that vary from each other both dimensionally and in measurement quality.

Test Objectives and Procedures

The objectives of these tests were to provide realistic experimental estimates of the natural frequencies and mode shapes that can be used as input to the XMOD program. The roving hammer method was used to collect accelerometer data which was processed into FRFs (Frequency Response Functions) by a digital signal analyzer as illustrated in figure 17. The natural frequencies and mass normalized mode shapes, along with other modal parameters were then estimated using the polyreference frequency domain method as implemented in the I-DEAS® software from Structural Dynamics Research Corporation. Additionally, the resulting experimental eigenvectors were constrained to preserve the symmetry of the system.

A photograph of the test configuration is shown in figure 18. The test article mounting fixture is attached to two cubic feet of concrete. The concrete, weighing approximately 300 pounds, served as a seismic mass thus providing a degree of isolation

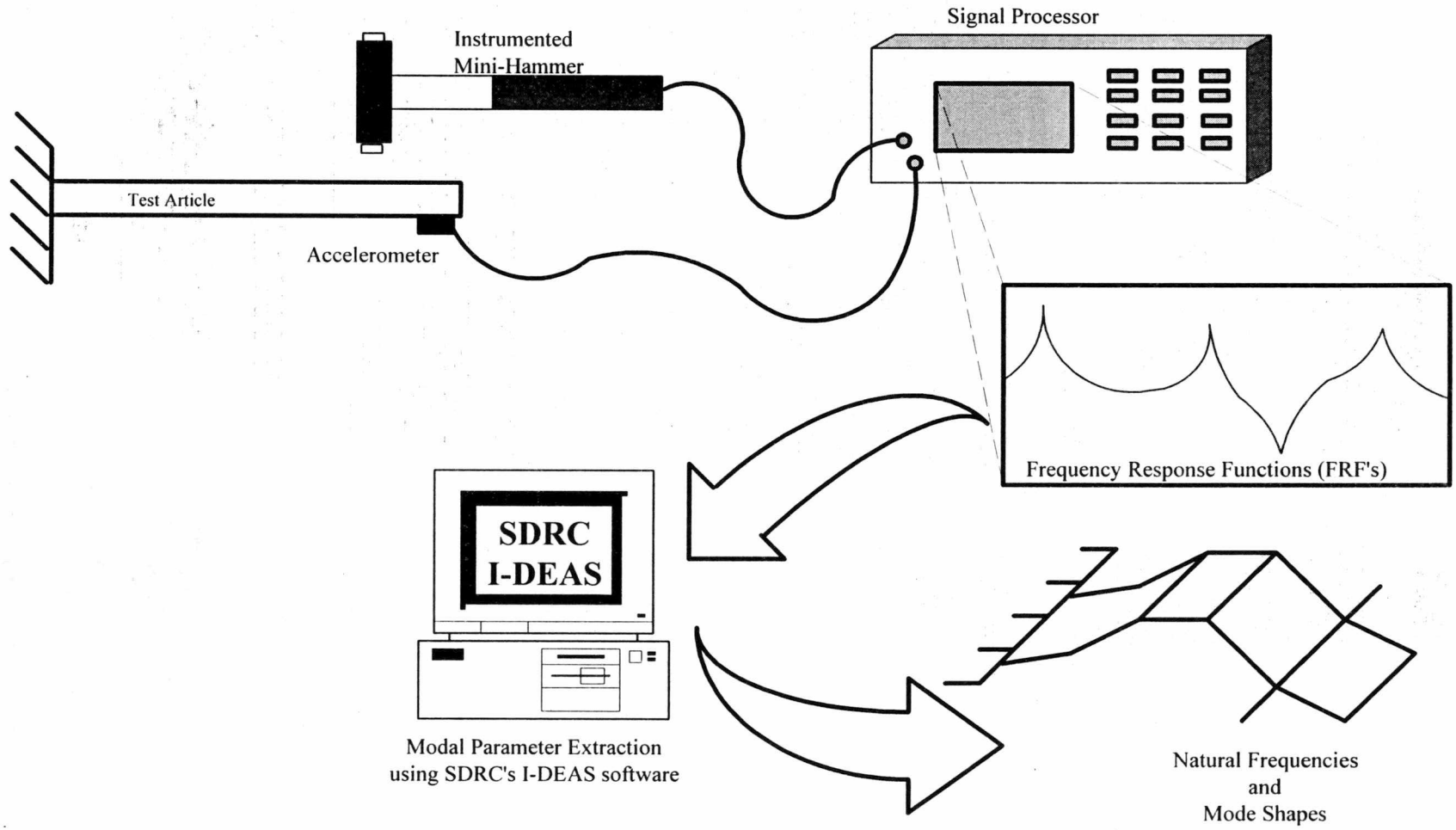


Figure 17, Schematic Representation of Experimental Set-up

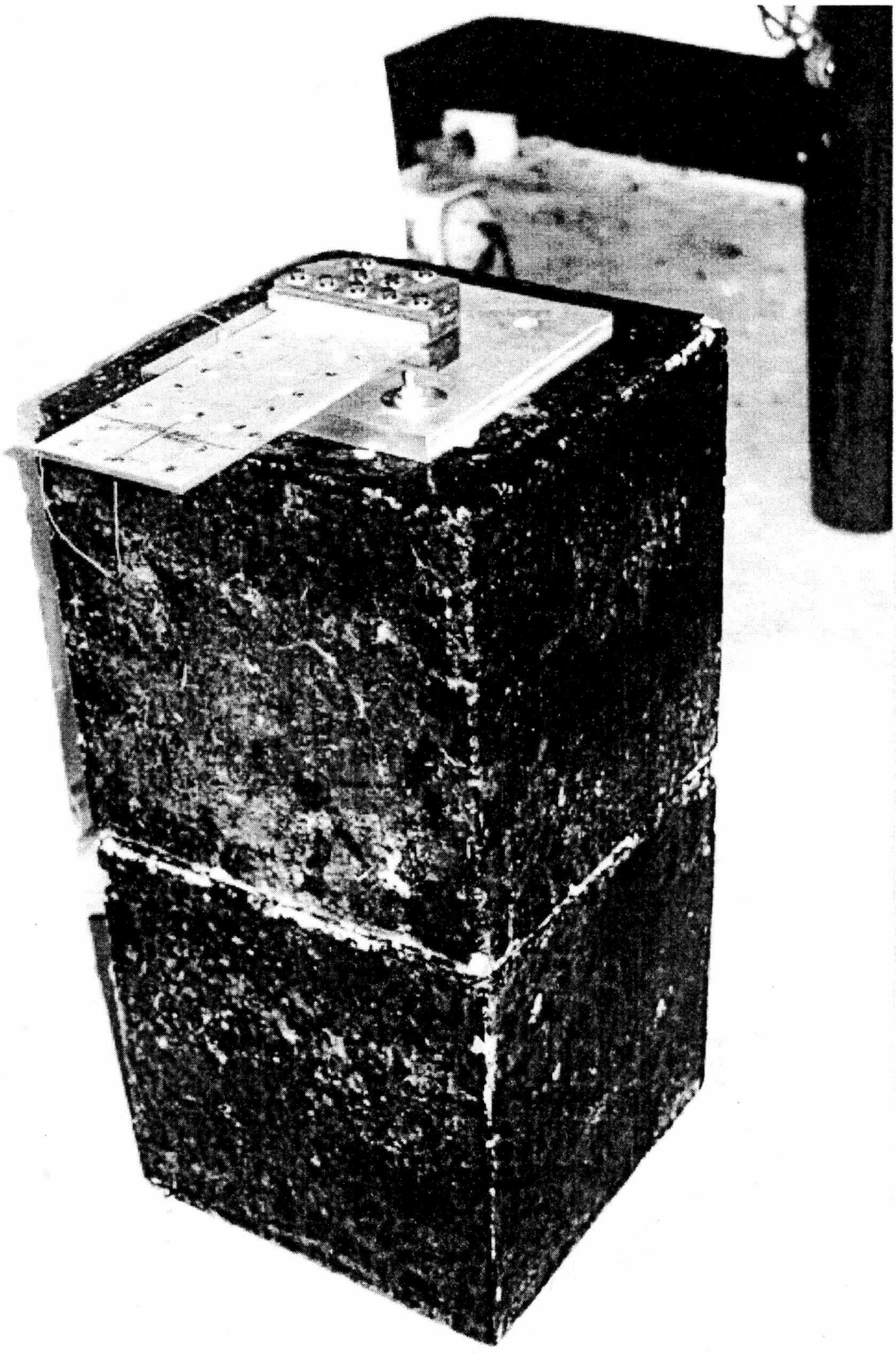


Figure 18, Cantilevered Plate Test Configuration

from ambient sources of vibration.

The accelerometer that was used to measure the response of the structure is shown in figure 19. This light weight accelerometer (approximately 1 gram) was selected, in order to avoid adversely affecting the system mass.

The excitation device was a mini-hammer designed especially for light weight structures such as turbine blades. The mini-hammer is shown in figure 20 along side a standard size hammer for perspective.

A detailed description of the test procedure is presented in appendix 1. Appendix 2 contains a summary of the resulting measurements.

Description of Test Articles

The structural systems that were used for experimental validation consisted of a set of three cantilevered thin plates. Each of the 4 inch wide aluminum plates has an overhanging length of 8.5 inches. The plates differ from each other only in their thickness and are illustrated in figures 21, 22, and 23 respectively. Table 4, below, lists

Table 4, Test Article Configurations

Test Article Designation	Cantilevered Length (inches)	Plate Width (inches)	Nominal Plate Thickness (inches)
P8540188	8.5	4	0.188
P8540100	8.5	4	0.100
P8540100M	8.5	4	0.140 over first 1.0625 inches from clamped end; 0.100 everywhere else.

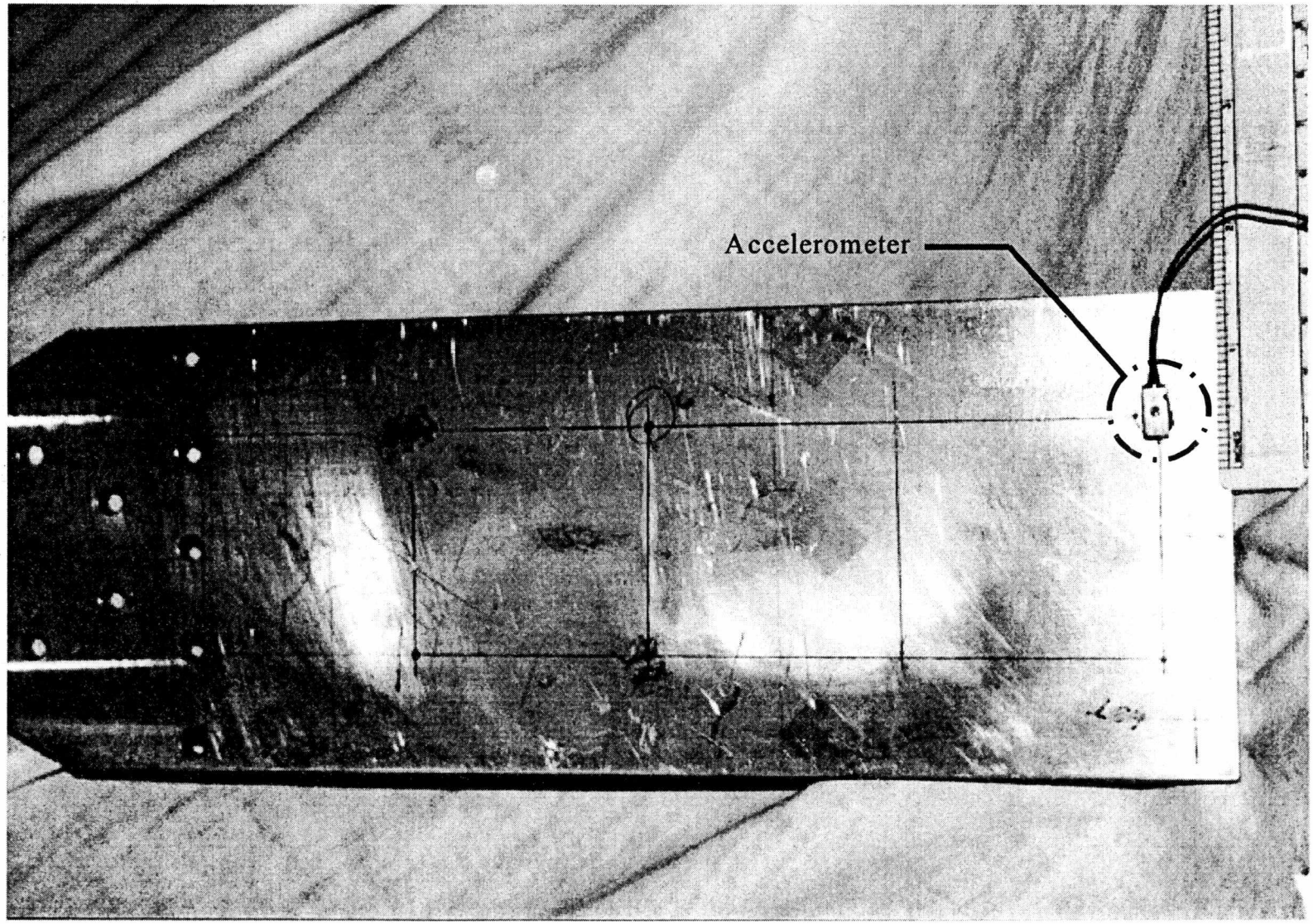


Figure 19, Light Weight Accelerometer, Shown Mounted on Test Article

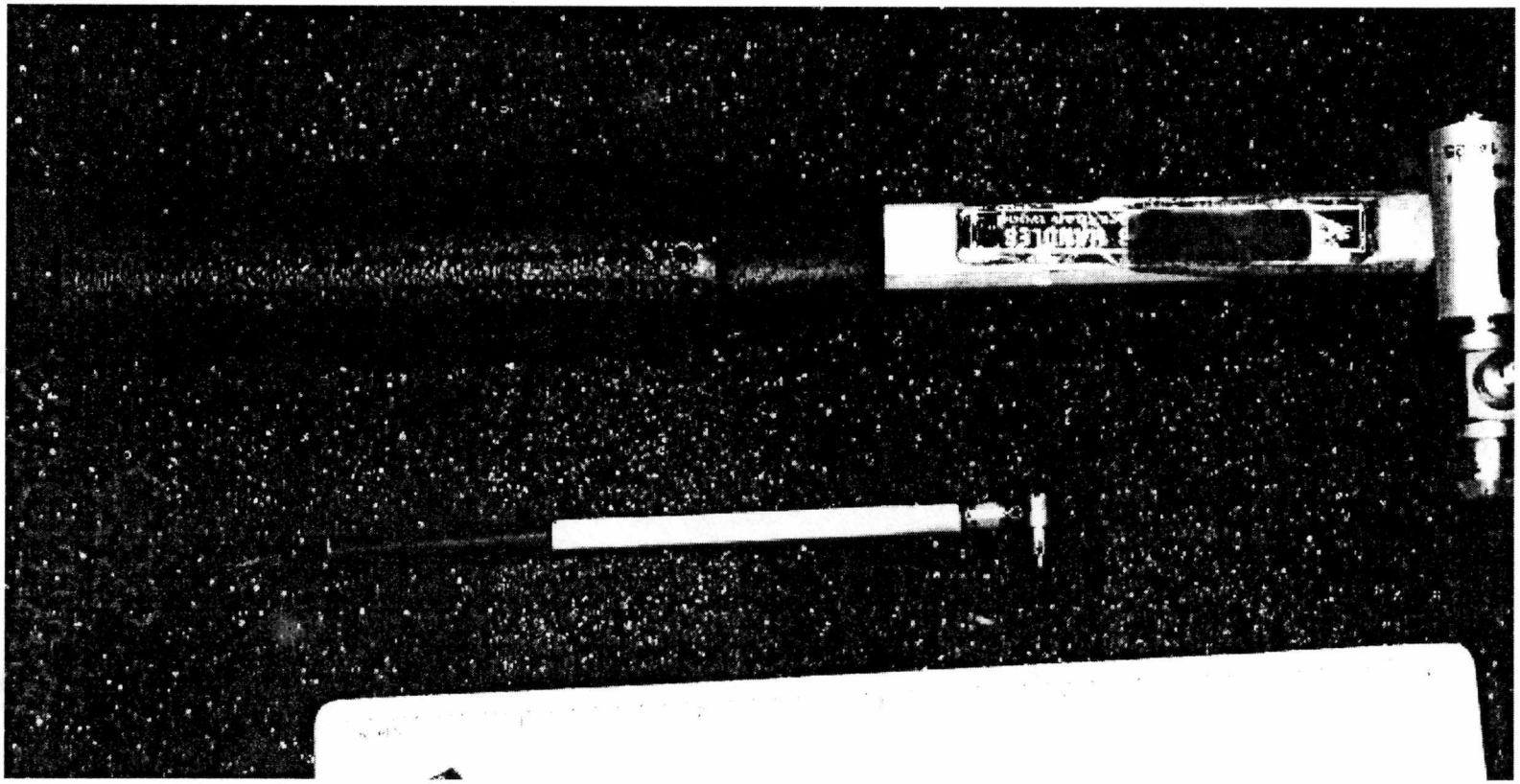


Figure 20, Instrumented Mini-Hammer (Shown with Standard Hammer)

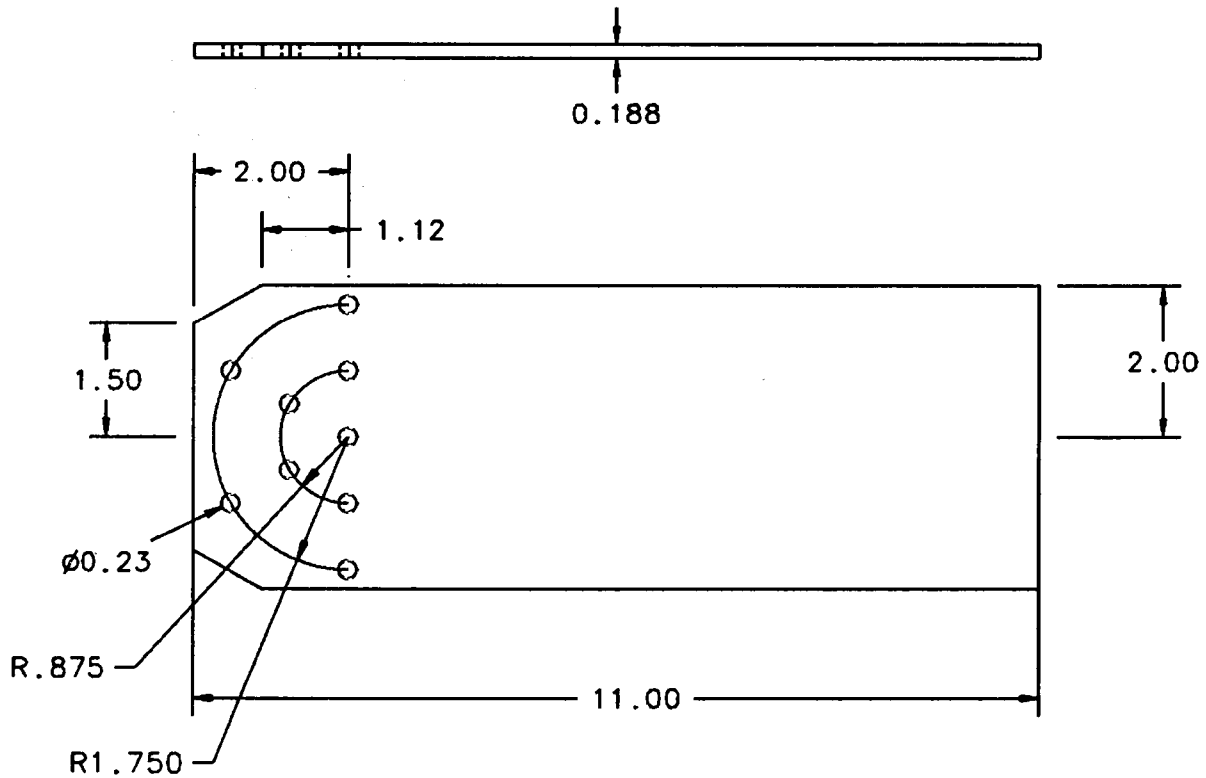


Figure 21, Test Article P8540188

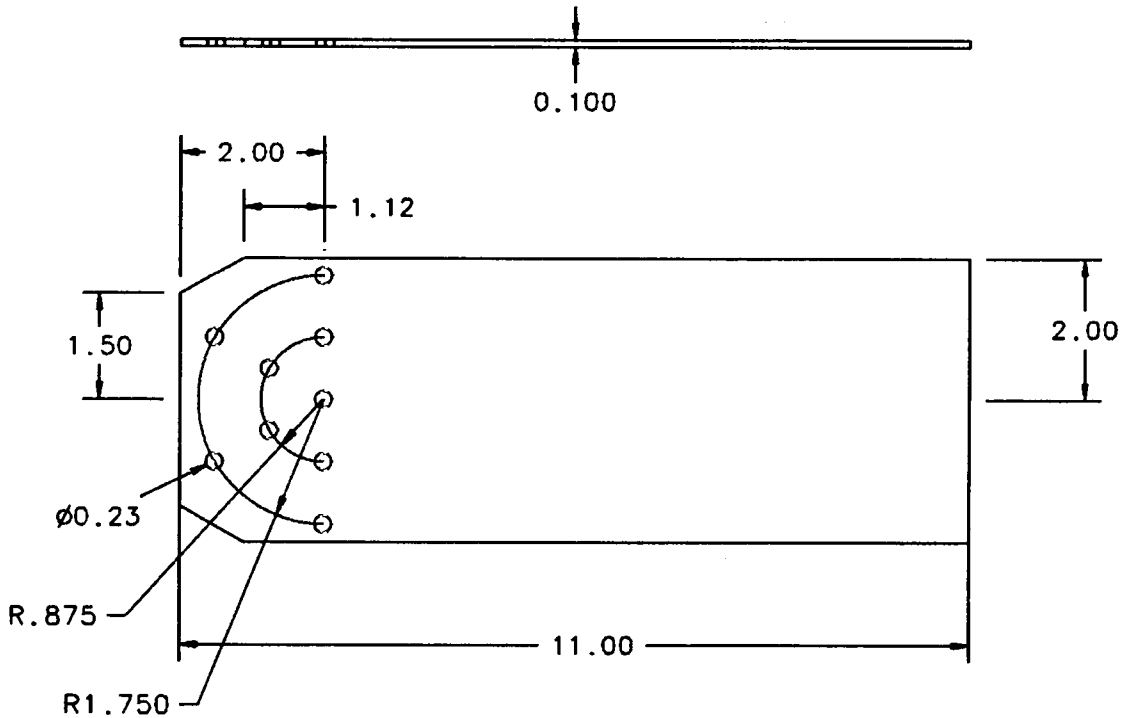


Figure 22, Test Article P8540100

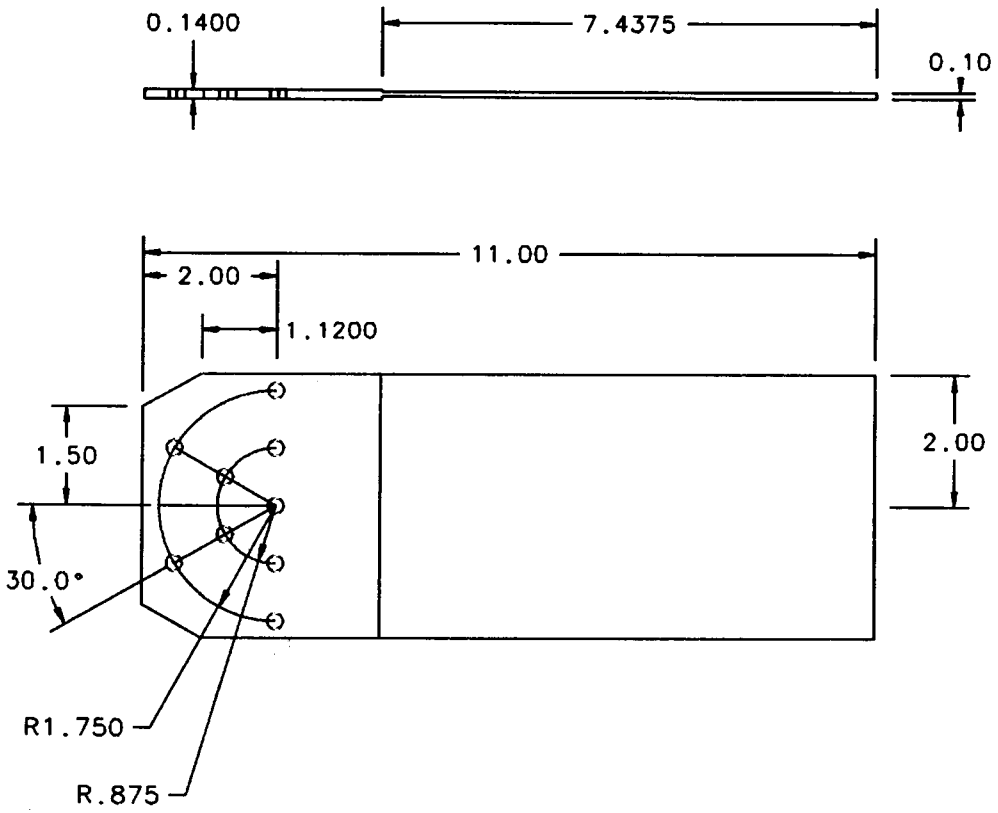


Figure 23, Test Article P8540100M

the designation for each plate. These dimensions were chosen in order to approximate a turbine engine compressor blade. The plate clamping fixture is illustrated in figure 24.

Test article P8540188 corresponds to the geometry that was used in the analytical validation described in the previous chapter. P8540188 and P8540100 are both used with unperturbed XMOD input finite element models that assume a higher stiffness near the boundary than is actually present in the test article (i.e. $E = 30 \times 10^6$ psi versus $E = 10.6 \times 10^6$ psi). Item P8540100M is thickened near the clamped end in order to approximate a stiffness corresponding to a Young's modulus equal to 30 million pounds per square inch and is used with an unperturbed XMOD input model of 10.6 million pounds per square inch.

Example 1, Test Article P8540188

Test article P8540188 was chosen as the first of the three test articles on which to demonstrate the semi-iterative technique because the measured frequencies corresponded the closest to the analytically determined values as shown in table 5. The input data to

Table 5, Comparison of Measured and Analytical Natural Frequencies, Example 1

Mode Number	Charaeteristic Shape	Theory (Gorman)	Finite Element	Measured Values
1	Bending	89.68 hz	90.09 hz	89.20 hz
2	Twisting	404.5 hz	386.6 hz	398.9 hz
3	Bending	558.8 hz	558.9 hz	547.7 hz
4	Twisting	1313. hz	1354. hz	1265. hz

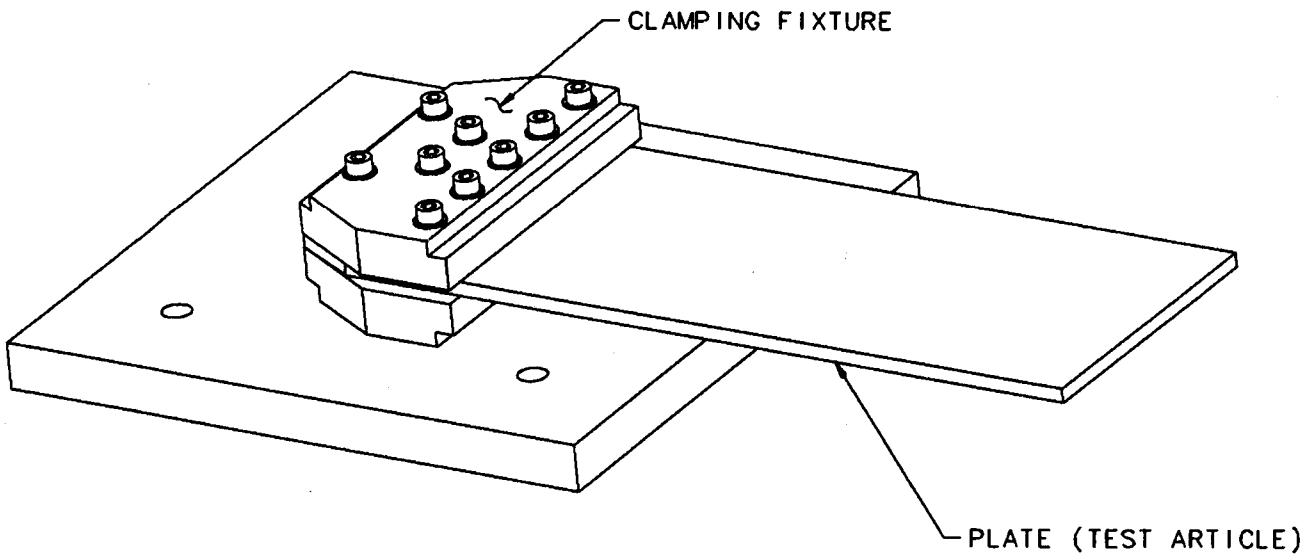


Figure 24, General Arrangement of Mounting Fixture and Test Article

the XMOD computer program consisted of the first four measured eigenvalues and the z-component of the first four eigenvectors at the points corresponding to nodes 122, 124, 152, 154, 212, and 214 (see figure 6). An eigenvector scaling factor of 0.4 was applied to the measured eigenvector. As can be seen in figure 25, the solution exhibited convergence characteristics consistent with the analytical validation model.

The values resulting from the fifth iteration were taken as the final results. The adjusted values for Young's modulus and Poisson's ratio were then used in the modified finite element model. A comparison of the measured natural frequencies with the natural frequencies calculated by the modified model is shown in table 6. Figures 26, 27, 28, and 29 show a comparison of the mode shapes for the initial unperturbed model (iteration 0) with the mode shapes calculated by the model modified with the values from the fifth iteration. As was the case in the analytical validation, the results are symmetric about an axis parallel to the x-axis down the center of the plate. Therefore, data is only presented along a line passing through nodes 122, 152, and 212. The measured data that was used as input is included in these plots as discrete data points.

Table 6, Measured versus Adjusted Frequencies, Example 1

Mode No.	Characteristic Shape	Measured Natural Frequency	Natural Frequency for Adjusted Model	Difference (per cent)
1	Bending	89.20 hz	87.46 hz	1.95%
2	Twisting	398.9 hz	383.6 hz	3.86%
3	Bending	547.7 hz	549.3 hz	-0.29%
4	Twisting	1265. hz	1255. Hz	0.80%

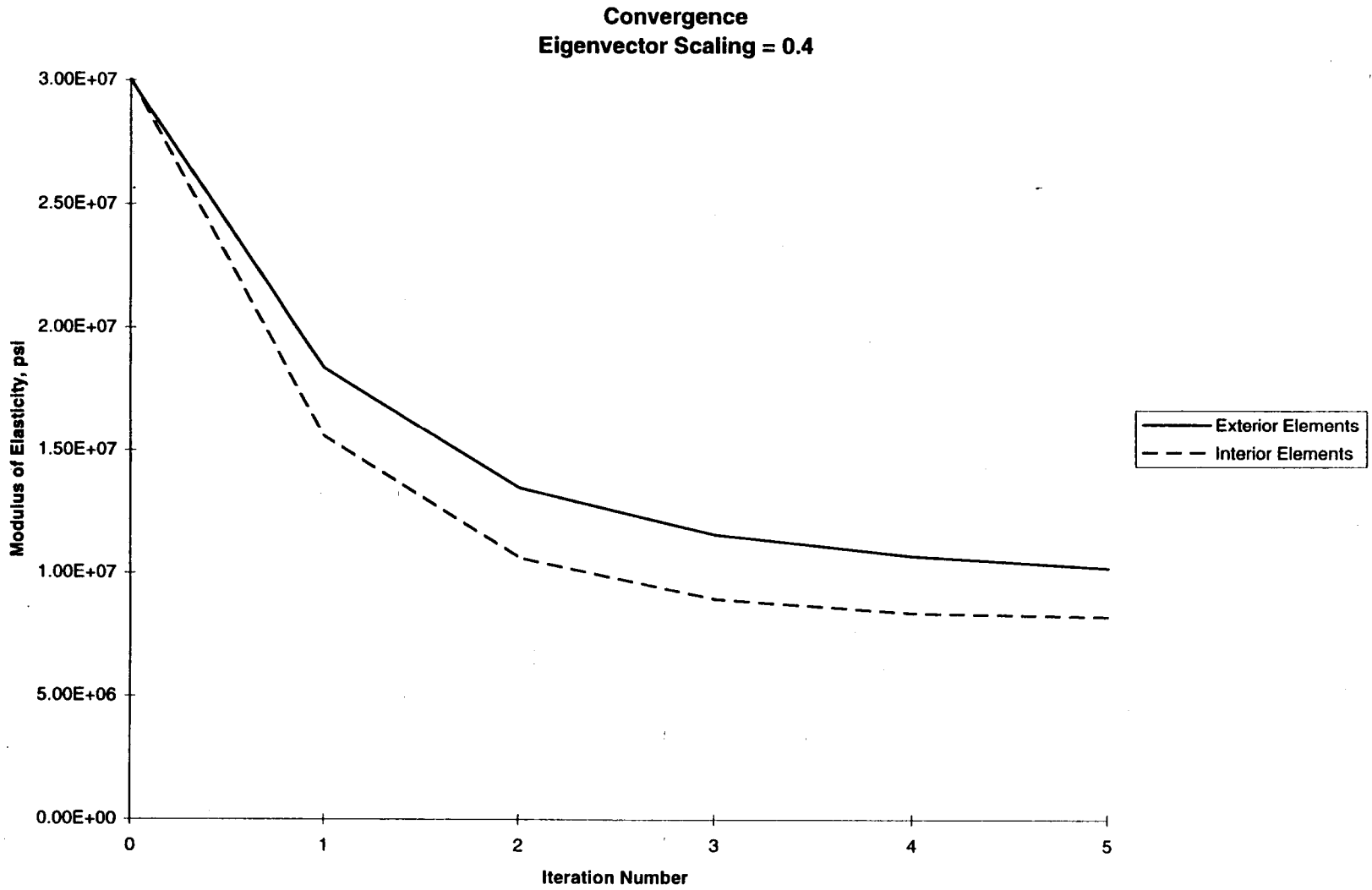


Figure 25, Convergence for Example 1, Eigenvector Scaling = 0.4

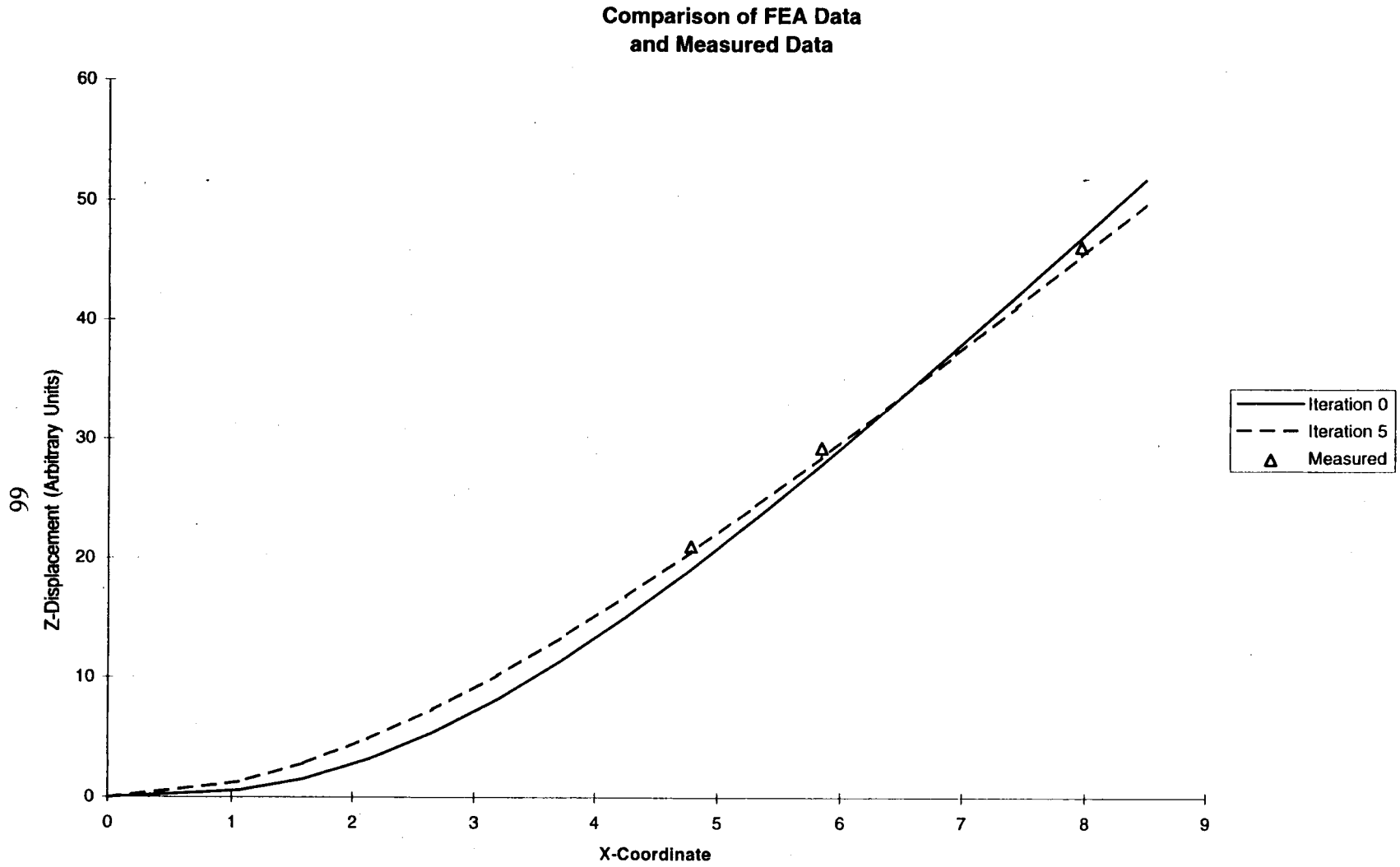


Figure 26, Comparison of Eigenvectors for Mode 1, Example 1

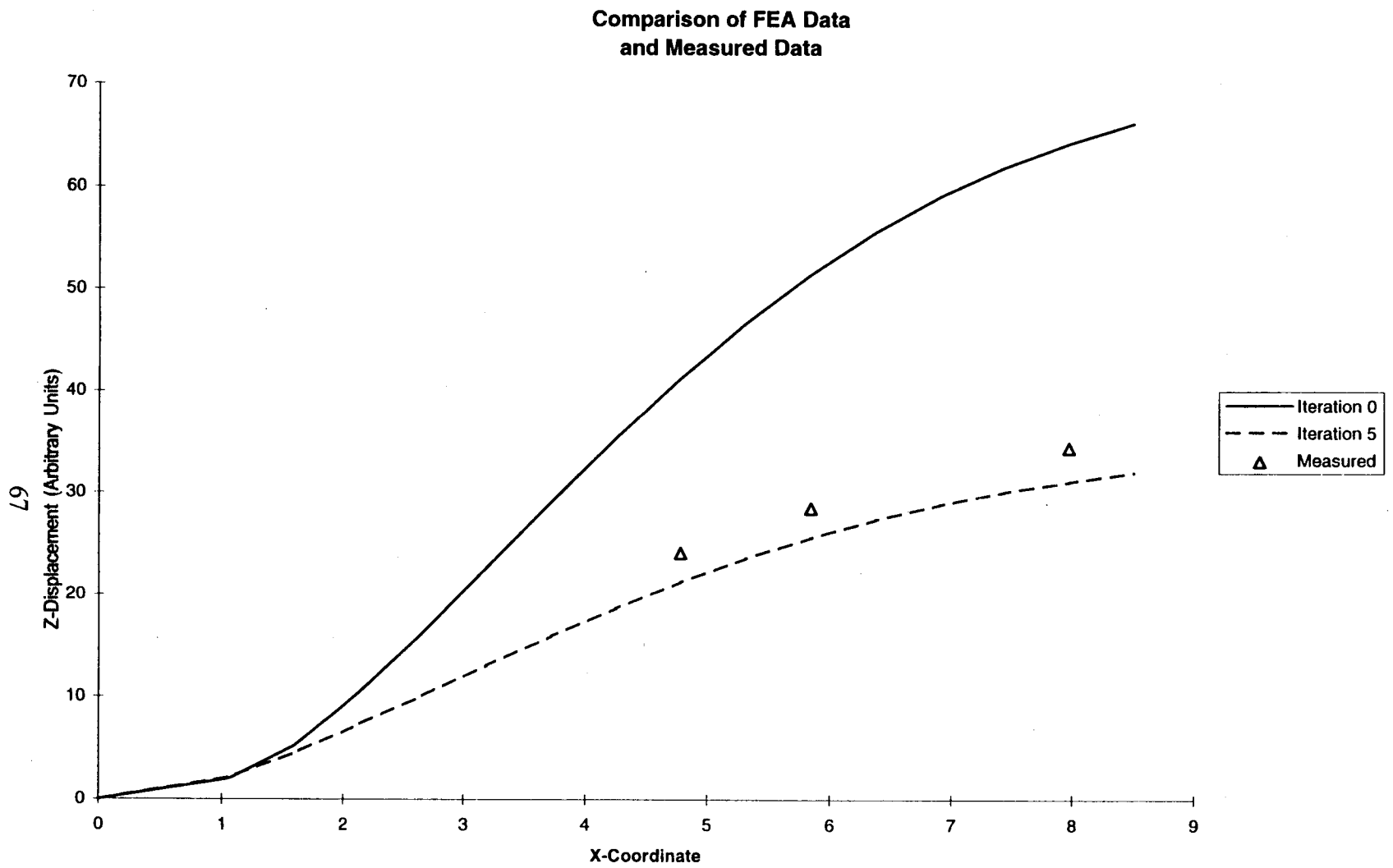


Figure 27, Comparison of Eigenvectors for Mode 2, Example 1

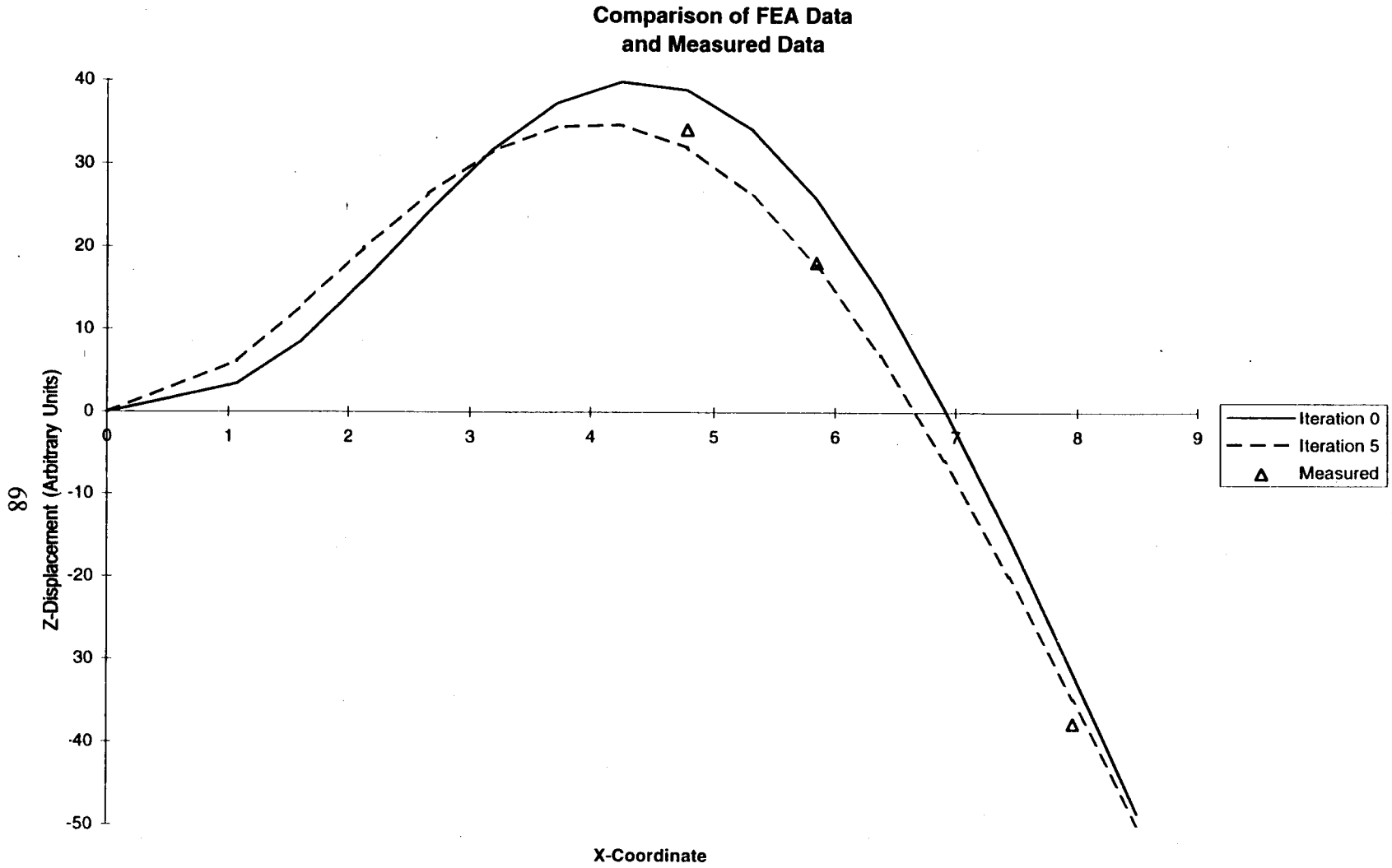


Figure 28, Comparison of Eigenvectors for Mode 3, Example 1

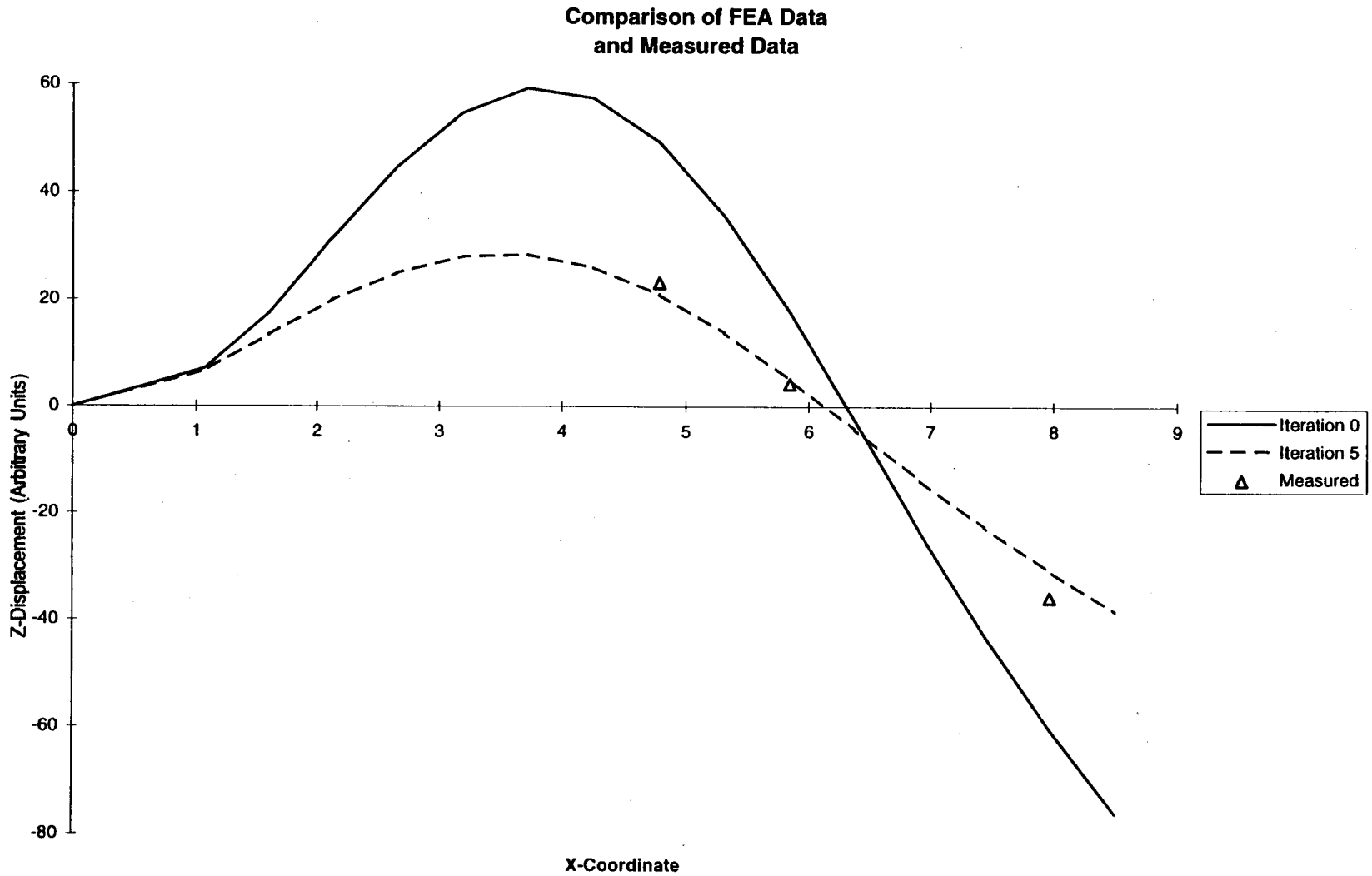


Figure 29, Comparison of Eigenvectors for Mode 4, Example 1

As can be seen from the data that is presented, the modifications selected by the XMOD program result in very good agreement with both the measured natural frequencies and the mass normalized mode shapes.

Example 2, Test Article P8540100

Test article P8540100 was chosen as the next test article for demonstrating the method. P8540100 is similar to P8540188 in that it is a homogeneous plate of uniform thickness, but the measured natural frequencies do not agree as well with the expected theoretical values (see table 7). The input data to the XMOD computer program also consisted of the first four measured eigenvalues, but the data points used for eigenvectors corresponded to nodes 92, 94, 122, 124, 212, and 214, as shown in figure 30. These nodes were selected because it was found that the magnitude of the eigenvector at nodes 152 and 154, previously used for P8540188, were close to node lines (i.e. lines where the mode shape amplitude is zero) for the third and forth mode shapes. It was found that,

Table 7, Comparison of Measured and Analytical Natural Frequencies, Example 2

Mode Number	Characteristic Shape	Theory (Gorman)	Finite Element	Measured Values
1	Bending	47.70 hz	48.20 hz	43.28 hz
2	Twisting	215.2 hz	218.0 hz	194.6 hz
3	Bending	297.2 hz	298.8 hz	271.3 hz
4	Twisting	698.5 hz	729.2 hz	630.9 hz

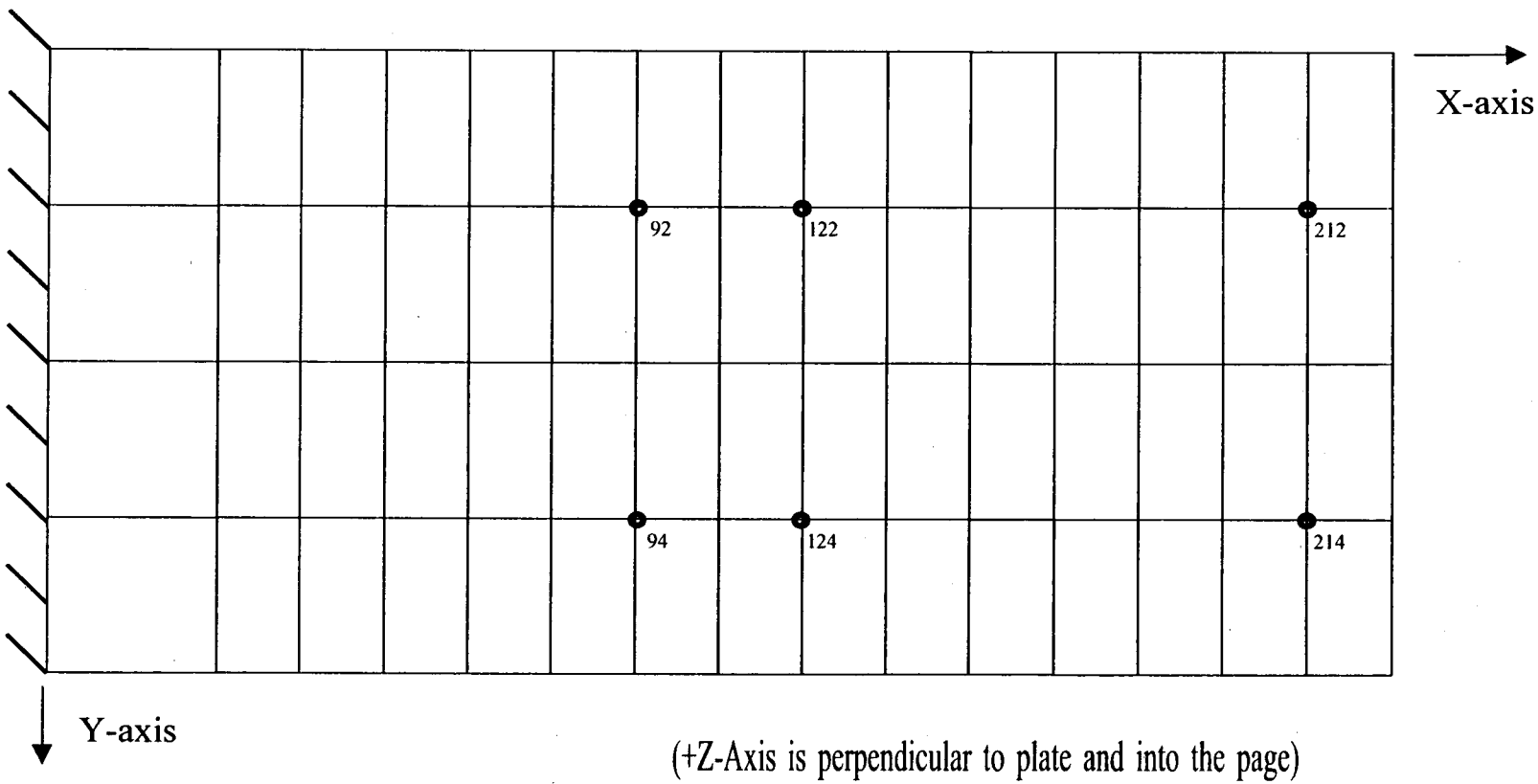


Figure 30, Nodes Corresponding to Measurement Data Points with P8540100

by using data points with values of the same order of magnitude, the stability of the solution was greatly enhanced. An eigenvector scaling factor of 0.5 was applied to the measured eigenvector. As can be seen in figure 31, this solution also exhibited convergence characteristics consistent with the previous examples.

The values resulting from the seventh iteration were taken as the final results and the adjusted values for Young's modulus and Poisson's ratio were applied to the modified finite element model. A comparison of the measured natural frequencies with the natural frequencies calculated by the adjusted model is shown in table 8 and figures 32, 33, 34, and 35 show the comparison of the mode shapes between the initial unperturbed model (iteration 0) and the mode shapes calculated by the model modified with the values from the seventh iteration presented in the same format as the previous examples. The measured data used as input is included in these plots as discrete data points.

As can be seen from the data that is presented, the modifications selected by the XMOD program result in slightly poorer agreement with both the measured natural frequencies and the mass normalized mode shapes than the previous example. The

Table 8, Measured versus Adjusted Frequencies, Example 2

Mode No.	Characteristic Shape	Measured Natural Frequency	Natural Frequency for Adjusted Model	Difference (per cent)
1	Bending	43.28 hz	45.46 hz	5.04%
2	Twisting	194.6 hz	213.9 hz	9.92%
3	Bending	271.3 hz	288.9 hz	6.49%
4	Twisting	630.9 hz	715.5 hz	13.4%

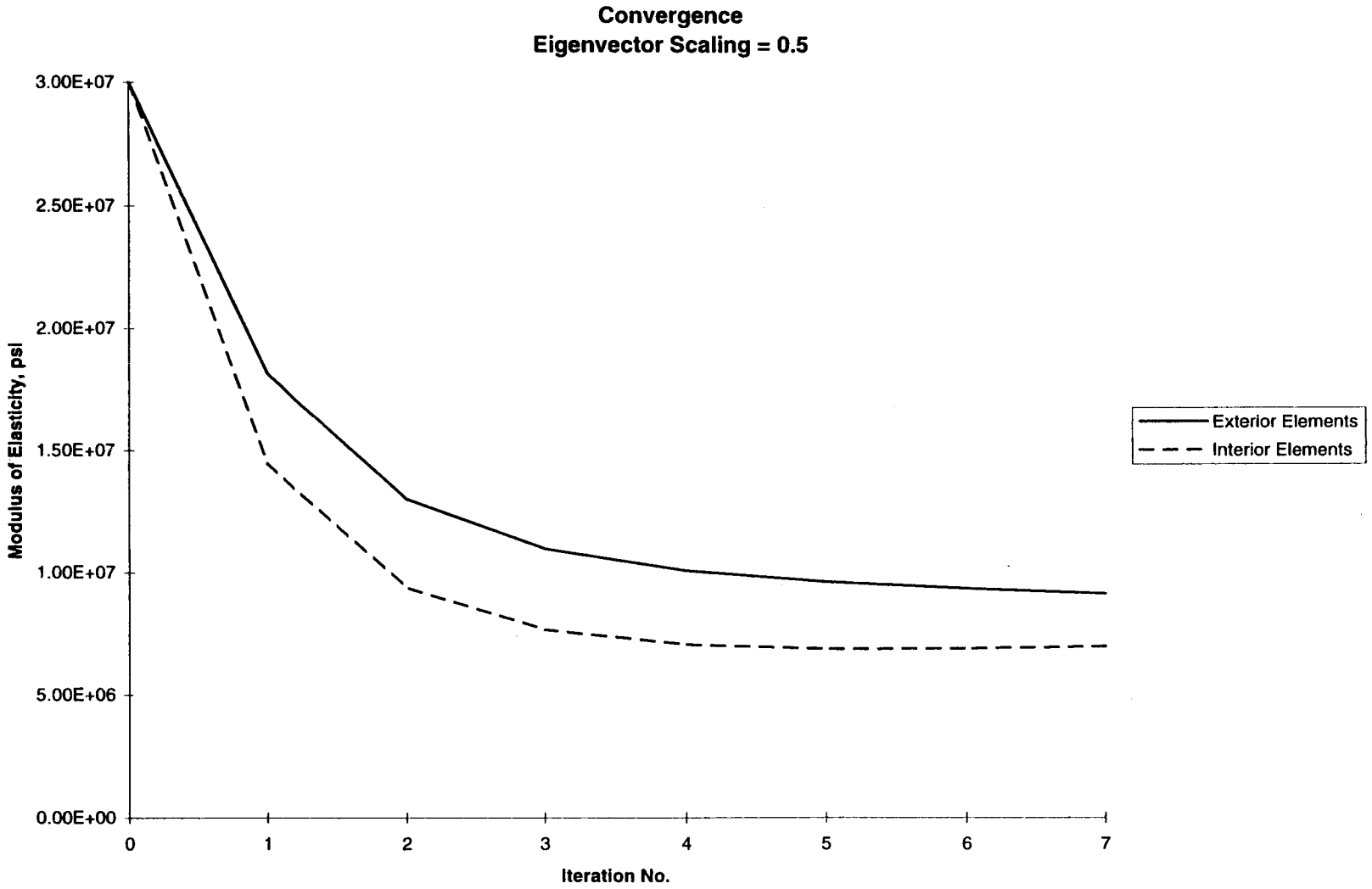


Figure 31, Convergence for Example 2, Eigenvector Scaling = 0.5

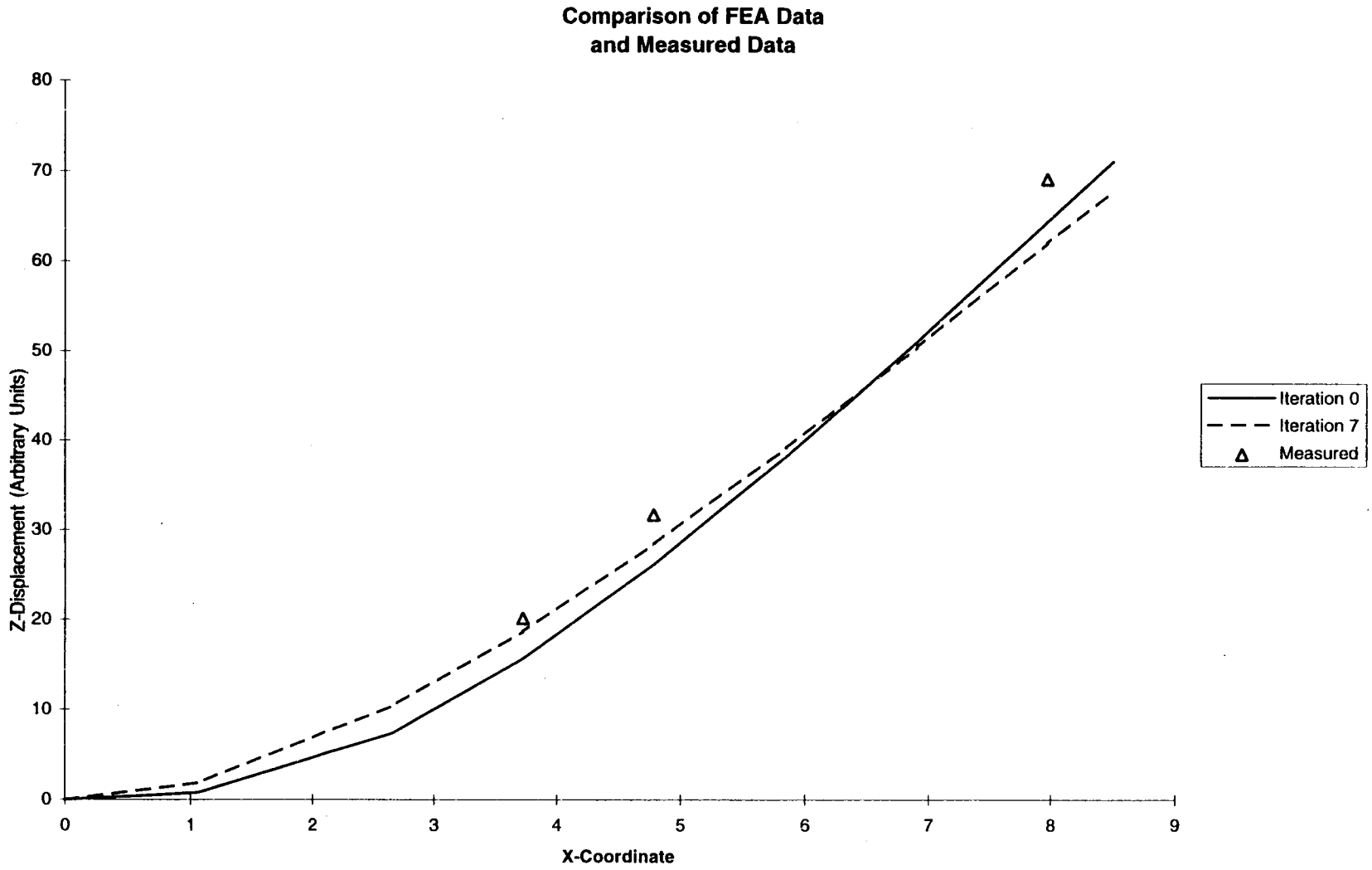


Figure 32, Comparison of Eigenvectors for Mode 1, Example 2

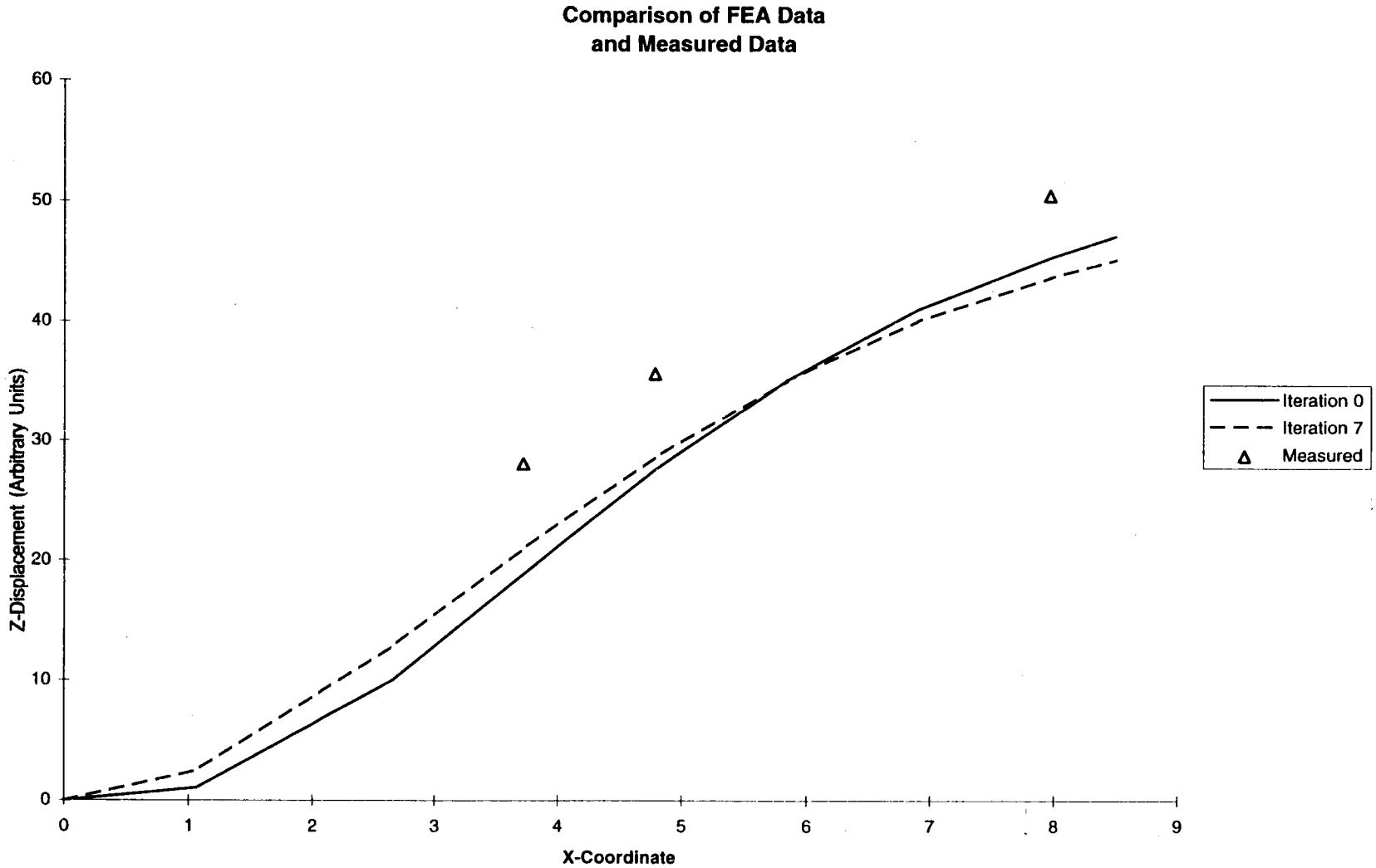


Figure 33, Comparison of Eigenvectors for Mode 2, Example 2

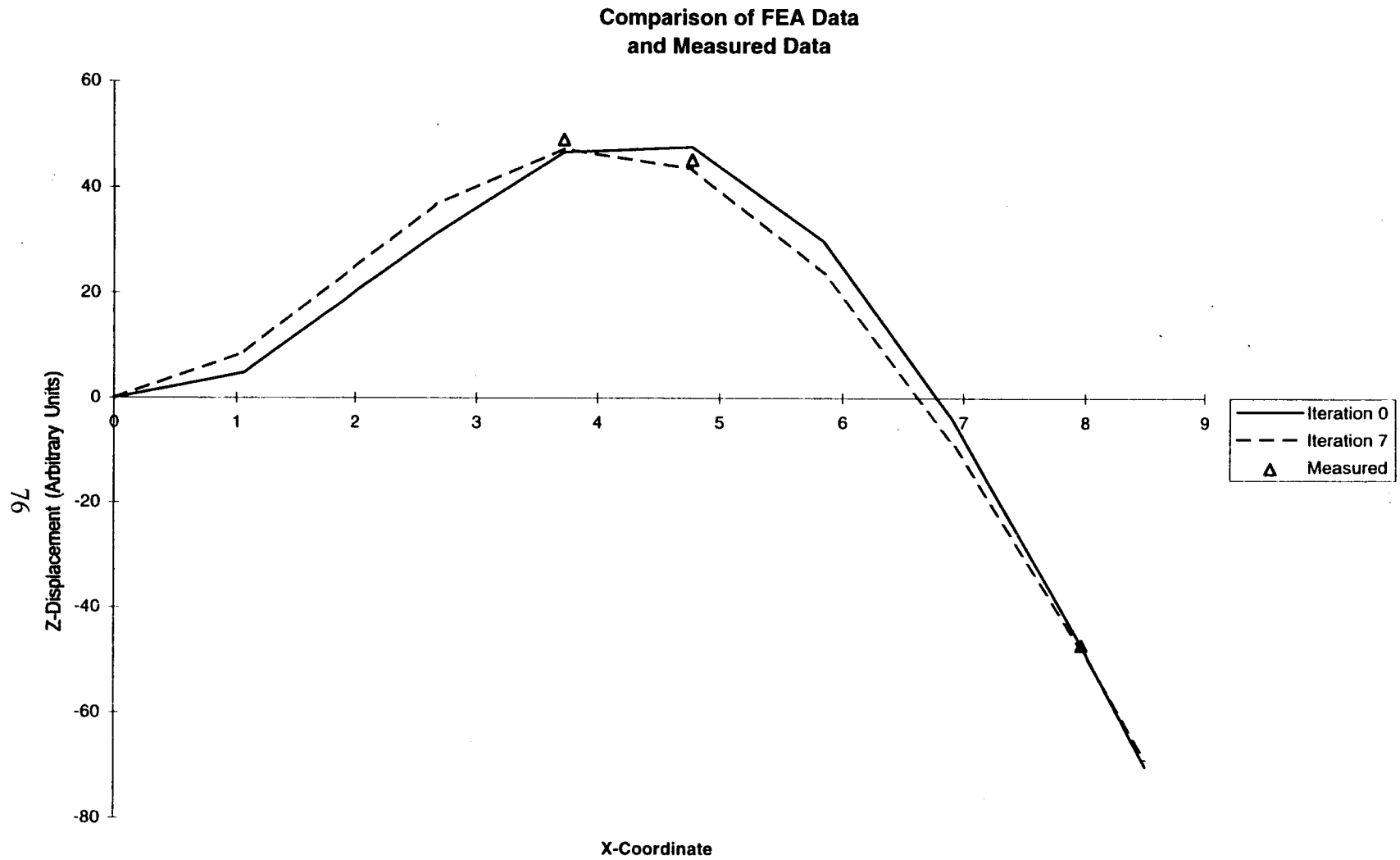


Figure 34, Comparison of Eigenvectors for Mode 3, Example 2

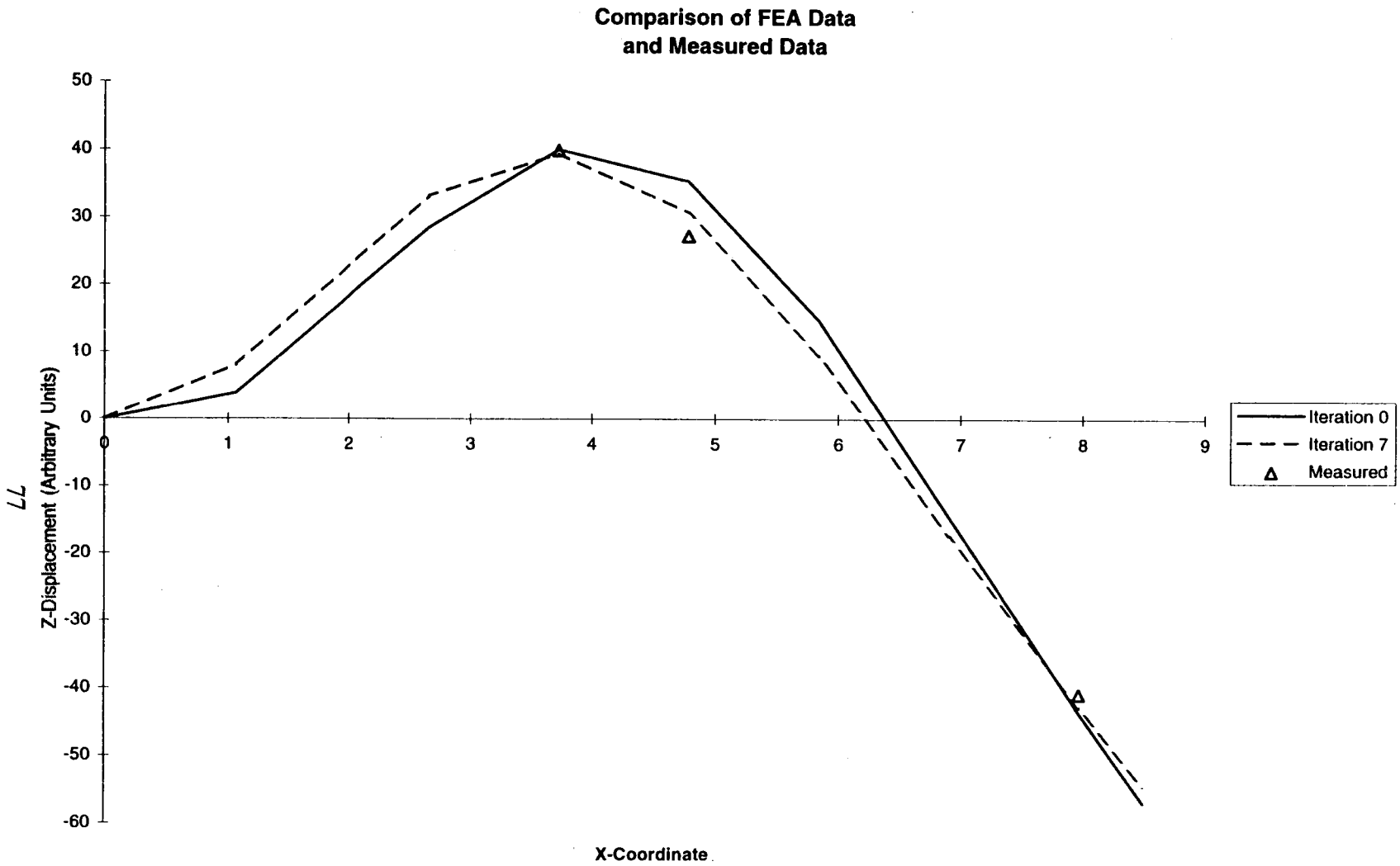


Figure 35, Comparison of Eigenvectors for Mode 4, Example 2

largest discrepancy in the eigenvector occurs for the second mode (first twisting mode).

From figure 33, it appears that the measured data is scaled by a factor that is inconsistent with the mass scaling of the vectors calculated by the finite element method. Figure 36 shows the second mode with the measured data scaled so as to shift the points into the range of the finite element data. From this it can be seen that the measured data has a shape that is consistent with the eigenvector resulting from the adjusted finite element model.

Example 3, Test Article P8540100M

The third test article that was used was P8540100M. This test article differs from the other two in that the measured data comes from a physical model with boundary conditions that are stiffer than the input model for the XMOD program. The increased thickness near the clamped boundary was chosen to simulate a Young's modulus of 30 million psi based on the first two bending modes. This approach does not necessarily insure a corresponding change in the twisting mode frequencies. The input data to the XMOD computer program also consisted of the first four measured eigenvalues and the data points used for eigenvectors corresponded to nodes 92, 94, 122, 124, 212, and 214, as with P8540100. An eigenvector scaling factor of 1.0 was applied to the measured eigenvector. As can be seen in figure 37, this solution exhibits convergence characteristics slightly different from the previous examples.

The values resulting from the eighth iteration were taken as the final results and the adjusted values for Young's modulus and Poisson's ratio were applied to the

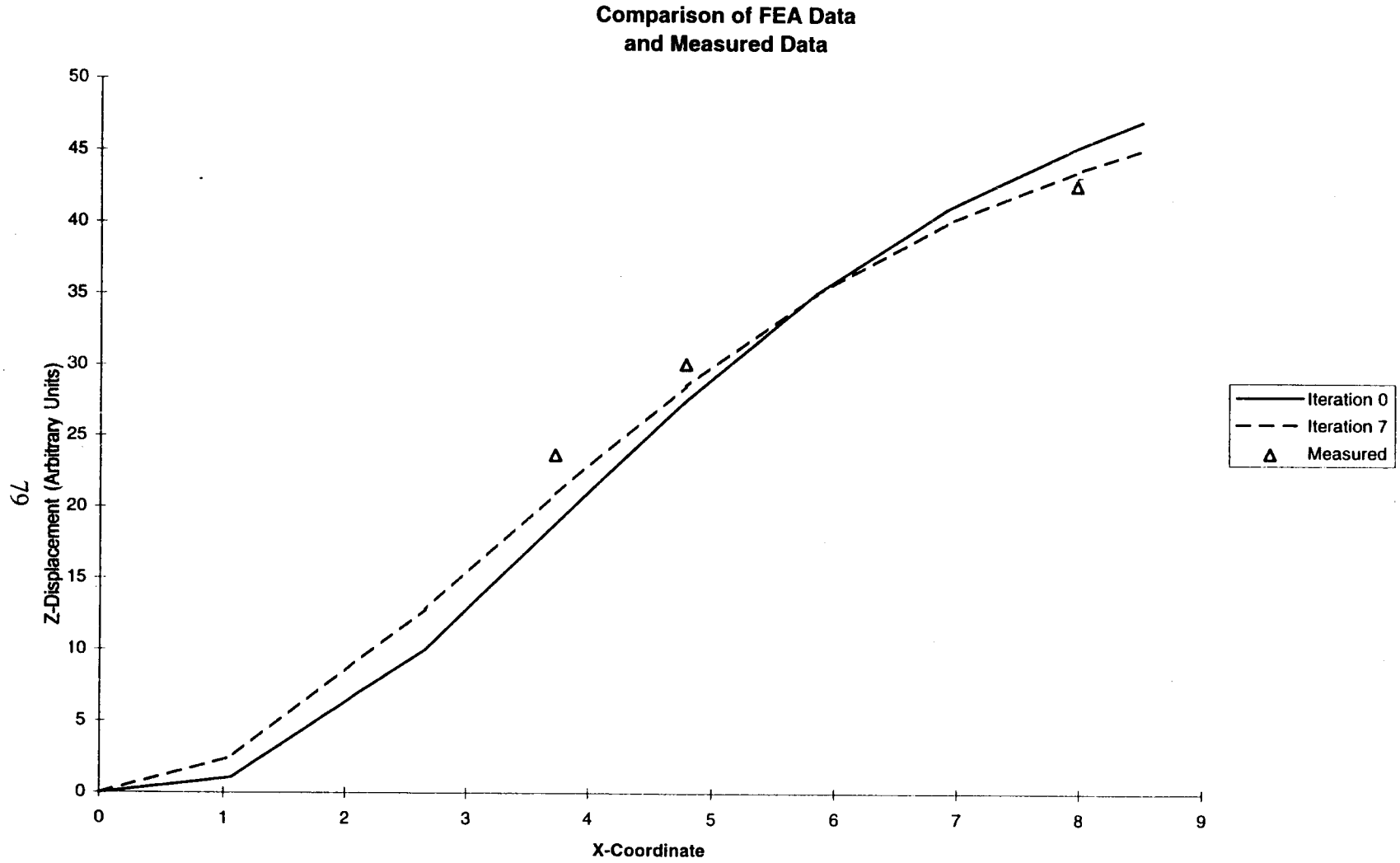


Figure 36, Comparison of Eigenvectors for Mode 2 with Scaled Data, Example 2

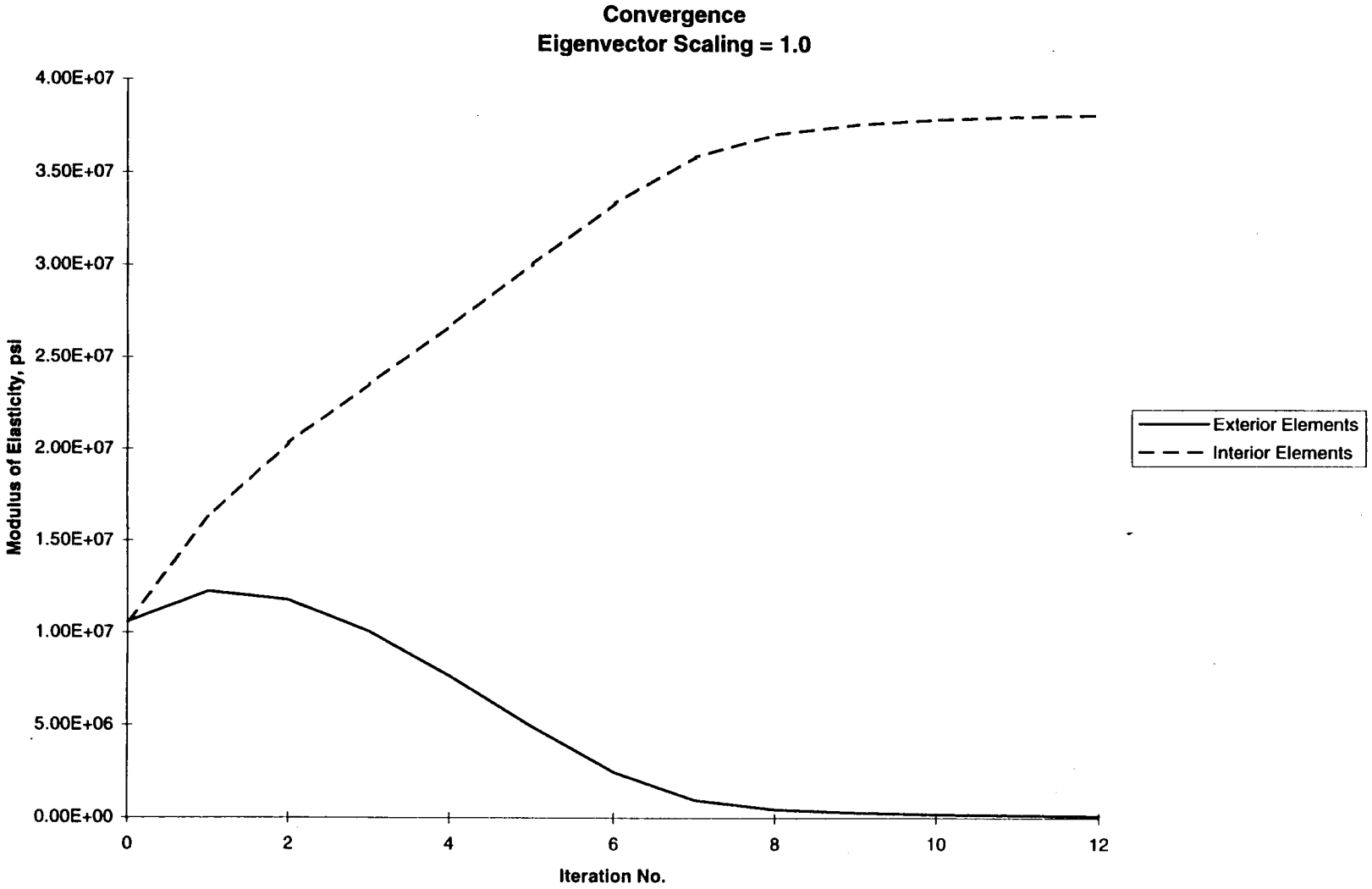


Figure 37, Convergence for Example 3, Eigenvector Scaling = 1.0

modified finite element model. Table 9 presents a comparison of the measured natural frequencies with the natural frequencies calculated by the adjusted model. From this comparison, it can be seen that the method converges to a solution that is within the accuracy limits of the measured data.

Figures 38, 39, 40, and 41 show the comparison of the mode shapes between the initial unperturbed model (iteration 0) and the mode shapes calculated by the model modified with the values from the eighth iteration presented in the same format as the previous examples. The measured data that was used as input to XMOD is included in these plots as discrete data points.

The modifications selected by the XMOD program produce somewhat ambiguous results. As can be seen in table 9, the natural frequencies resulting from the adjusted model compare favorably with the measured natural frequencies, but the differences in the mode shapes between unadjusted XMOD model and the eighth iteration are too small to demonstrate definitive improvements. As with P8540100, the largest discrepancy in the eigenvector occurs for the second mode (first twisting mode),

Table 9, Measured versus Adjusted Frequencies, Example 3

Mode No.	Characteristic Shape	Measured Natural Frequency	Natural Frequency for Adjusted Model	Difference (per cent)
1	Bending	54.95 hz	52.93 hz	-3.69%
2	Twisting	227.6 hz	218.4 hz	-4.04%
3	Bending	329.7 hz	317.0 hz	-3.87%
4	Twisting	732.1 hz	727.7 hz	-0.60%

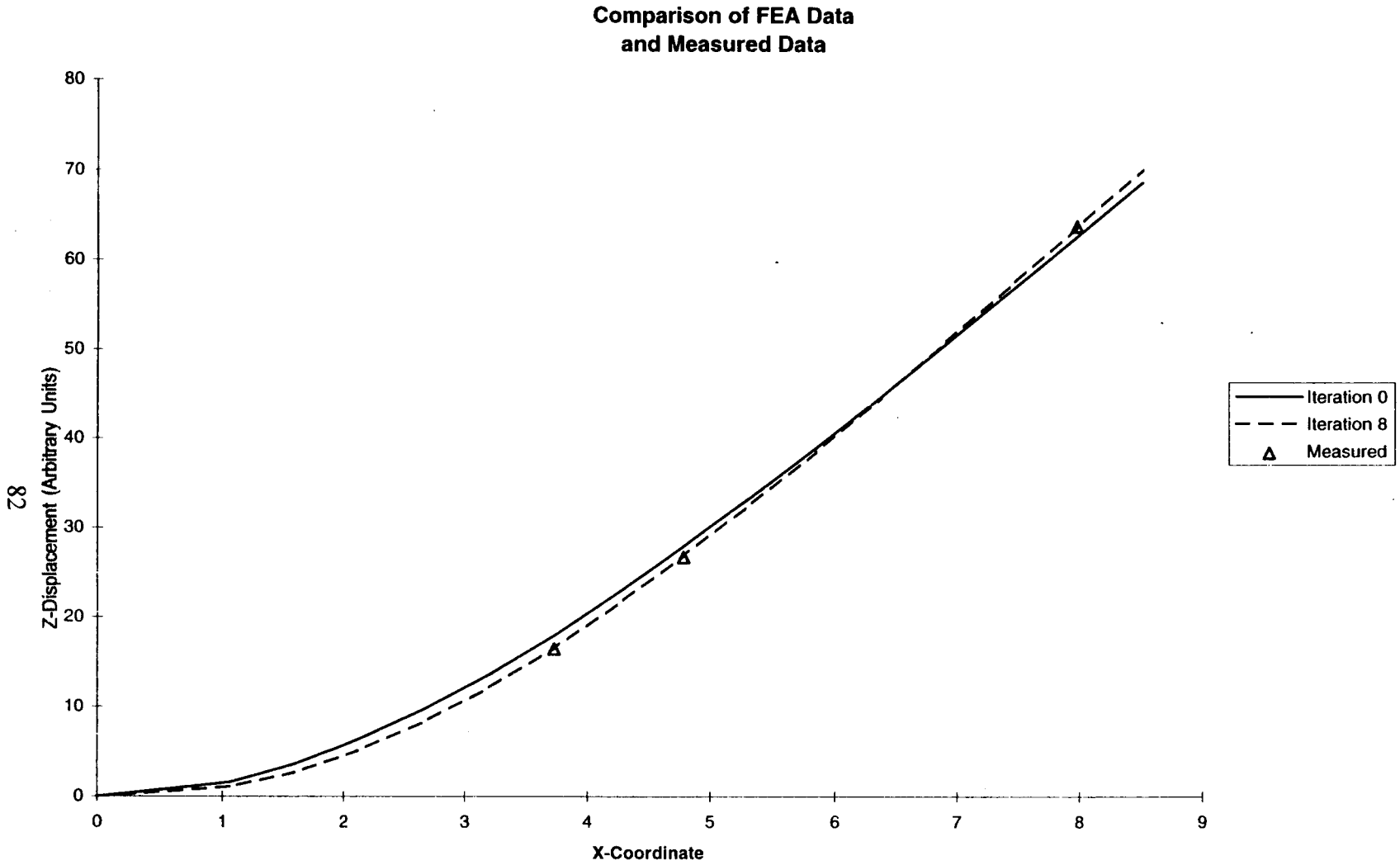


Figure 38, Comparison of Eigenvectors for Mode 1, Example 3

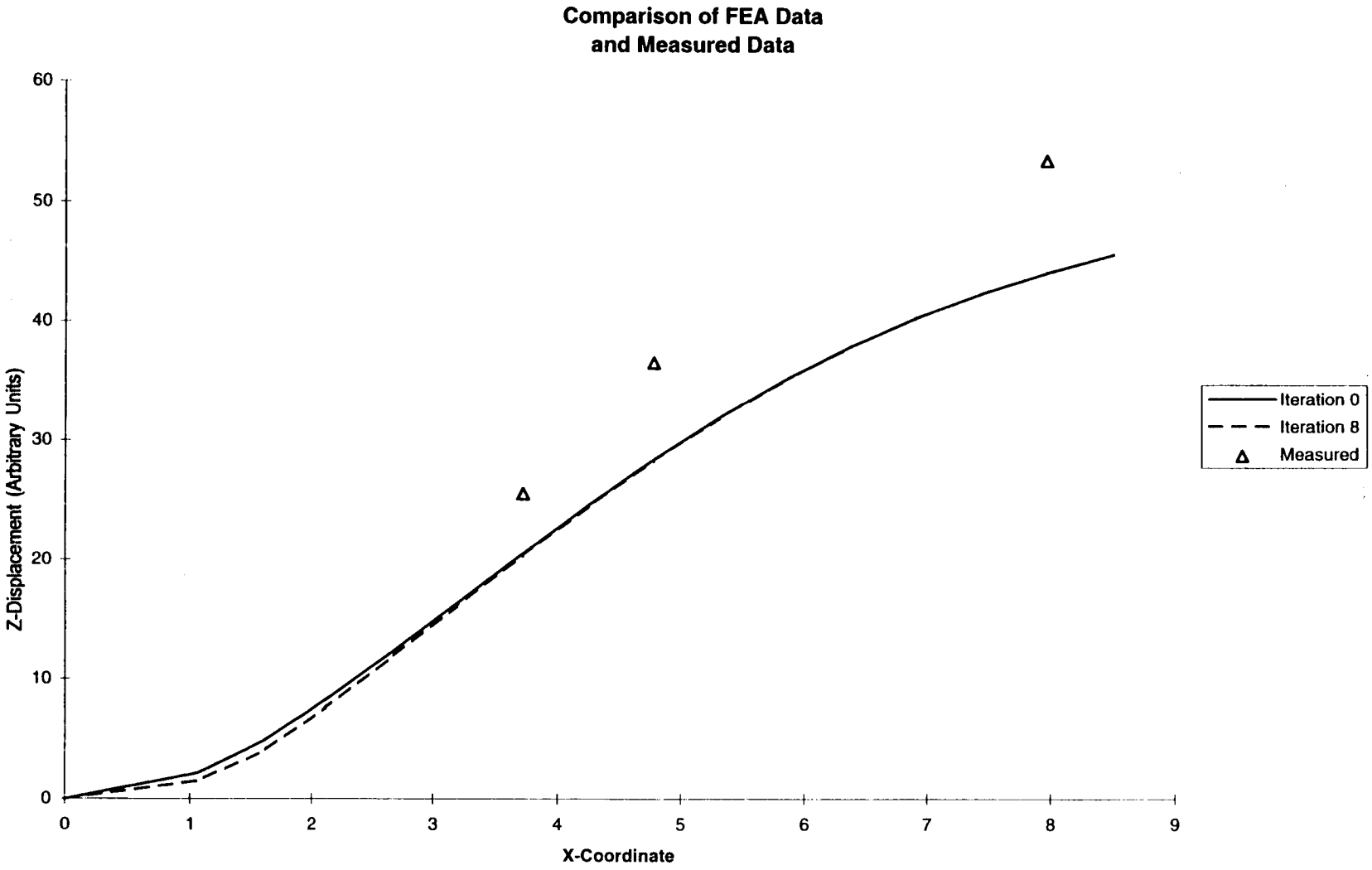


Figure 39, Comparison of Eigenvectors for Mode 2, Example 3

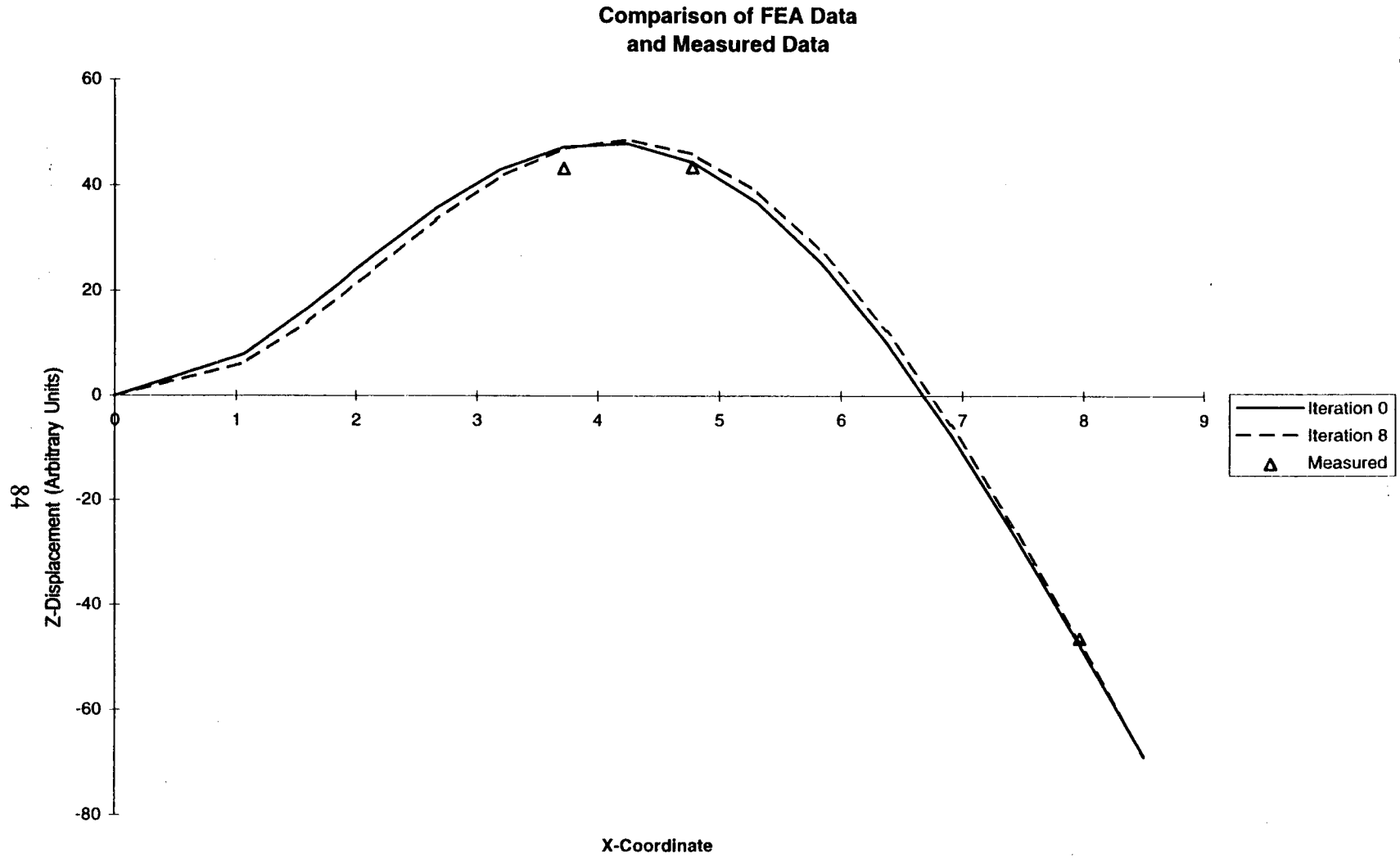


Figure 40, Comparison of Eigenvectors for Mode 3, Example 3

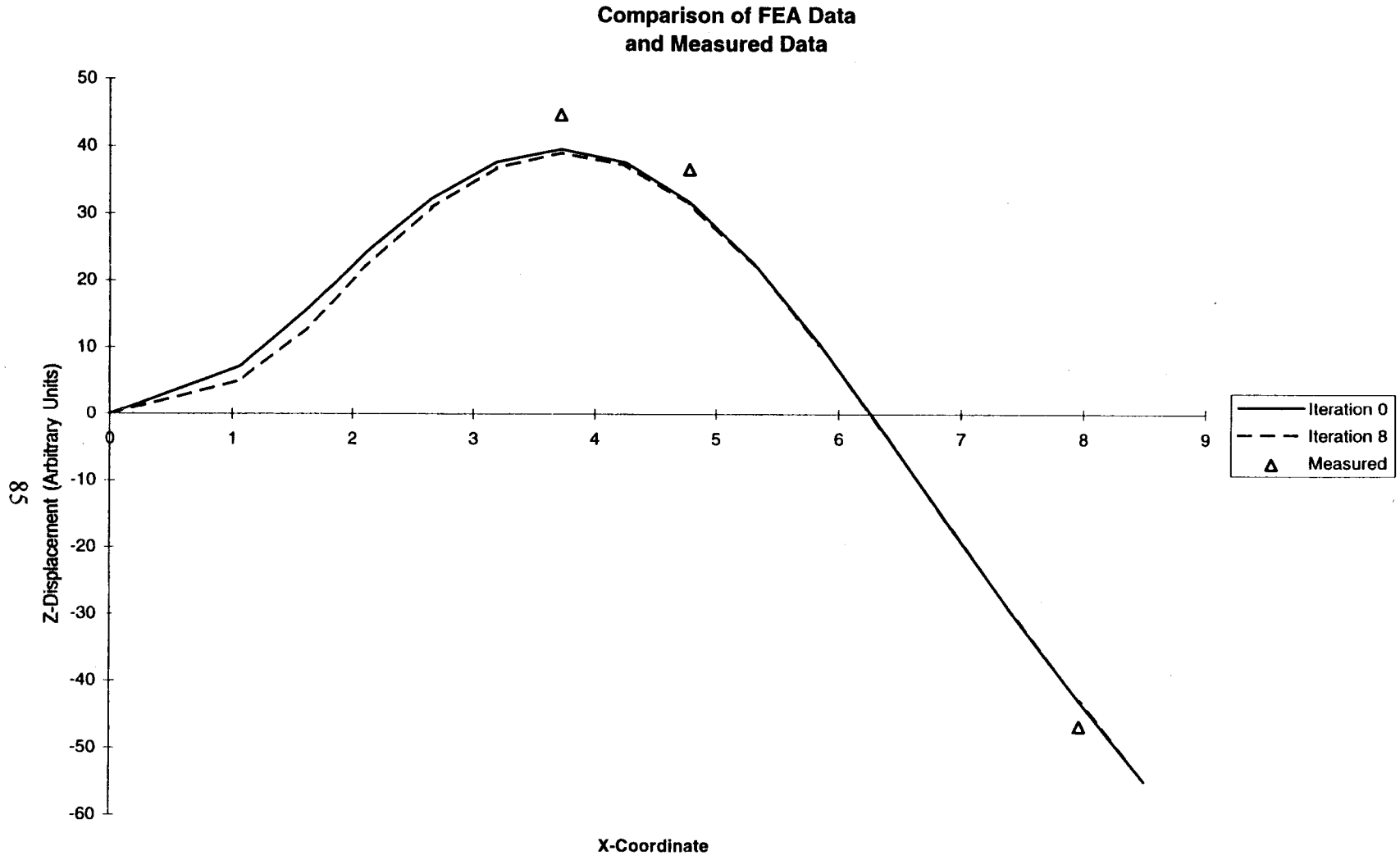


Figure 41, Comparison of Eigenvectors for Mode 4, Example 3

indicating the likelihood that the measured data is scaled by a factor that is inconsistent with the mass scaling of the vectors calculated by the finite element method. By shifting the measured data points into the range of the finite element data, as in figure 42, it can be seen that while the measured data has a shape that is consistent with the eigenvector resulting from the adjusted finite element model it is not measurably different from the unadjusted XMOD model. This ambiguity in results for P8540100M is more than likely due to the similarity between the measured natural frequencies and the natural frequencies of the unadjusted XMOD model. As can be seen in table 10, with the exception of the first natural frequency, the frequencies of the unadjusted XMOD model are within 10% of each other.

Table 10, Measured versus Unadjusted Frequencies, Example 3

Mode No.	Characteristic Shape	Measured Natural Frequency	Natural Frequency for Unadjusted Model	Difference (per cent)
1	Bending	54.95 hz	48.20 hz	-12.28%
2	Twisting	227.6 hz	218.0 hz	-4.20%
3	Bending	329.7 hz	298.8 hz	-9.37%
4	Twisting	732.1 hz	729.2 hz	-0.40%

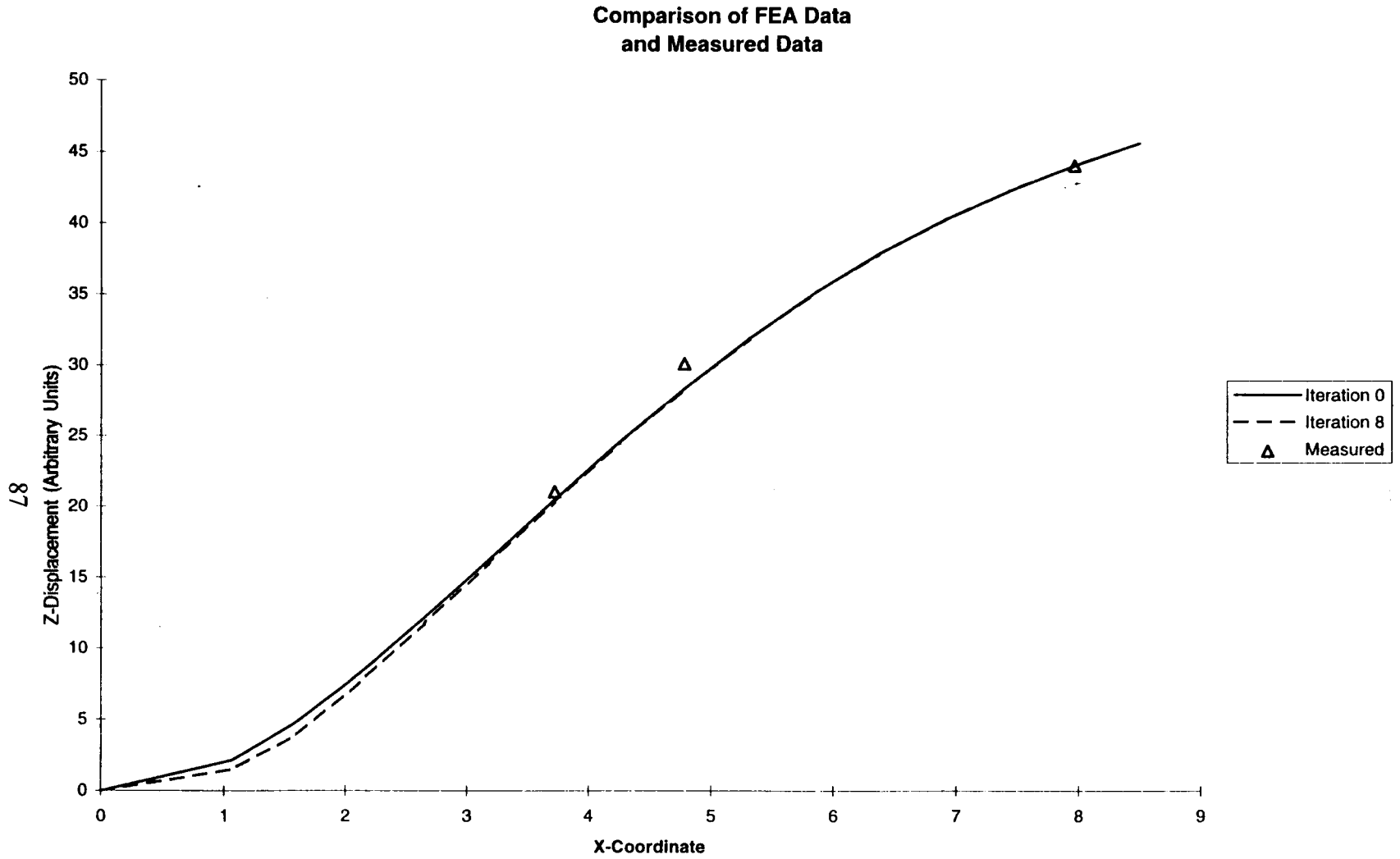


Figure 42, Comparison of Eigenvectors for Mode 2 with Scaled Data, Example 3

6. CONCLUSIONS

The semi-iterative technique is shown to be effective in predicting needed adjustments to finite element models in regions near physical boundaries. This was demonstrated with a high degree of accuracy for the examples using test article P8540188 and to a somewhat lesser extent with the other two test articles.

Discussion of Results

It became apparent during the reduction of the test data that P8540188 showed a closer agreement with the mass normalized mode shapes that result from the corresponding finite element solution. Furthermore, the finite element solution for P8540188 exhibited very little difference between the solution resulting from a lumped mass matrix formulation as compared with the consistent mass matrix formulation. This was not the case with P8540100 and P8540100M. Both of the finite element models for the latter two test articles exhibited marked differences between the lumped and consistent mass formulations. In both cases, the consistent mass matrix solutions came closer to matching the measured mass normalized mode shapes. While this does not affect the overall performance of XMOD, it does explain the differences exhibited in scaling for the twisting modes.

The third example (test article P8540100M) demonstrated an important characteristic of the method regarding the role of the eigenvector scale factors. This

example used an initial unperturbed XMOD model that had lower eigenvalues than the physical model from which measurements were taken. This condition produces a set of Δp_1^k 's and Δp_2^k 's that are initially positive, which results in values for Poisson's ratio that are also positive. Because Poisson's ratio remains positive, there is a diminished need to slow the solution by scaling the eigenvectors. This is reflected in the fact that the XMOD solution for example 3 converges to a satisfactory solution using an eigenvector scale factor equal to one. In fact, scale factors greater than one tended to accelerate convergence with little or no degradation in the quality of the solution.

When examining the three examples together, it also becomes apparent that the heaviest test article, P8540188, resulted in the best overall results. This may, in fact, be due to possible inconsistencies in the measured data resulting from changes to the system mass due to the added weight of the accelerometer. This influence would be more apparent for the lighter weight cases where the accelerometer represents a larger percentage of the overall system mass.

Areas of Further Study

As with any new method, there are still aspects of the semi-iterative technique that would benefit from further study. First of all, the examples that have been presented here have all been simple uniform homogeneous structures. The method should now be applied to more complex structures such as turbine blades to further investigate the practical nuances of the method.

Secondly, the influence of the specific element formulation used in the initially

unadjusted model needs to be investigated. For example, a means of uncoupling the stiffness relationship between Young's modulus and Poisson's ratio could lead to a stable solution without the need for eigenvector scaling. Also, the use of a consistent mass matrix formulation could improve the methods agreement with the data collected by physical measurement.

Third, an analytical study of the role of scaling the eigenvectors is indicated. Such a study could lead to a better way of selecting the scale factors to be used.

LIST OF REFERENCES

[1] Cooley, James W. and Tukey, John W., "An Algorithm for the Machine Calculation of Complex Fourier Series," Mathematics of Computation, Vol. XIX, 1965, pp. 297-301.

[2] Engels, Remi C., Final Report, Support for the Finite Element Model Improvement Technique Program, Work Order No. A96W-18, The University of Tennessee Space Institute, Tullahoma, TN, September 1996.

[3] Collins, J. D., Young, J. P., and Kifling, L.A., "Methods and Applidcations of System Identificaton in Shock and Vibrations," System Identification of Vibrating Structures - Mathematical Models from Test Data, ed. Pilkey, W. and Cohen, R., 1972, Annual meeting of the ASME, 1972.

[4] Hart, G. C. and Yao, J. T. P., "System Identification in Structural Dynamics," Dynamic Response of Structures: Instrumentation, Testing Methods, and System Identification, ASCE/EMD Technical Conference, UCLA, March 30, 1976.

[5] Ibáñez, Paul, "Review of Analytical and Experimental Techniques for Improving Structural Dynamic Models," Welding Research Council Bulletin, No. 249, June 1979, Welding ResearchCouncil, New York, NY.

[6] Guyan, Robert J., "Reduction of Stiffness and Mass Matrices," AIAA Journal, Vol 3, No. 2, February 1965, p. 380.

[7] Paz, Mario, "Dynamic Condensation," AIAA Journal, Vol. 22, No. 5, 1984, pp. 724-727.

[8] Kidder, R. L. "Reduction of Structural Frequency Equations," AIAA Journal, Vol. 11, No. 6, June 1973, p. 892.

[9] Lieven, N.A. J. and Ewins, D. J., "Correlation of Modeshapes, the Coordinate Modal Assurance Criterion (COMAC)", Proceedings of the Sixth International Modal Analysis Conference, 1988, p. 690.

[10] Lipkens, J. and Vandeurzen, U., "The Use of Smoothing Techniques for Structural Modificaiton Aplications," 12th International Seminar on Modal Analysis, Leuven, Belgium, 1987.

[11] To, W. M., Lin, R. M., and Ewins, D. J., "A Criterian for Localization of Structural Modification Sites Using Modal Data," Proceedings of the Eighth International Modal Analysis Conference, February 1990, pp. 961-967.

[12] Farhat, C. and Hemez, F. M.,"Updating Finite Element Dynamic Models Using an Element-By-Element Sensitivity Methodology," AIAA Journal, Vol. 31, No. 9, September 1993, pp.1702-1711.

[13] Fox, R. L. and Kapoor, M. P. "Rates of Change of Eigenvalues and Eigenvectors," AIAA Journal, Vol. 6, No. 12, December 1968, pp. 2426-2429.

[14] Nash, M., "An Approach to the Reconciliation of Finite Element and Modal Test Studies," Proceedings of the Eighth International Modal Analysis Conference, February 1990, Orlando, Florida, pp. 187-194.

[15] Ibrahim, S. R., "Analytical Dynamic Model Updating: The Challenge for the Nineties," Transactions of Mechanical Engineering, Vol. ME 16, No. 1, July 1991, The Institution of Engineers, Australia.

[16] Gorman, D. J., Free Vibration Analysis of Rectangular Plates, New York, Amsterdam, and Oxford: Elsevier, 1982.

APPENDICES

APPENDIX 1

TEST PLAN

TEST PLAN

This test plan outlines the procedure for performing modal testing of three simple test articles by the accelerometer based roving hammer impact method.

Objective:

To provide accurate experimental values for natural frequencies and frequency response functions (FRF's) to be used in the verification of the improved model modification method. The resulting FRF's will undergo further data reduction to eventually result in eigenvalues and mass normalized mode shapes.

Test Article:

The test articles consist of three different 4 inch wide plates each with a cantilevered length of 8.5 inches when installed in the mounting fixture (total end-to-end length of the plates is 11 inches). The three plates have different thicknesses and are described in figures 21, 22, and 23. Each plate is marked with a grid of seventeen measurement points as shown in figure A1-1. These points are located so as to correspond with specific nodal locations in the initial finite element model. The test articles are designated as:

P8540188	8.5" × 4" × 0.188"
P8540100	8.5" × 4" × 0.100"
P8540100M	8.5" × 4" × Varying Thickness

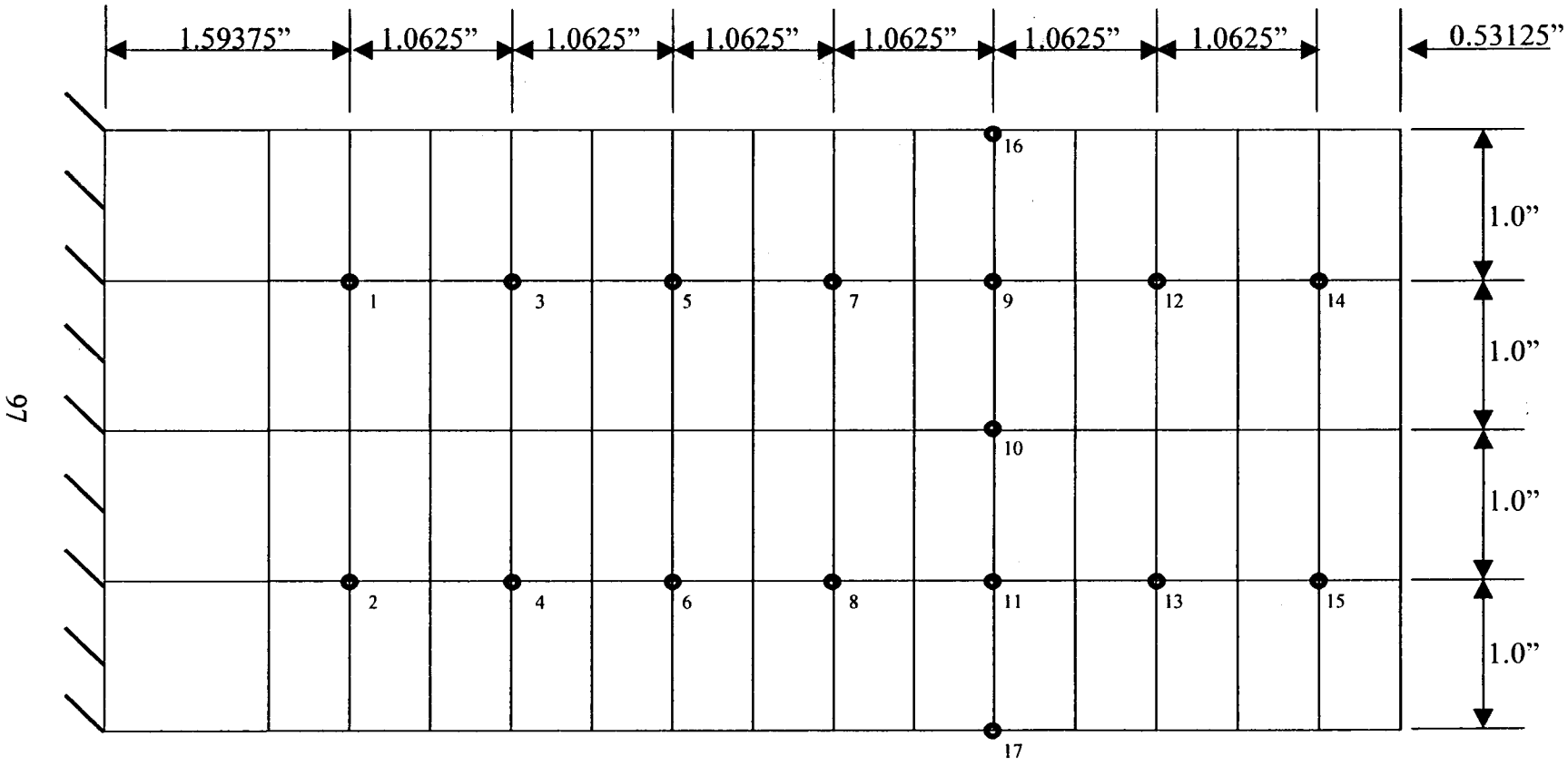


Figure A1-1, Data Point Locations

Test Equipment:

The test equipment to be used for this test consists of:

Hewlett Packard model HP 35665A Dynamic Signal Analyzer
Kistler model 8732A500 accelerometer (10mV/g nominal excitation, mass = 1 gram) with pre-amplifier
PCB Piezotronics model 086C80 miniature impulse hammer (100 mV/lb_f nominal excitation).

Test Procedure:

The following test procedure is to be followed for each of the three test articles:

1. Insert the test article into the test fixture as shown in figure 24 and tighten the eight socket-head cap screws. The clamping fixture is intended to simulate a clamped boundary condition that restrains all displacement and rotation. It is also important not to over torque the bolts. Therefore, prior to taking data, the effect of bolt torque on measurement quality must be assessed by taking trial measurements for various amounts of torque. Apply an initial light torque (finger tight) followed by a trial measurement at various locations. Then apply additional torque in small increments, followed by more trial measurements. Repeat this procedure until there is no noticeable variation in the resulting FRF.

2. Attach the accelerometer at reference location #5 using bee's wax, making sure that there is an adequate bond between the metal plate and the accelerometer.

3. Proceed to take data readings by striking the hammer lightly at the first response location. The response data point will be struck several times in order to get a good average response function for this location. Examine the quality of both the wave form of the hammer impulse and the accelerometer time record for each strike to determine whether to accept or reject the data as a part of the averaged time record. The goal is to obtain enough measurements that the form of the FRF becomes unchanging with each subsequent data set added to the average.

4. Proceed to the next data point and repeat step 4 until all data locations have been measured.

5. Move the accelerometer to reference location #14 and attach it to the plate using bee's wax and repeat steps 3,4, and 5.

6. Move the accelerometer to reference location #15 and attach it to the plate using bee's wax and repeat steps 3,4, and 5.

The resulting data is to be stored on DOS diskettes in the form of FRF's, to be further analyzed by the SDRC I-DEAS software.

APPENDIX 2

TEST DATA SUMMARY

TEST DATA SUMMARY

This is a summary of the test data acquired for the three test articles over the period of time from July 14, 1998 to July 16, 1998. The HP 35665A had the following settings:

Windowing:

Type: Force Exponential
Force Width: 4 ms
Exponential Decay: 50 ms

Channel 1:

Source: Miniature Impulse Hammer
EU Conversion: 95.2 mV/lb, (per calibration)

Channel 2:

Source: Accelerometer
EU Conversion: 10.27 mV/g (per mfr specifications)

Number of Lines of Data:

800

Frequency Span:

Test Article P8540188	0 to 1.6 khz
Test Article P8540100M	0 to 800 hz
Test Article P8540100	0 to 800 hz

Number of Averages:

5

The accompanying plots are the output from the dynamic signal analyzer. Figures A2-1, A2-2, and A2-3 show the FRF's for test articles P8540188, P8540100, and

P8540100M respectively. The notation beneath the x-axis for each plot indicates the accelerometer location followed by the hammer strike location (e.g. 05-01 indicates the accelerometer is located at point 5 with the impulse hammer input at point 0 1

Using simple peak picking techniques, we can estimate the natural frequencies of each test article. The first five natural frequencies below 1.6 khz for P8540188 were estimated as 89 hz, 399 hz, 547 hz, 1266 hz, and 1496 hz. For P8540100 the first five frequencies were 43 hz, 195 hz, 271 hz, 631 hz, and 757 hz. There were only four natural frequencies below 800 hz for P8540100M. These were estimated to be 55 hz, 227 hz, 329 hz, 732 hz.

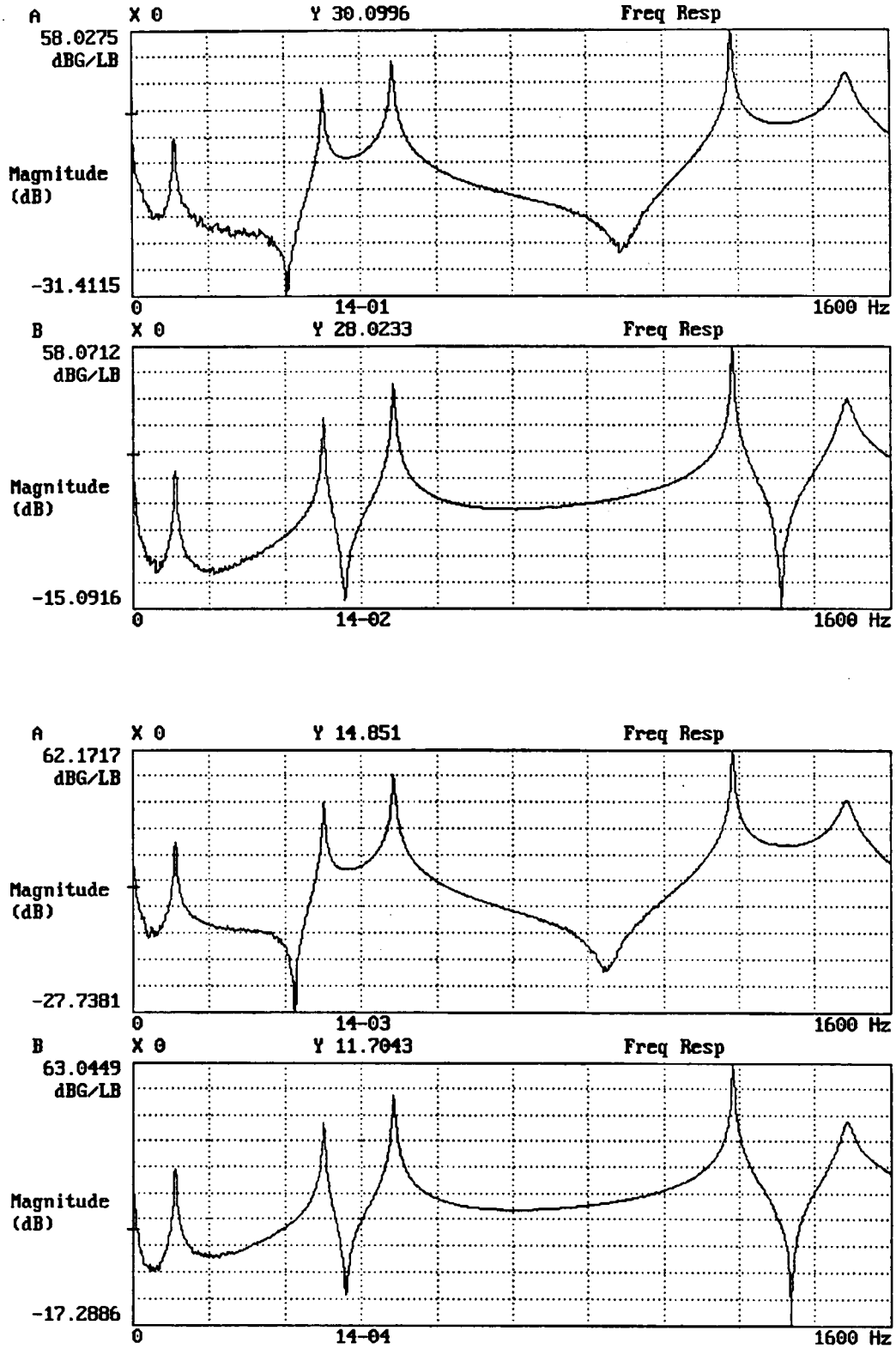


Figure A2-1, Test Article P8540188, Frequency Response Plots

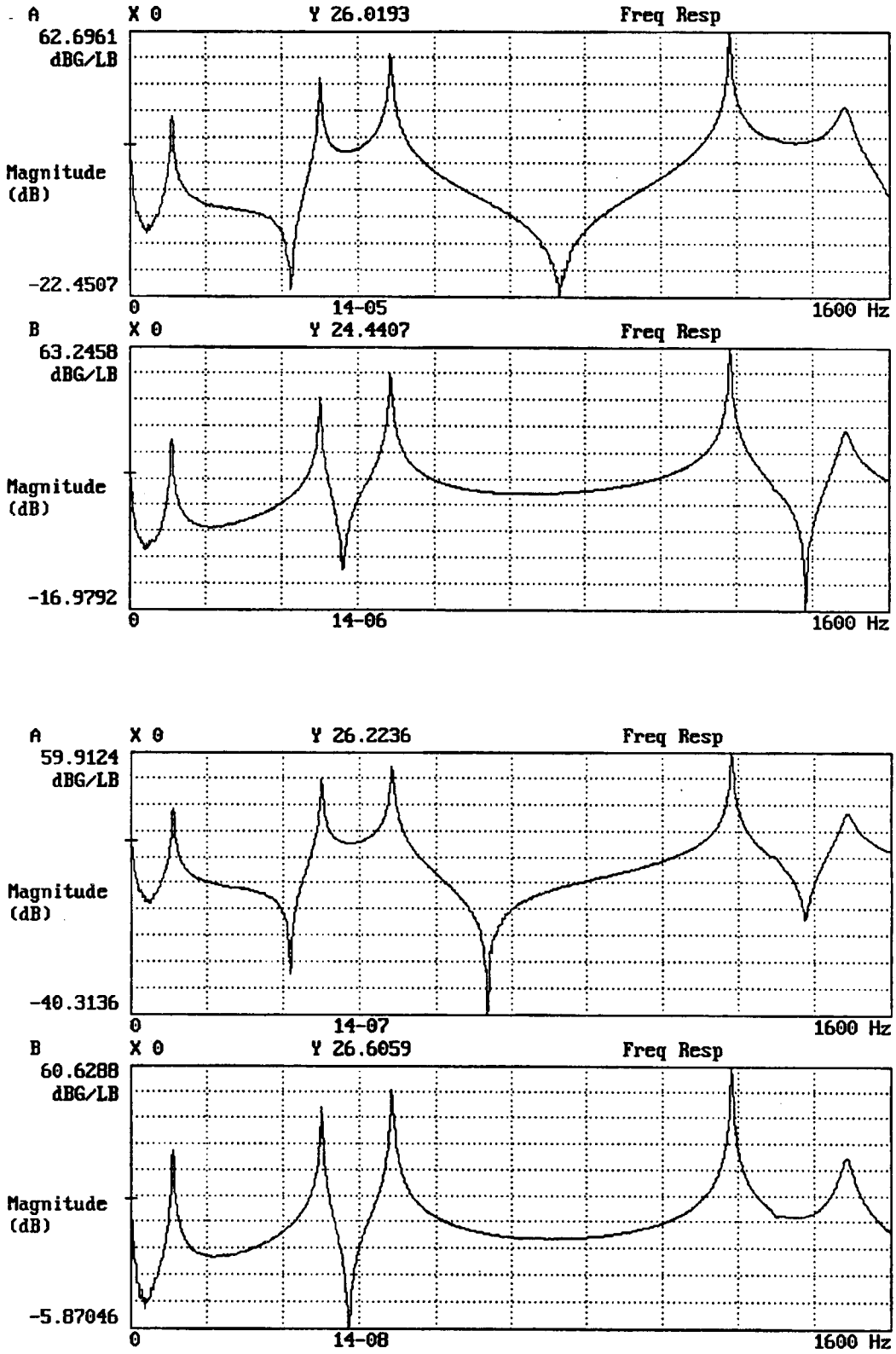
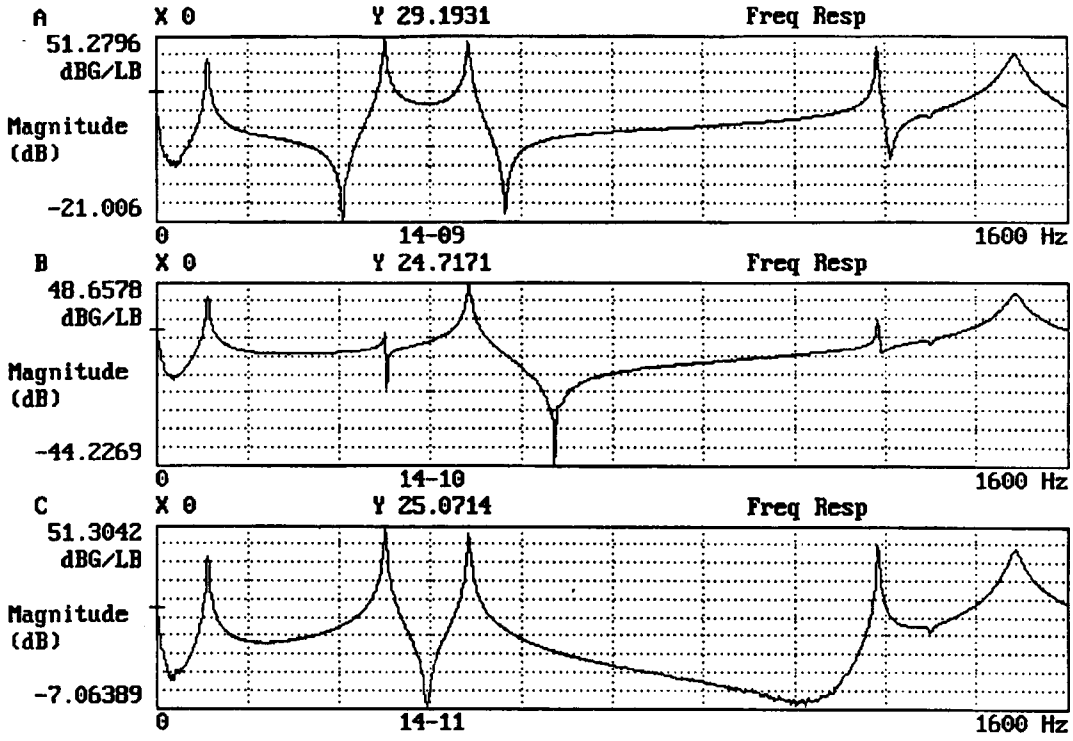


Figure A2-1, Test Article P8540188, Frequency Response Plots (continued)



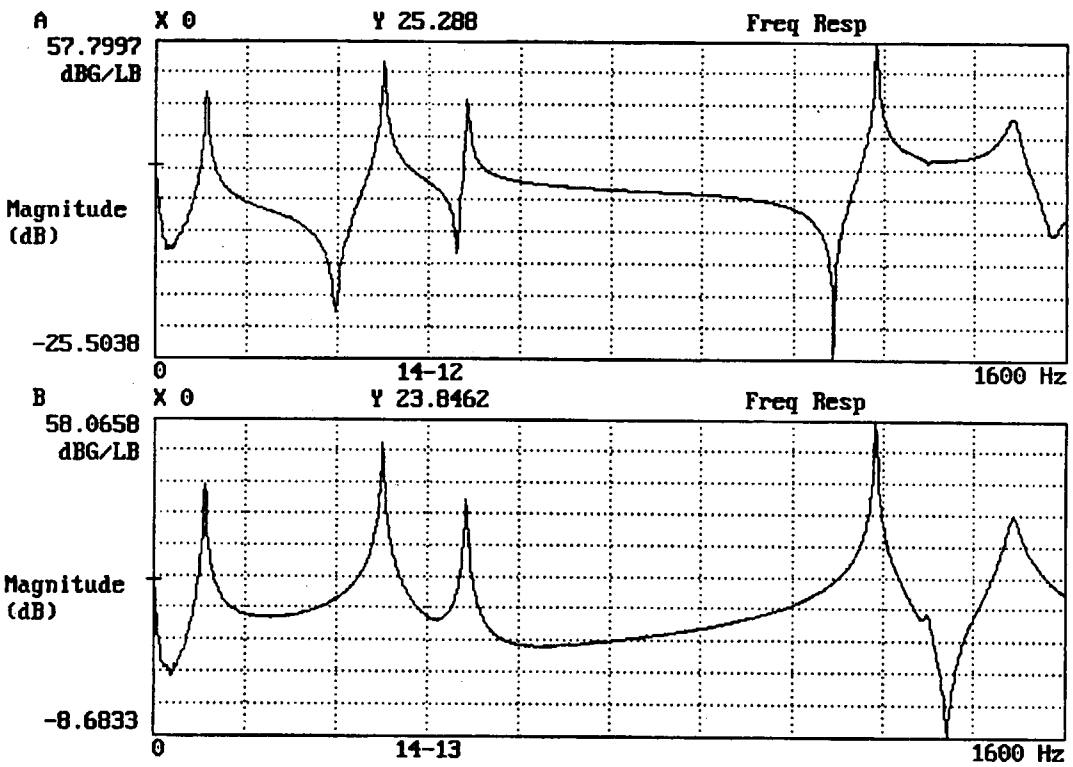


Figure A2-1, Test Article P8540188, Frequency Response Plots (continued)

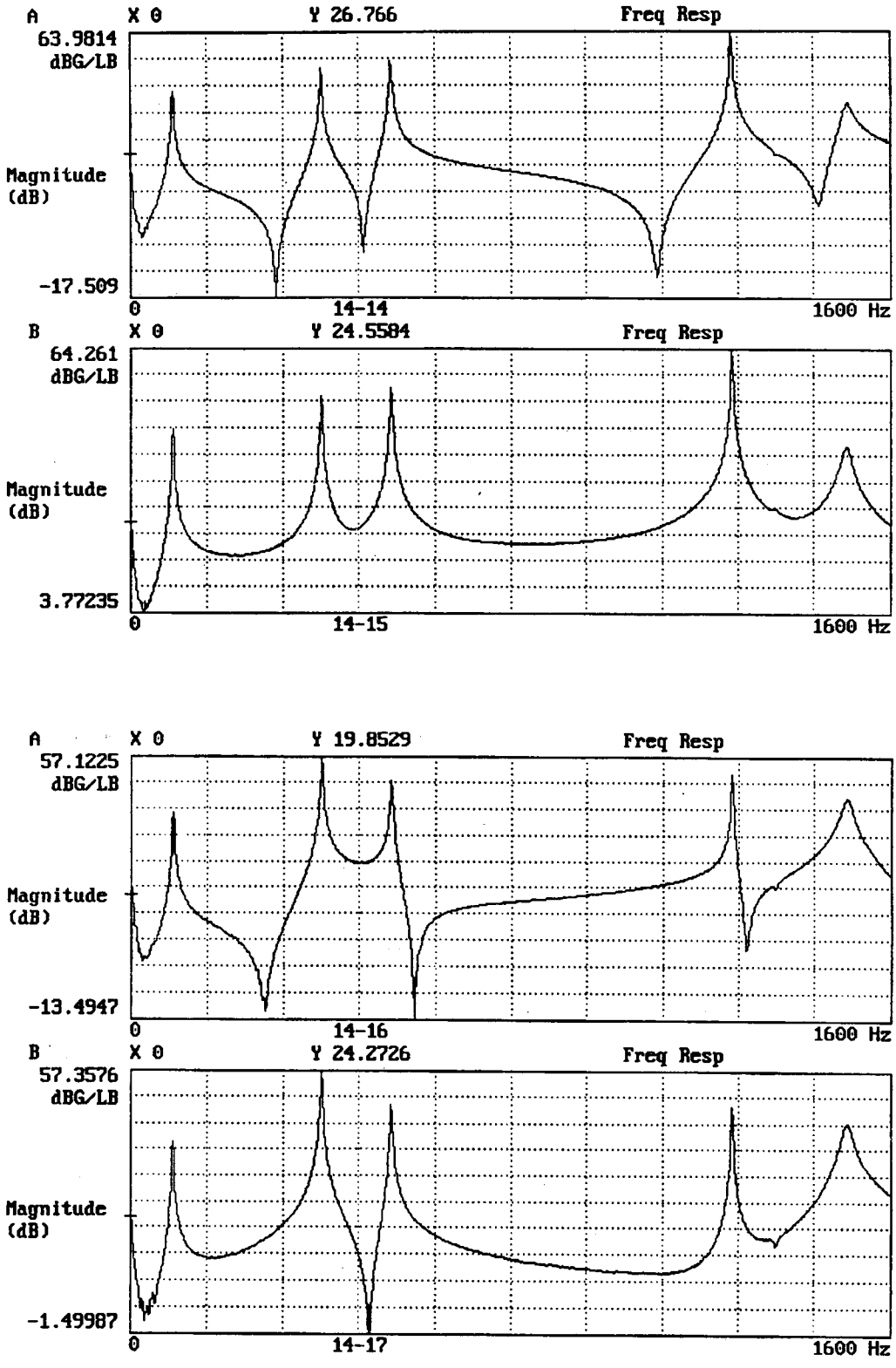


Figure A2-1, Test Article P8540188, Frequency Response Plots (continued)

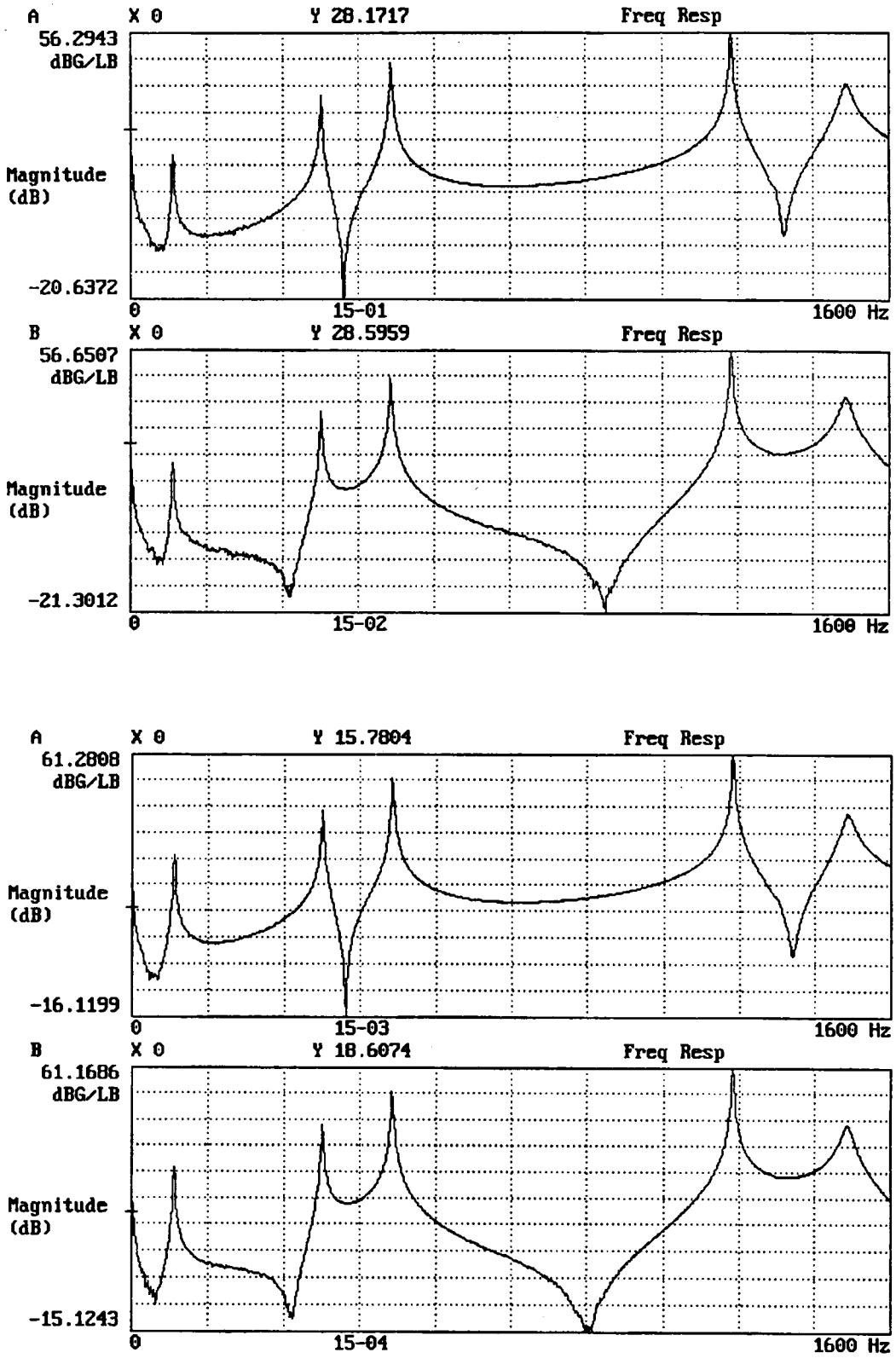


Figure A2-1, Test Article P8540188, Frequency Response Plots (continued)

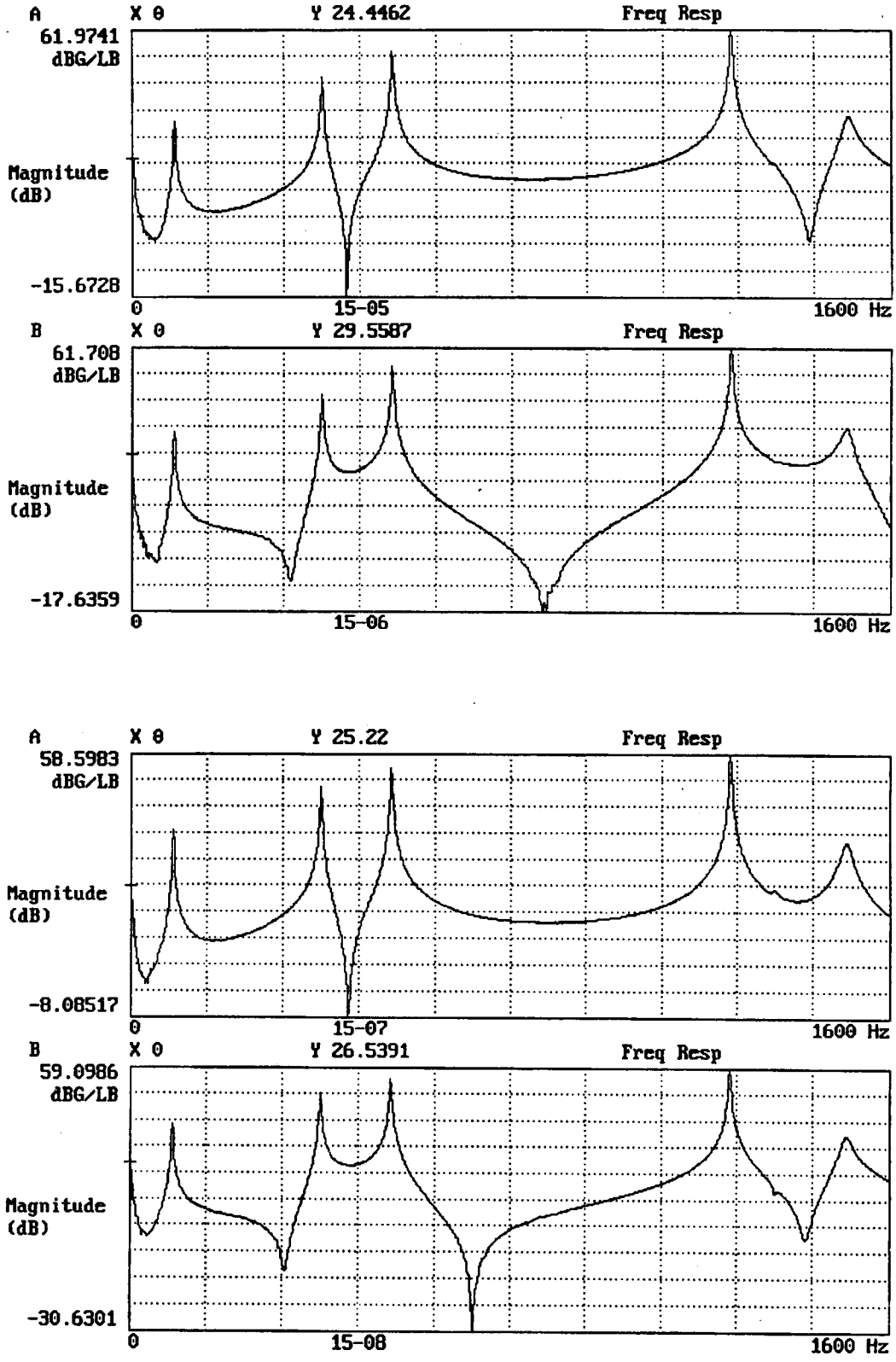


Figure A2-1, Test Article P8540188, Frequency Response Plots (continued)

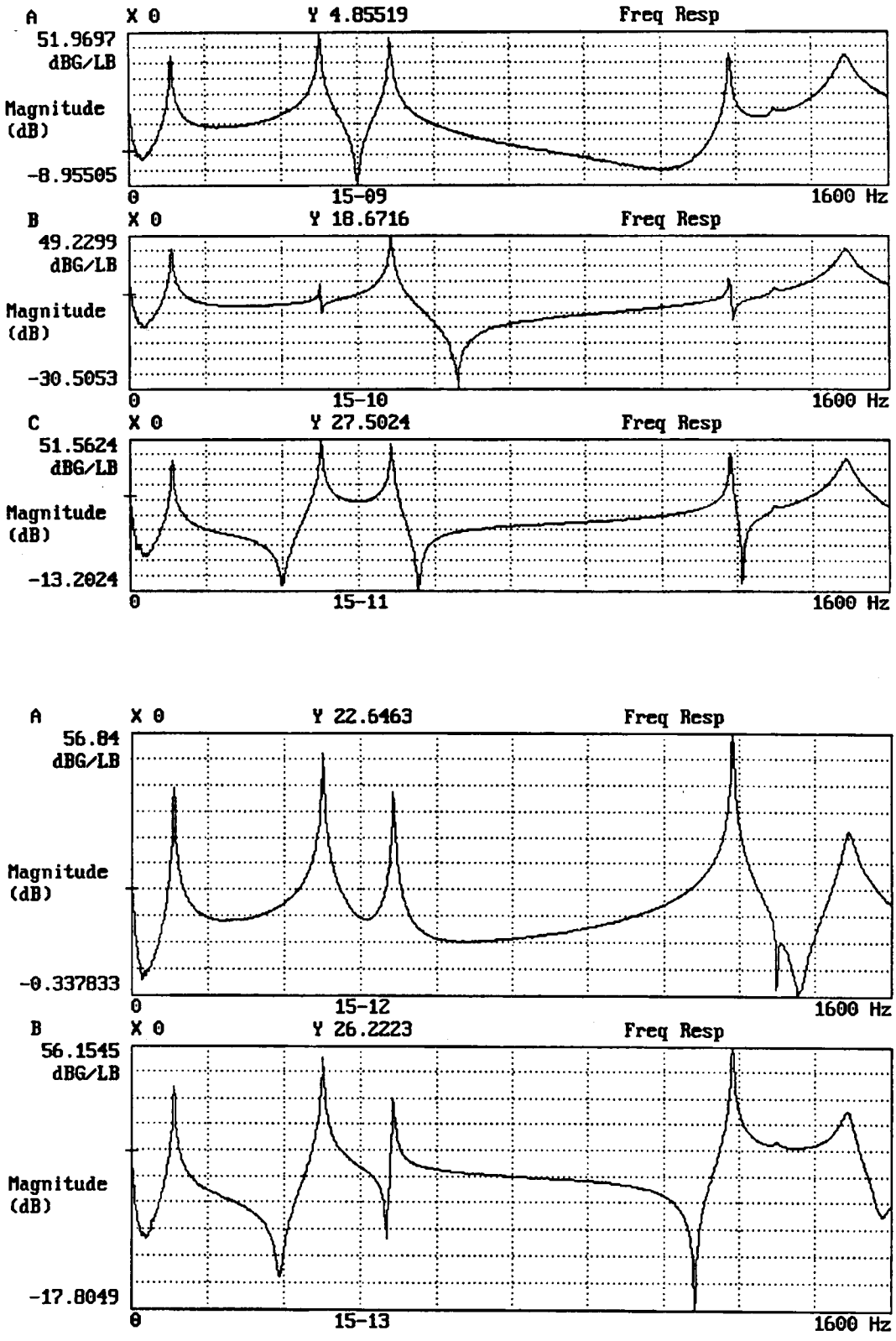


Figure A2-1, Test Article P8540188, Frequency Response Plots (continued)

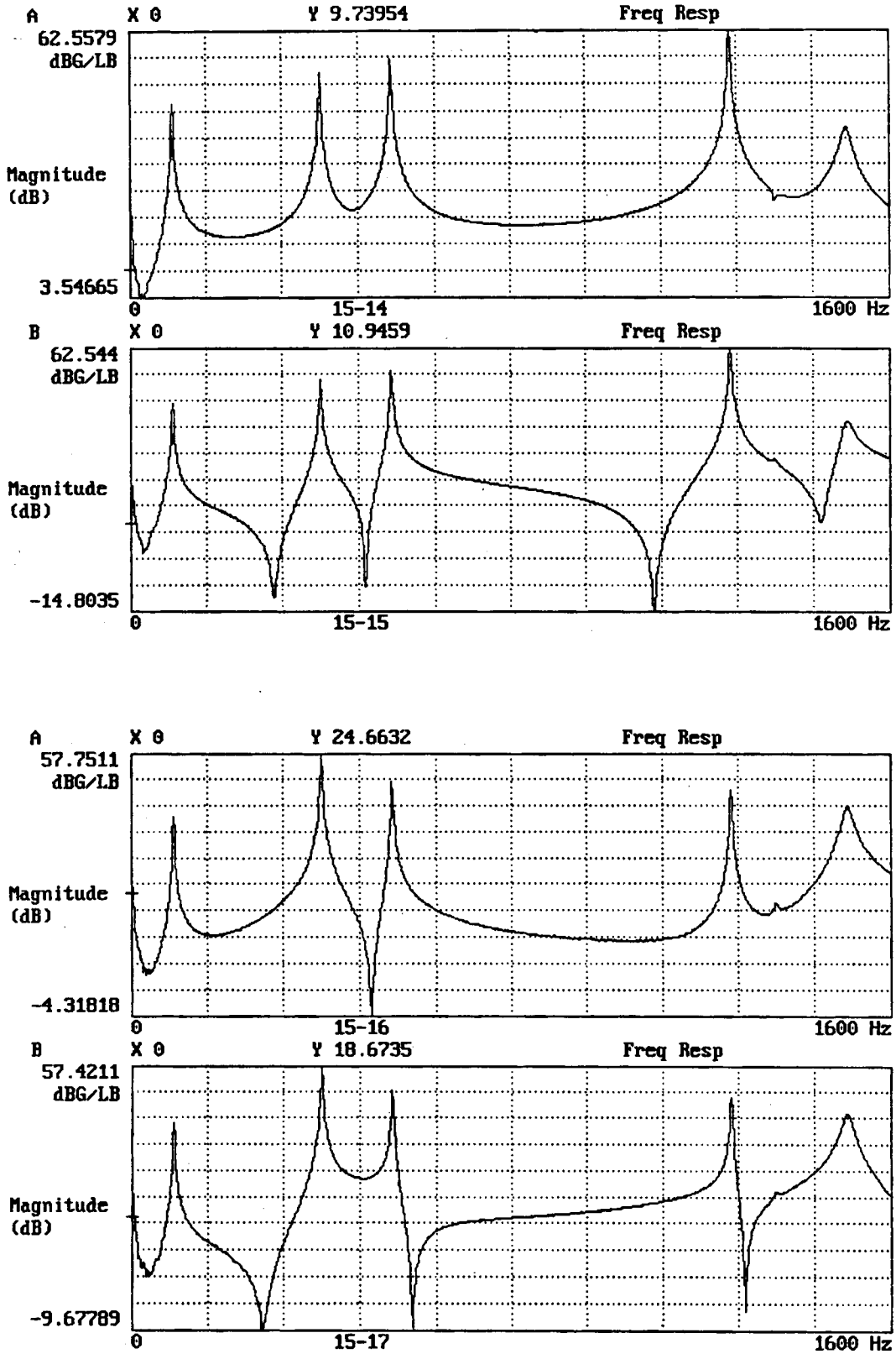


Figure A2-1, Test Article P8540188, Frequency Response Plots (concluded)

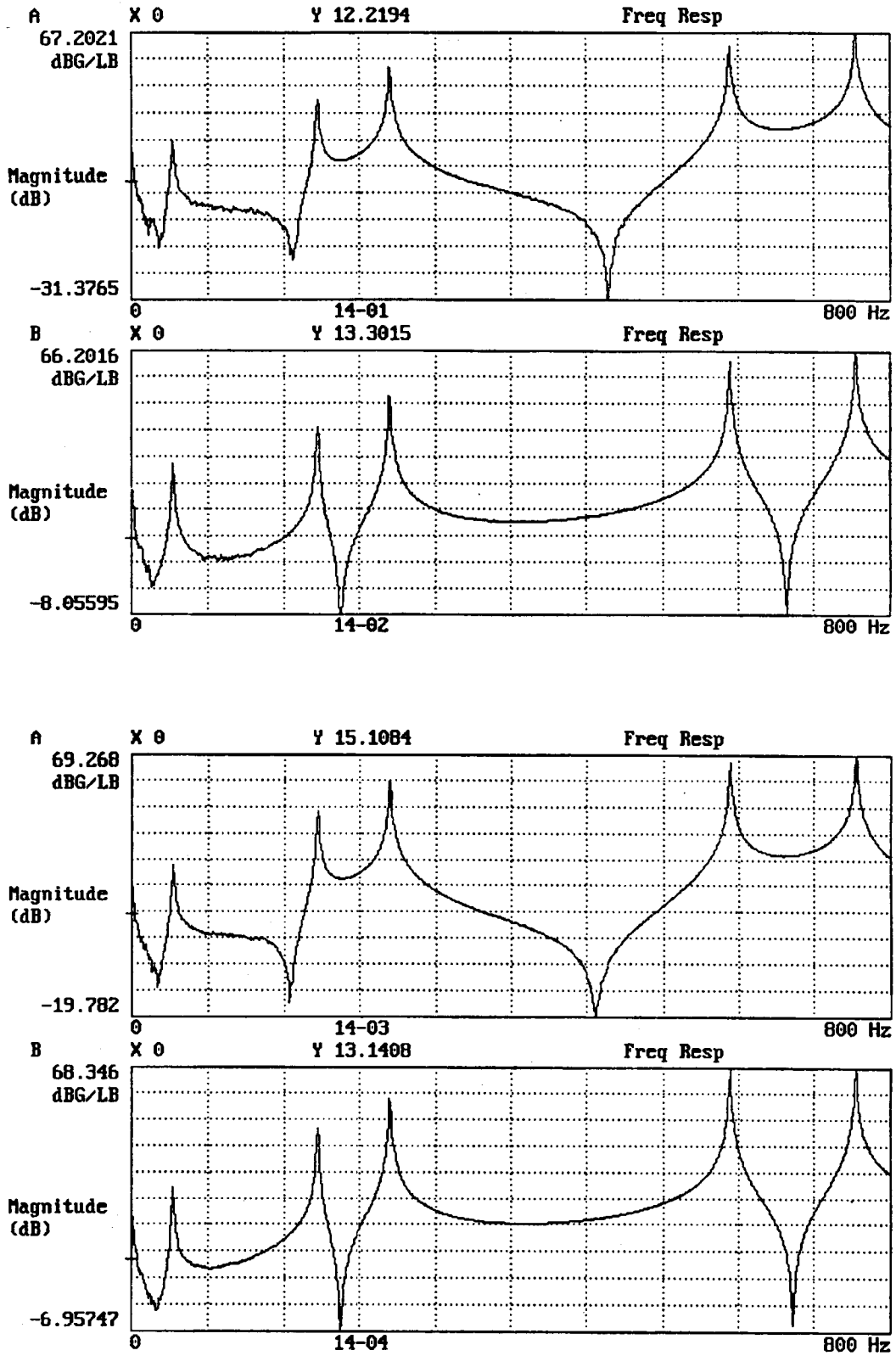


Figure A2-2, Test Article P8540100, Frequency Response Plots

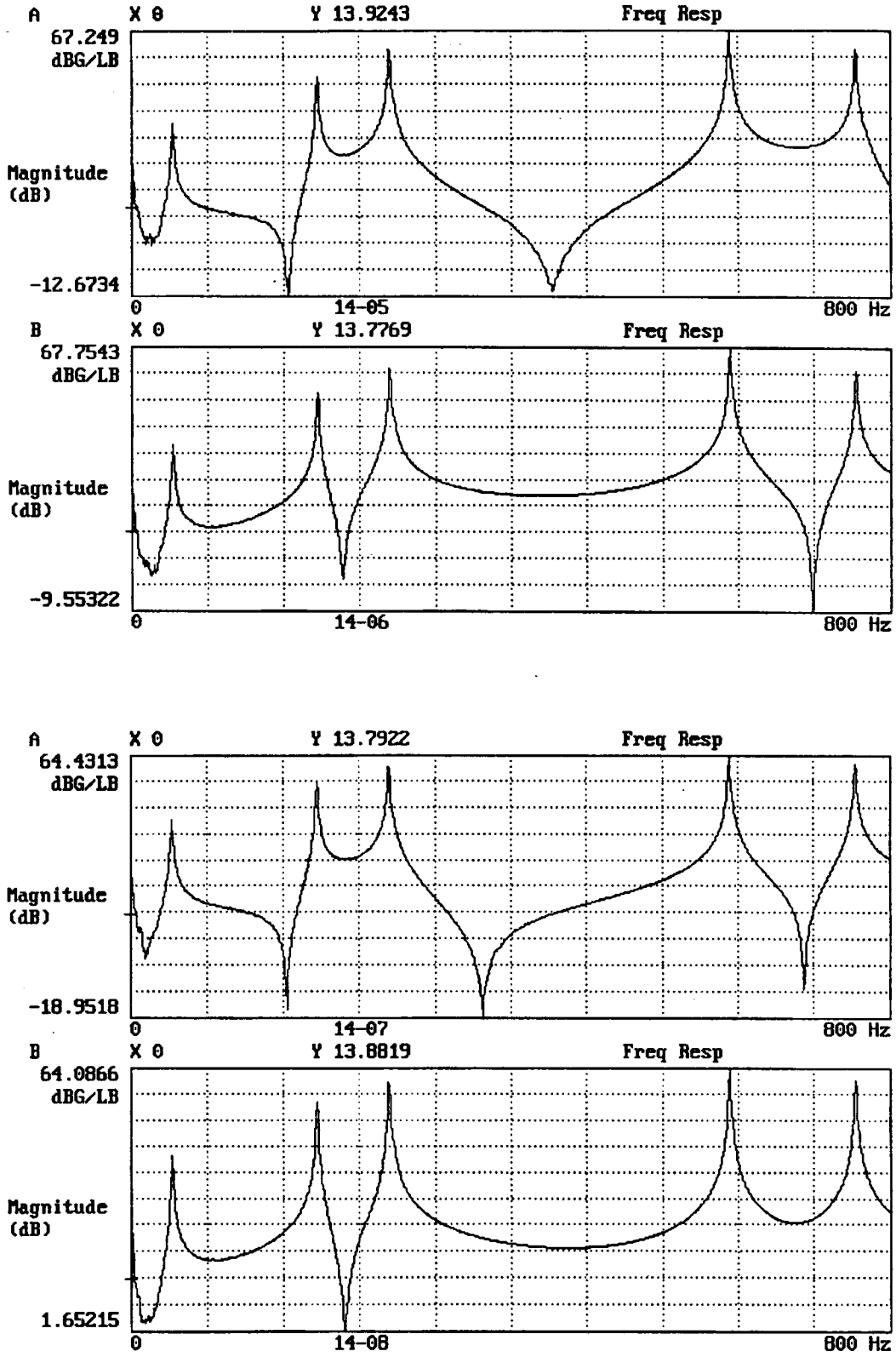
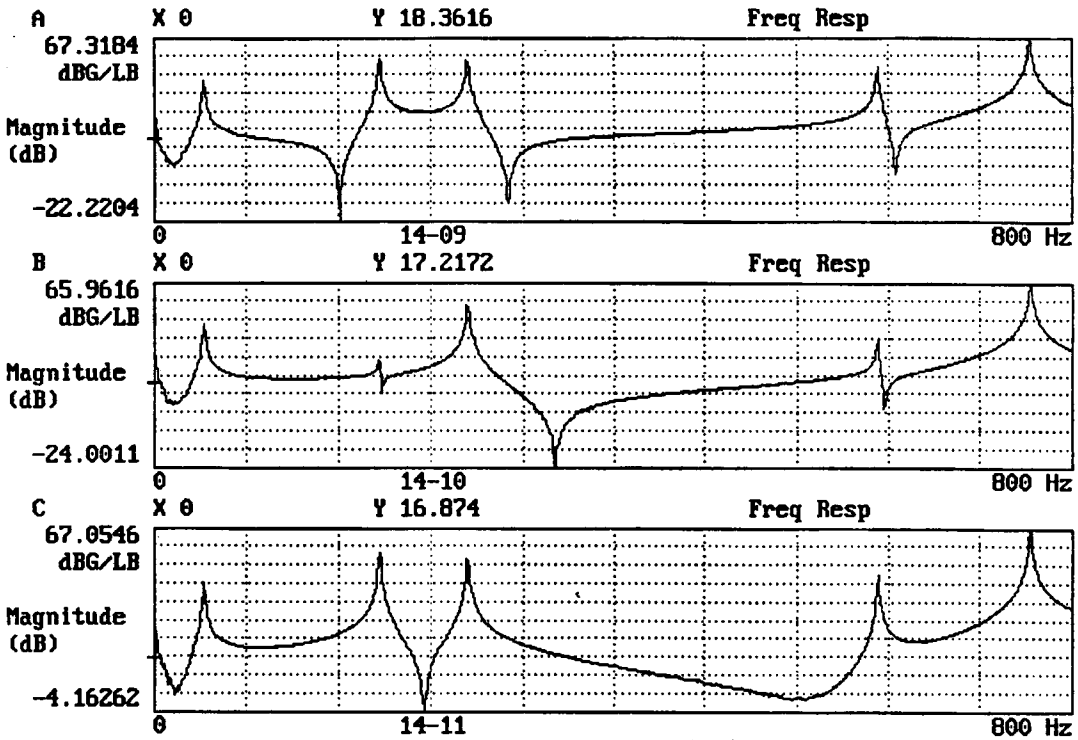


Figure A2-2, Test Article P8540100, Frequency Response Plots (continued)



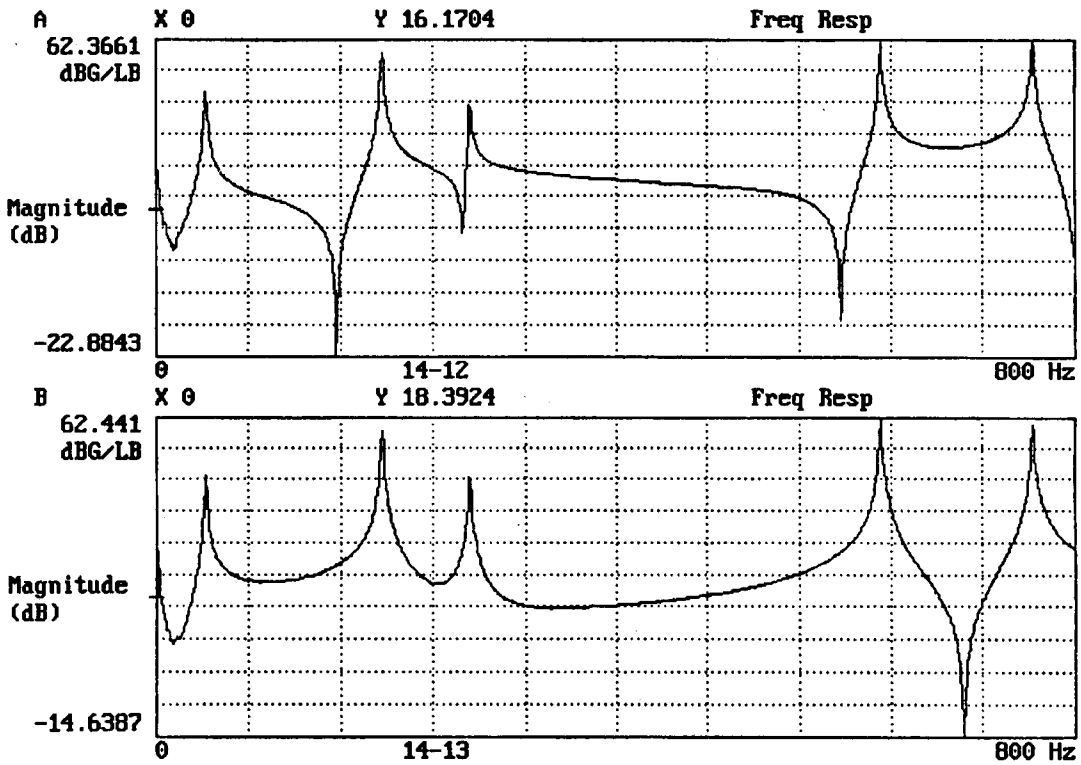


Figure A2-2, Test Article P8540100, Frequency Response Plots (continued)

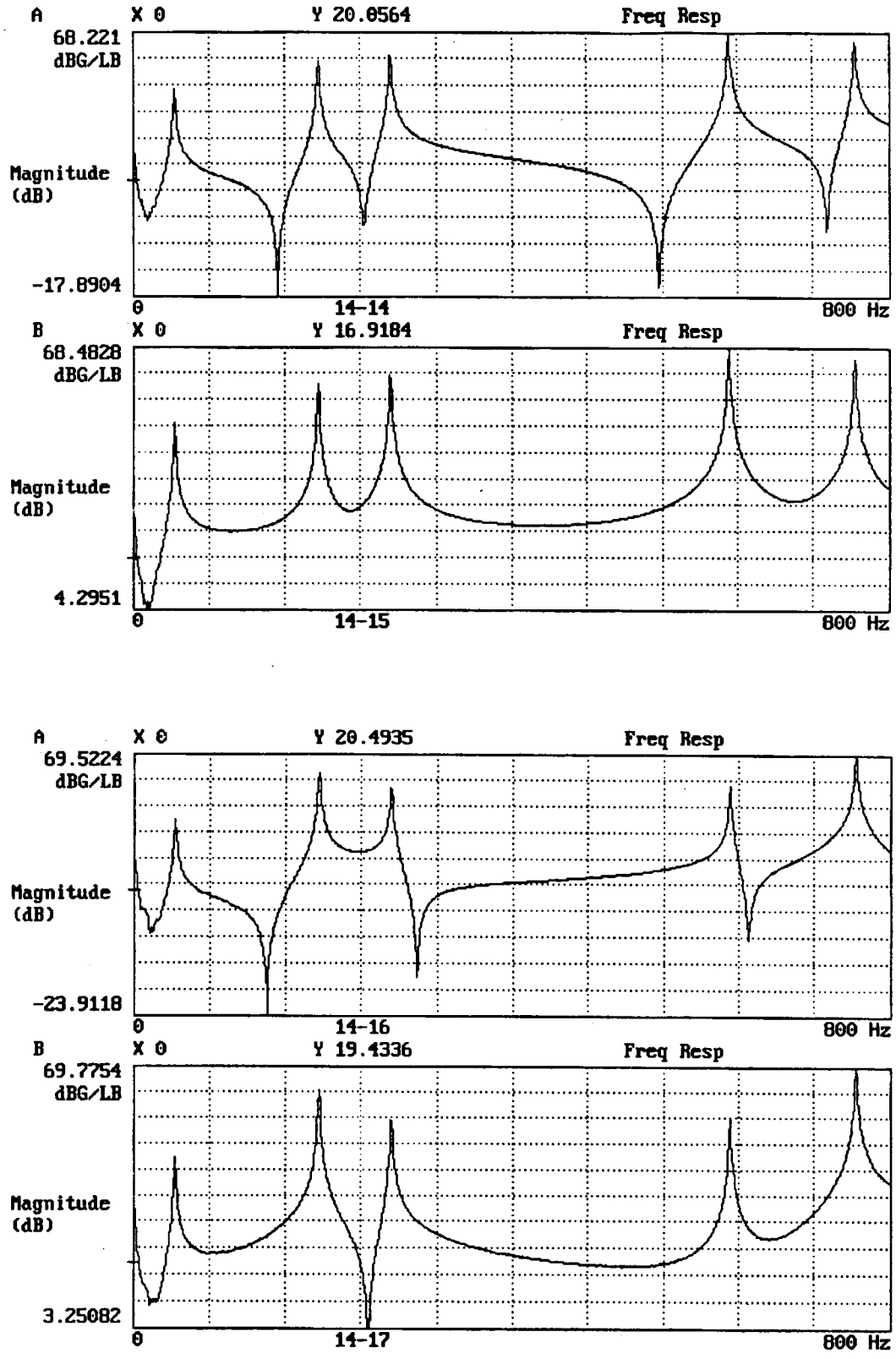


Figure A2-2, Test Article P8540100, Frequency Response Plots (continued)

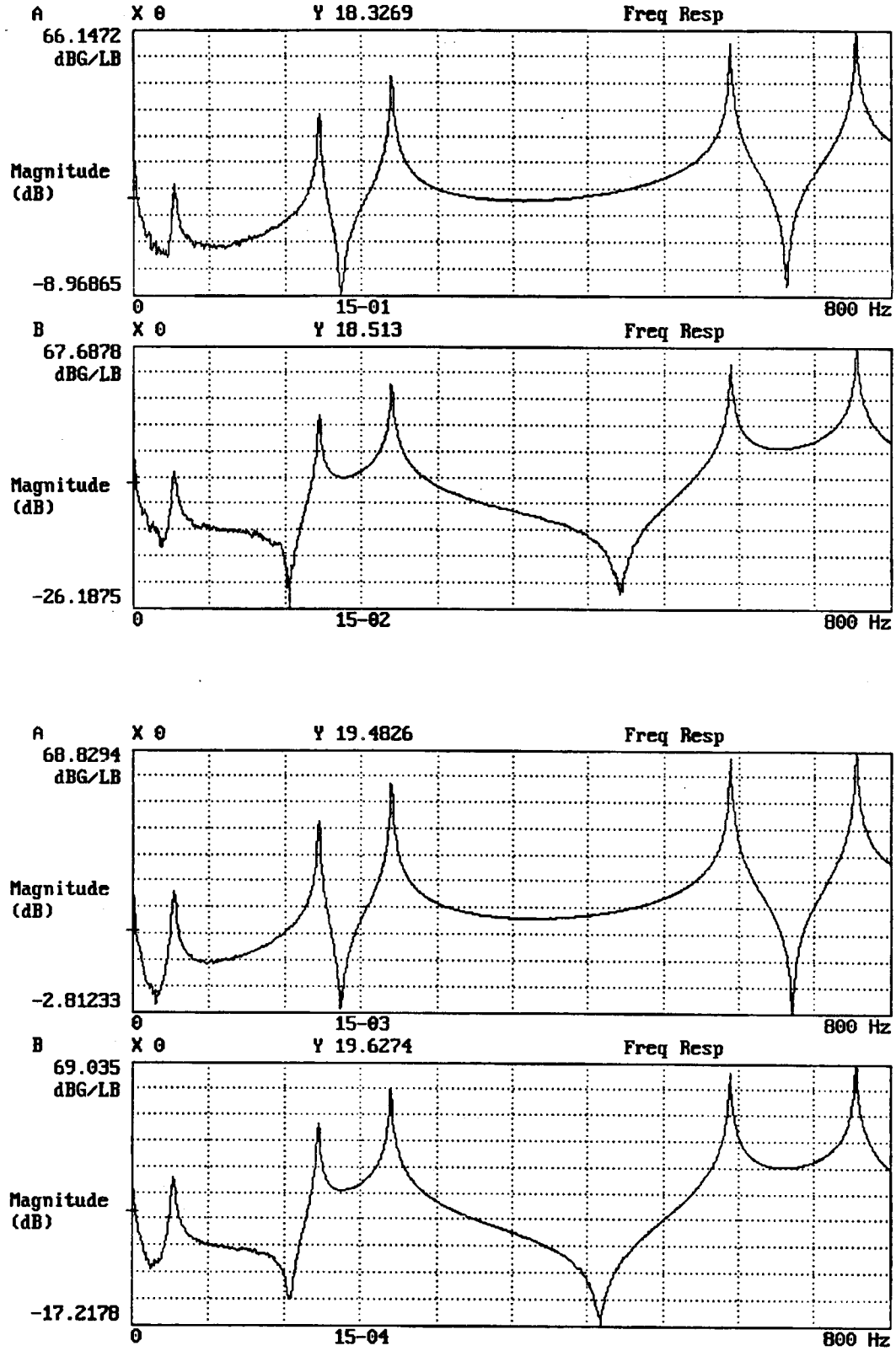


Figure A2-2, Test Article P8540100, Frequency Response Plots (continued)

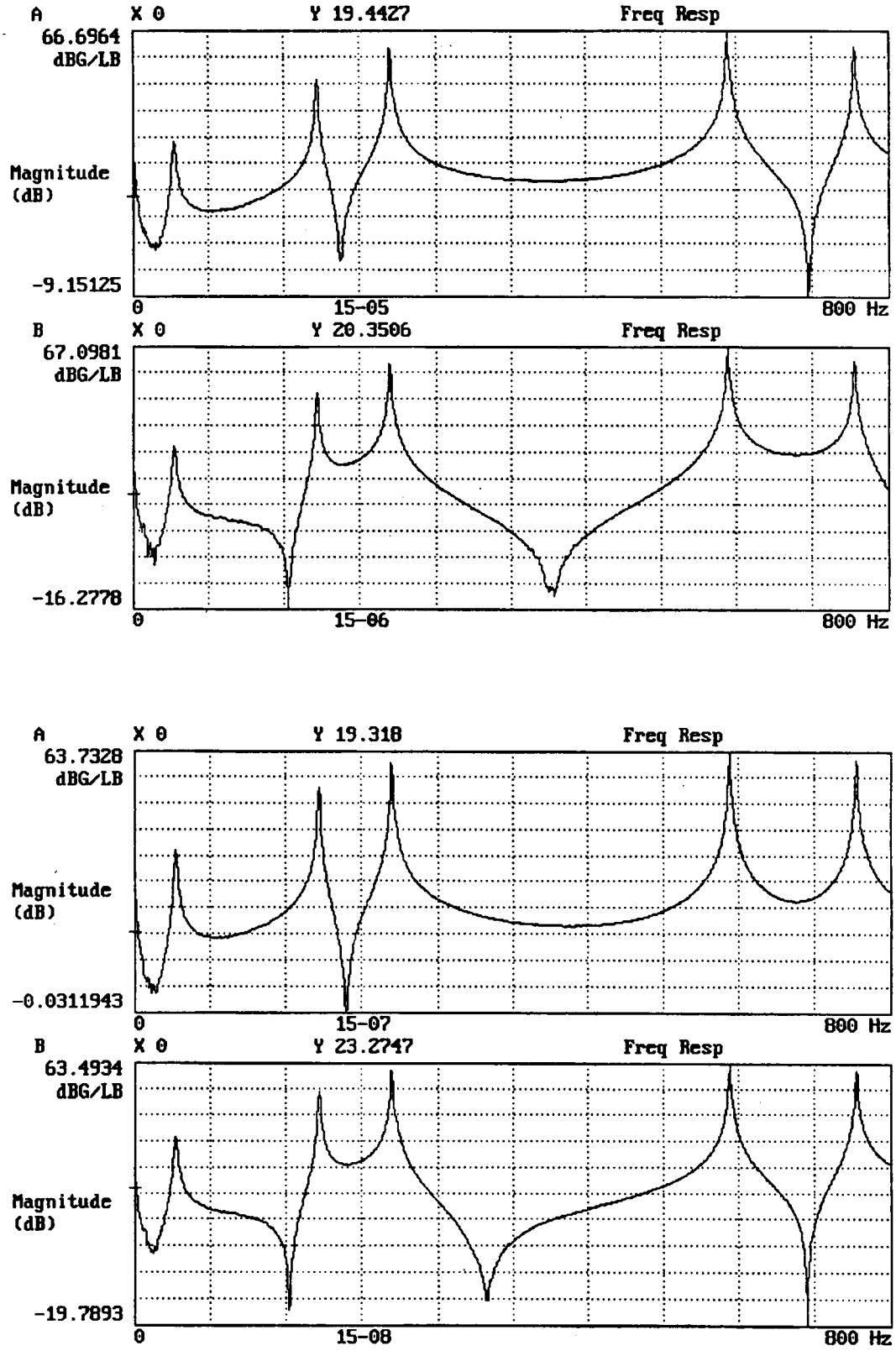


Figure A2-2, Test Article P8540100, Frequency Response Plots (continued)

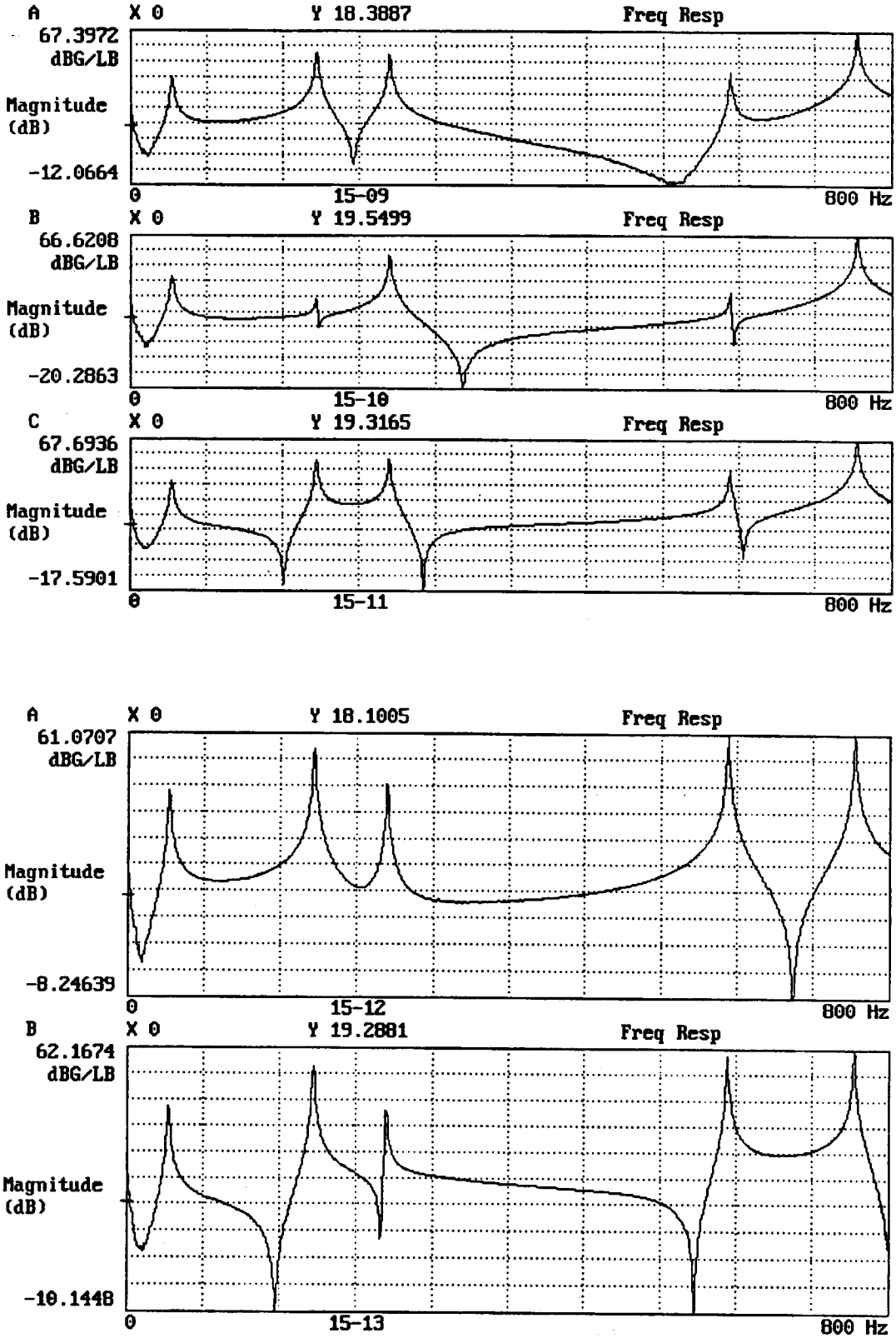


Figure A2-2, Test Article P8540100, Frequency Response Plots (continued)

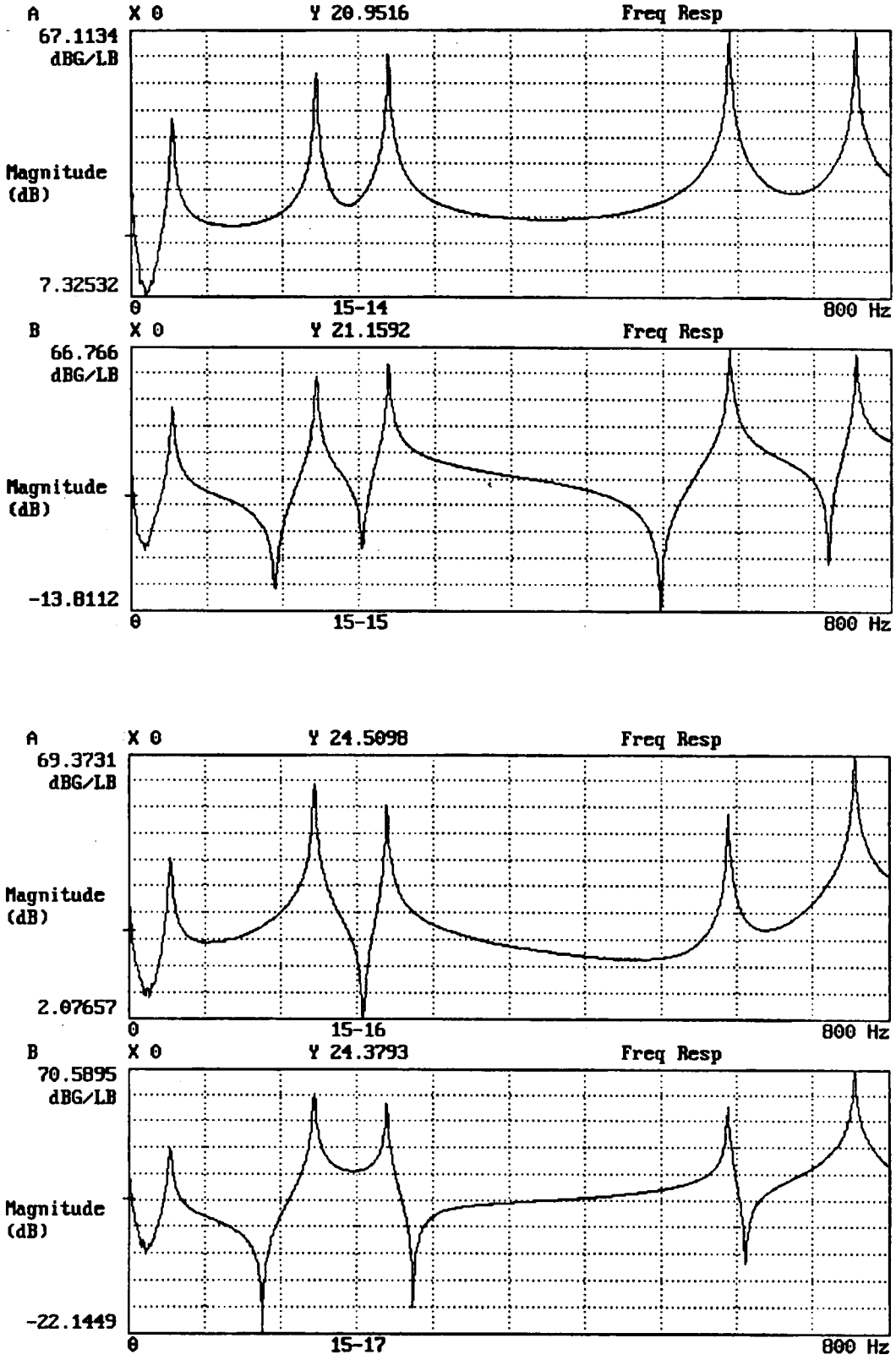


Figure A2-2, Test Article P8540100, Frequency Response Plots (concluded)

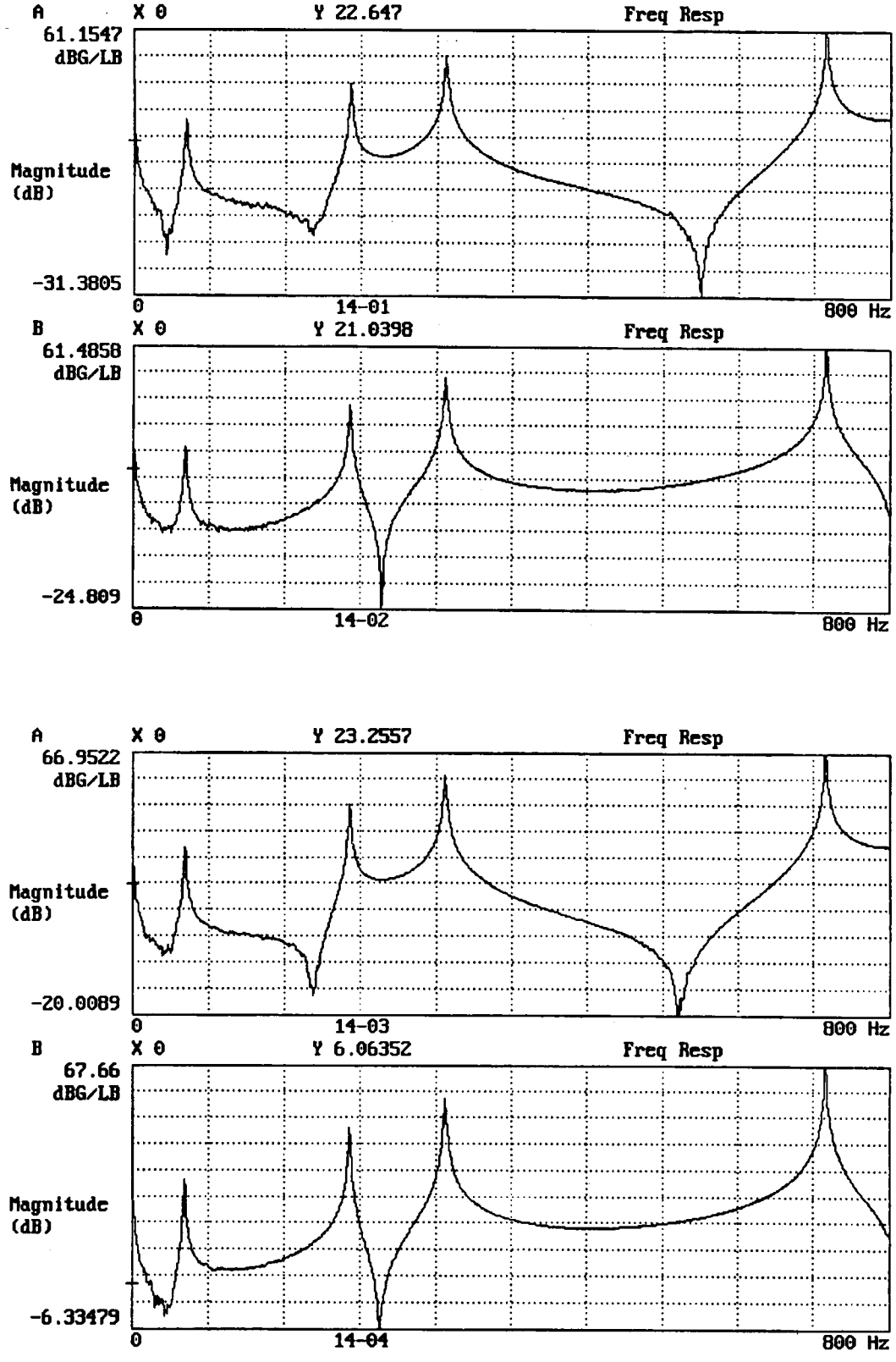


Figure A2-3, Test Article P8540100M, Frequency Response Plots

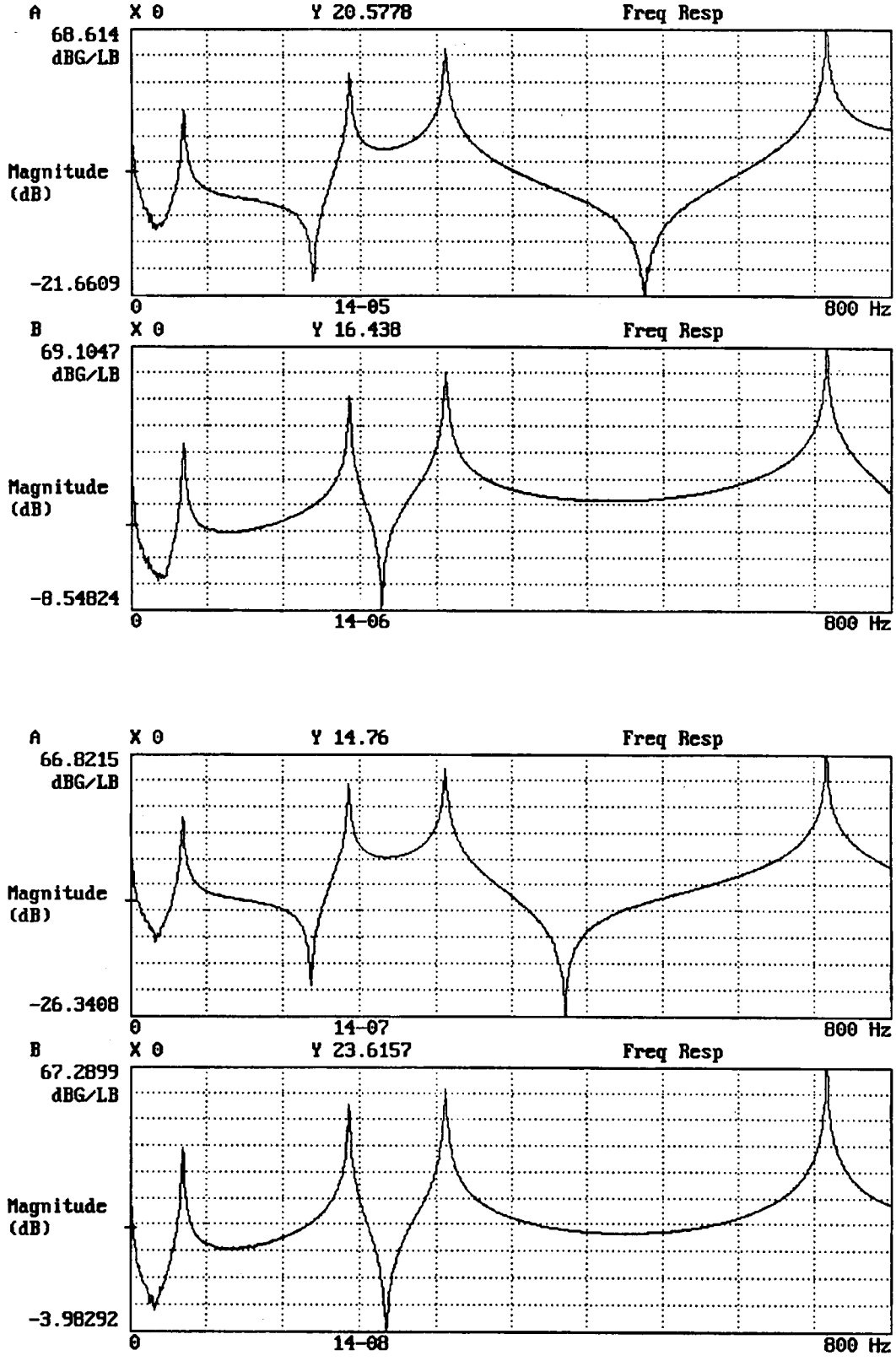


Figure A2-3, Test Article P8540100M, Frequency Response Plots (continued)

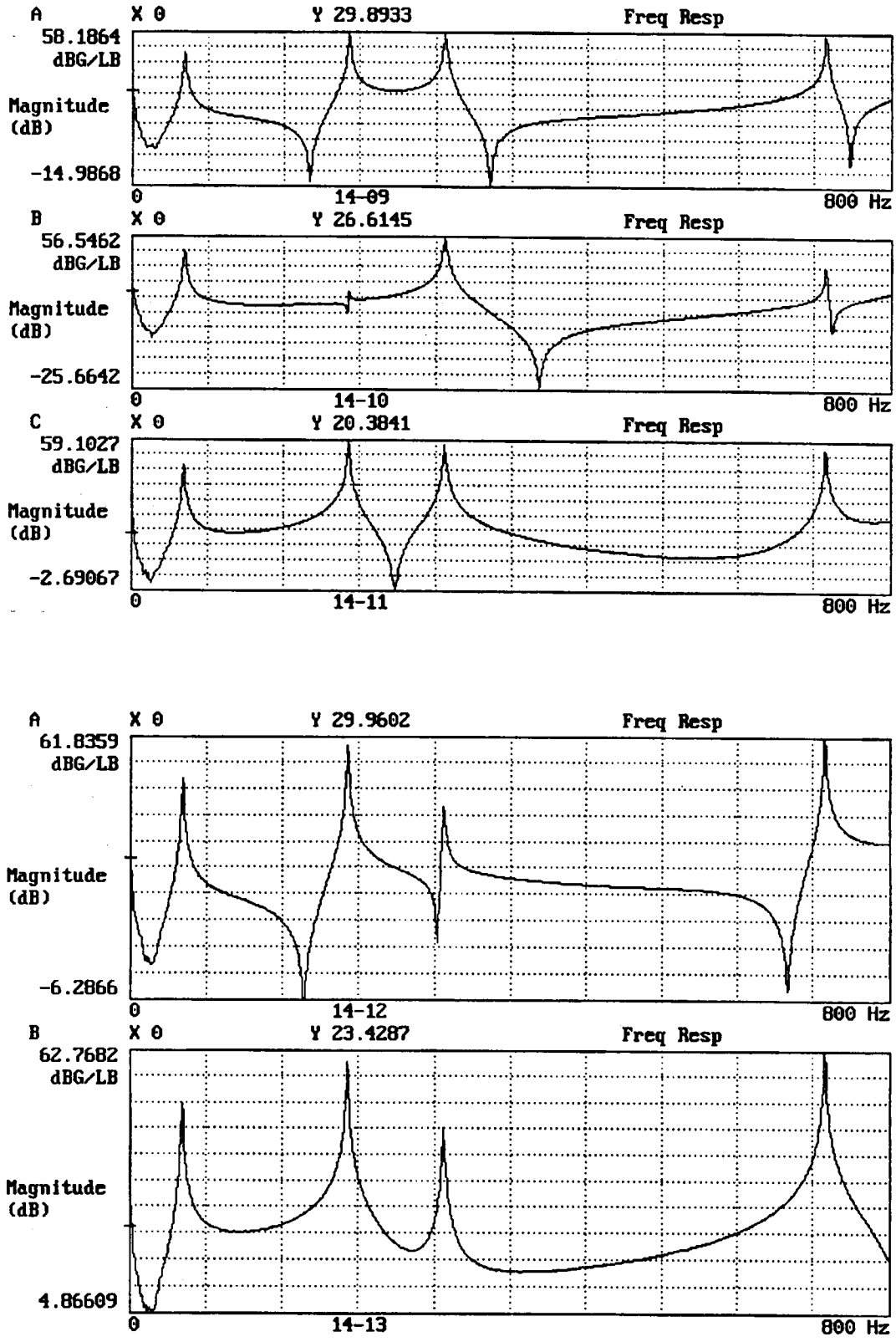


Figure A2-3, Test Article P8540100M, Frequency Response Plots (continued)

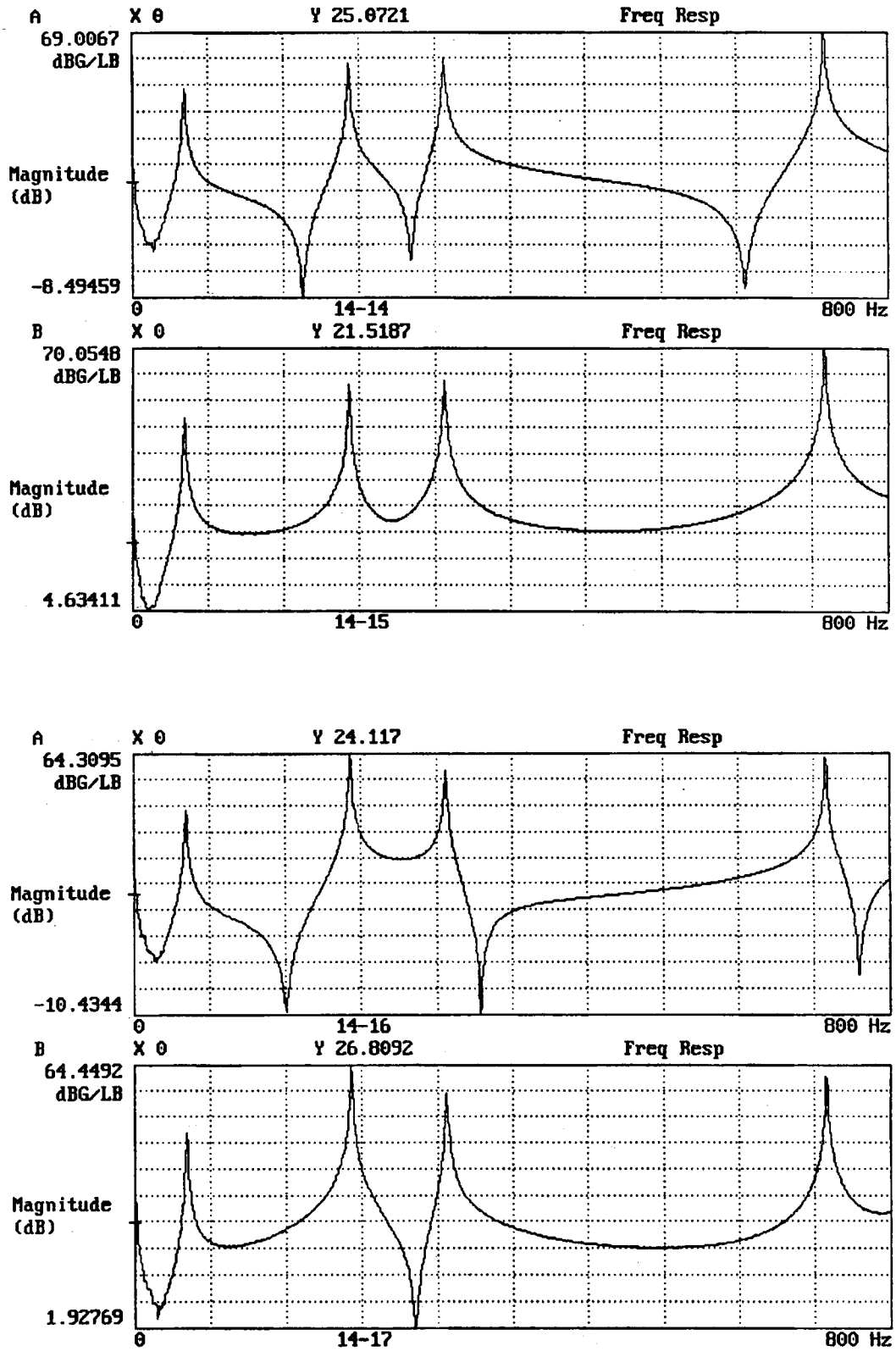


Figure A2-3, Test Article P8540100M, Frequency Response Plots (continued)

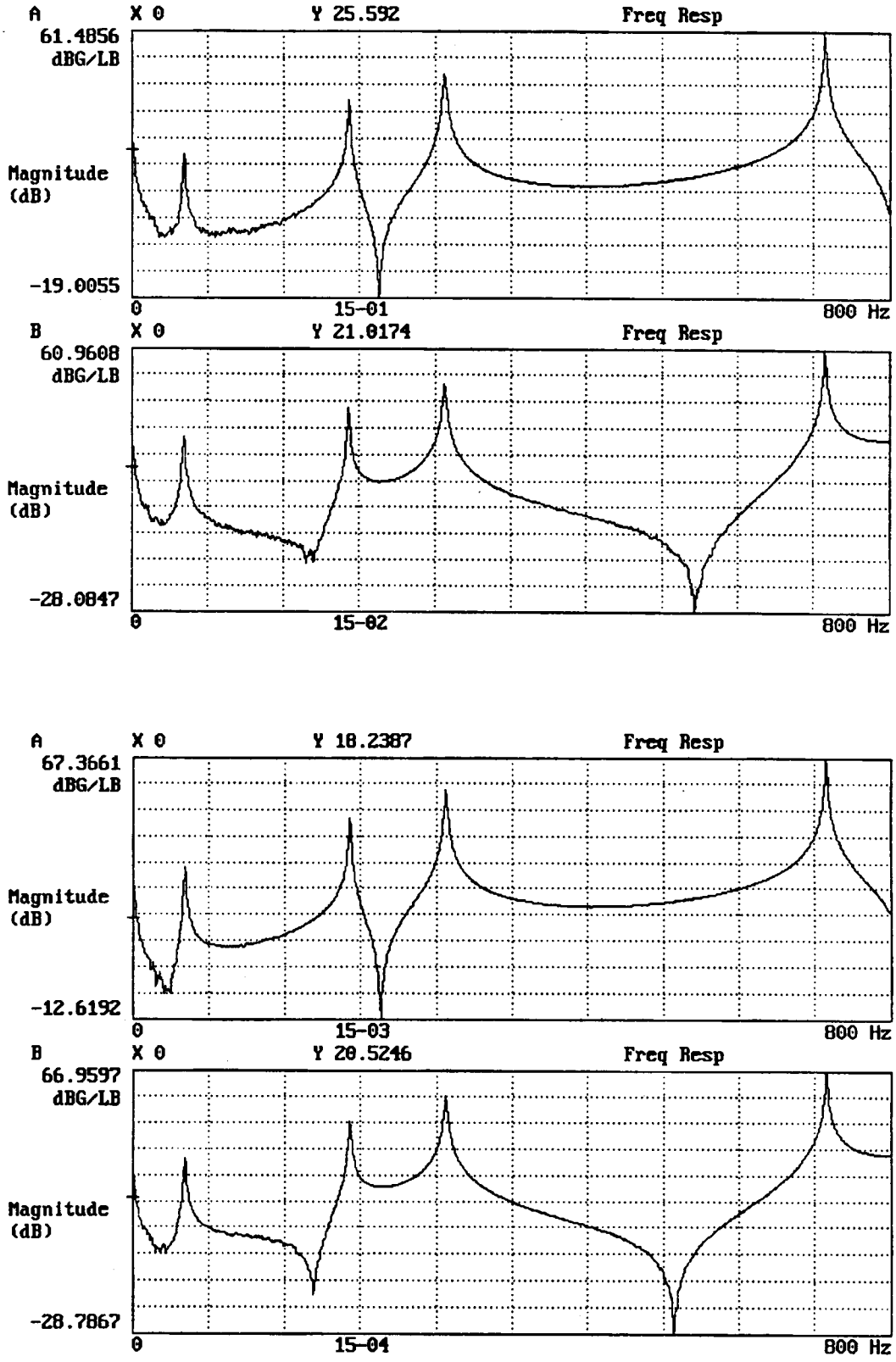


Figure A2-3, Test Article P8540100M, Frequency Response Plots (continued)

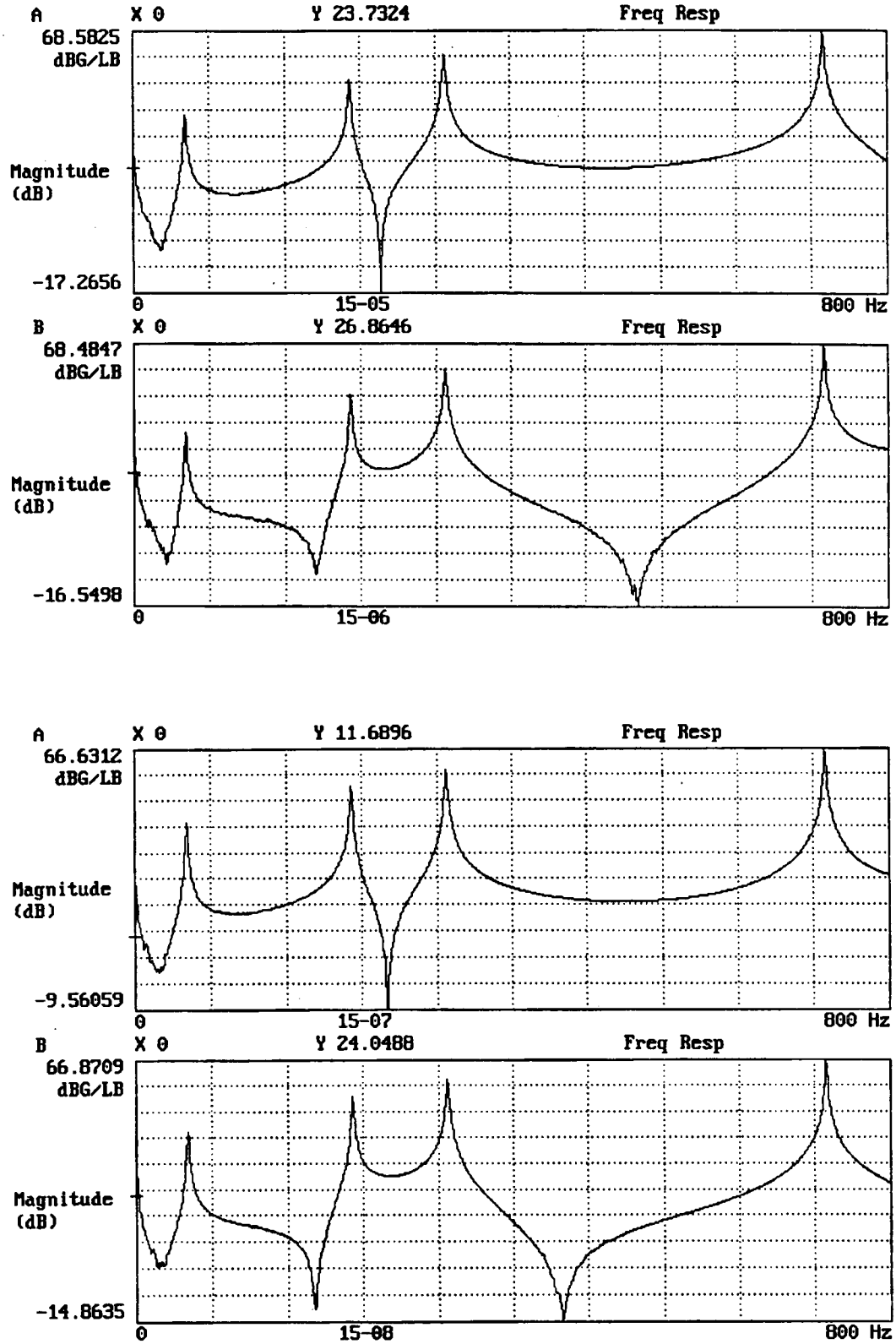


Figure A2-3, Test Article P8540100M, Frequency Response Plots (continued)

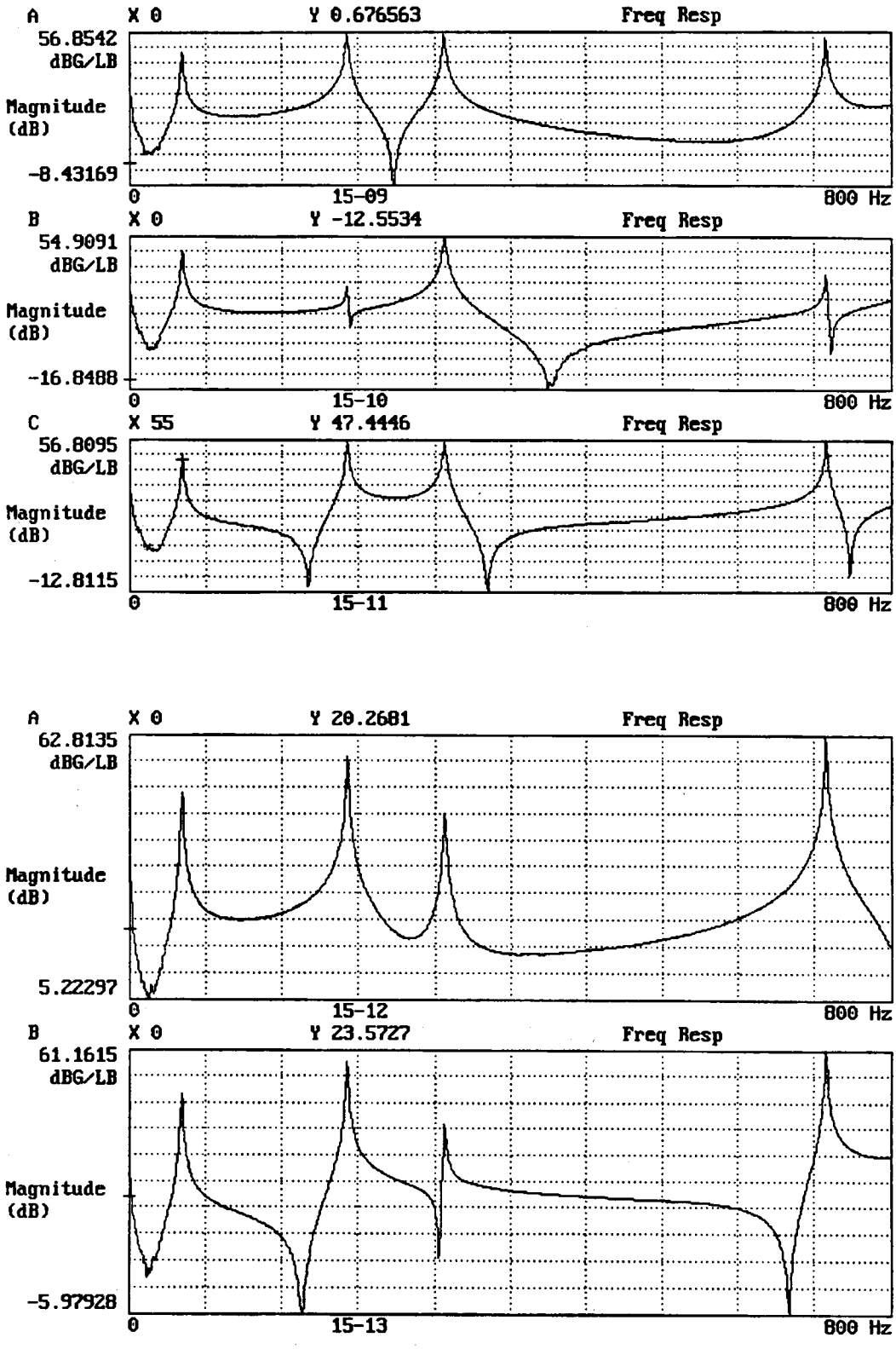


Figure A2-3, Test Article P8540100M, Frequency Response Plots (continued)

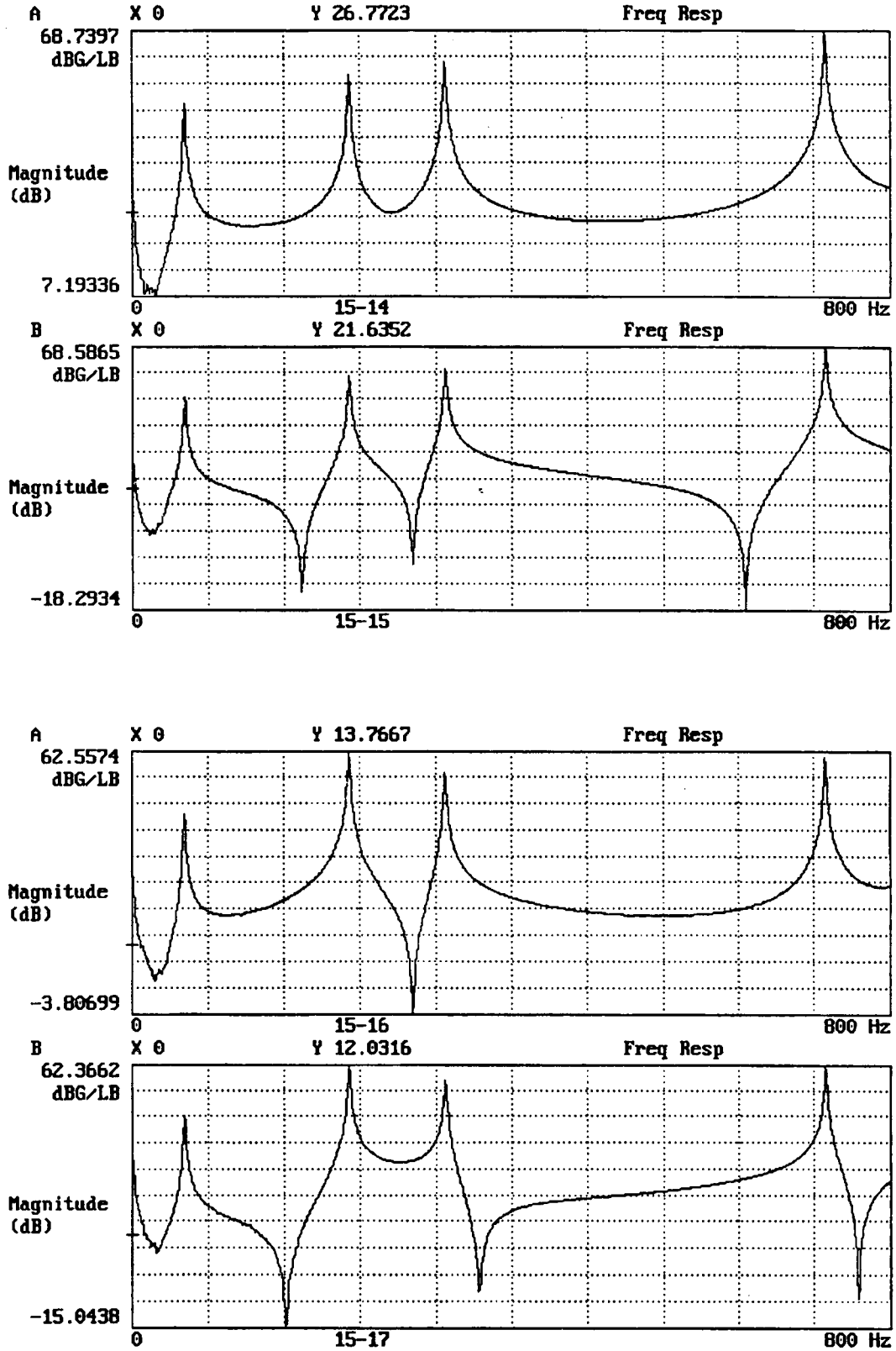


Figure A2-3, Test Article P8540100M, Frequency Response Plots (concluded)

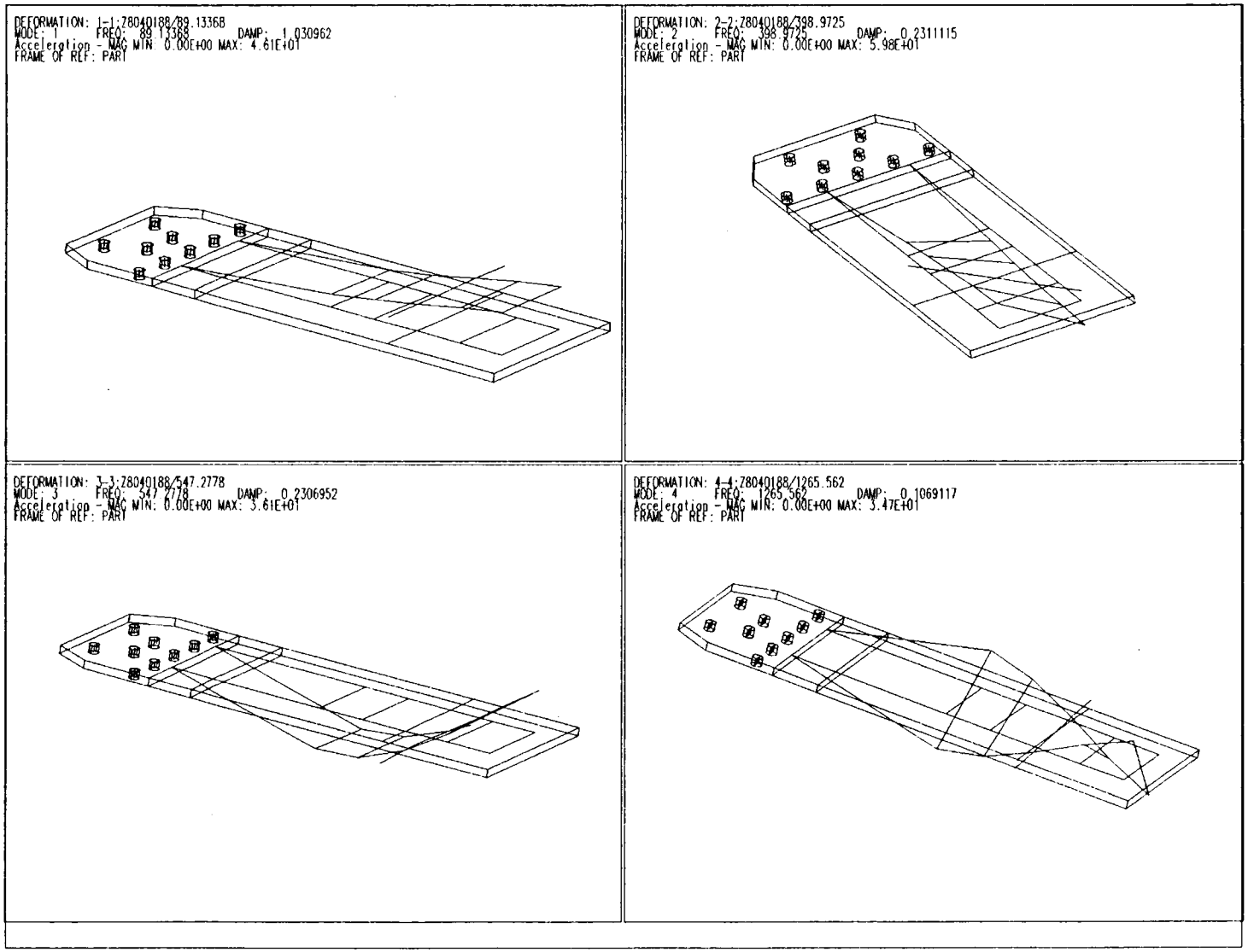


Figure A2-4, Mode Shapes for P8540188 as Generated From Test Data by the I-DEAS® Software

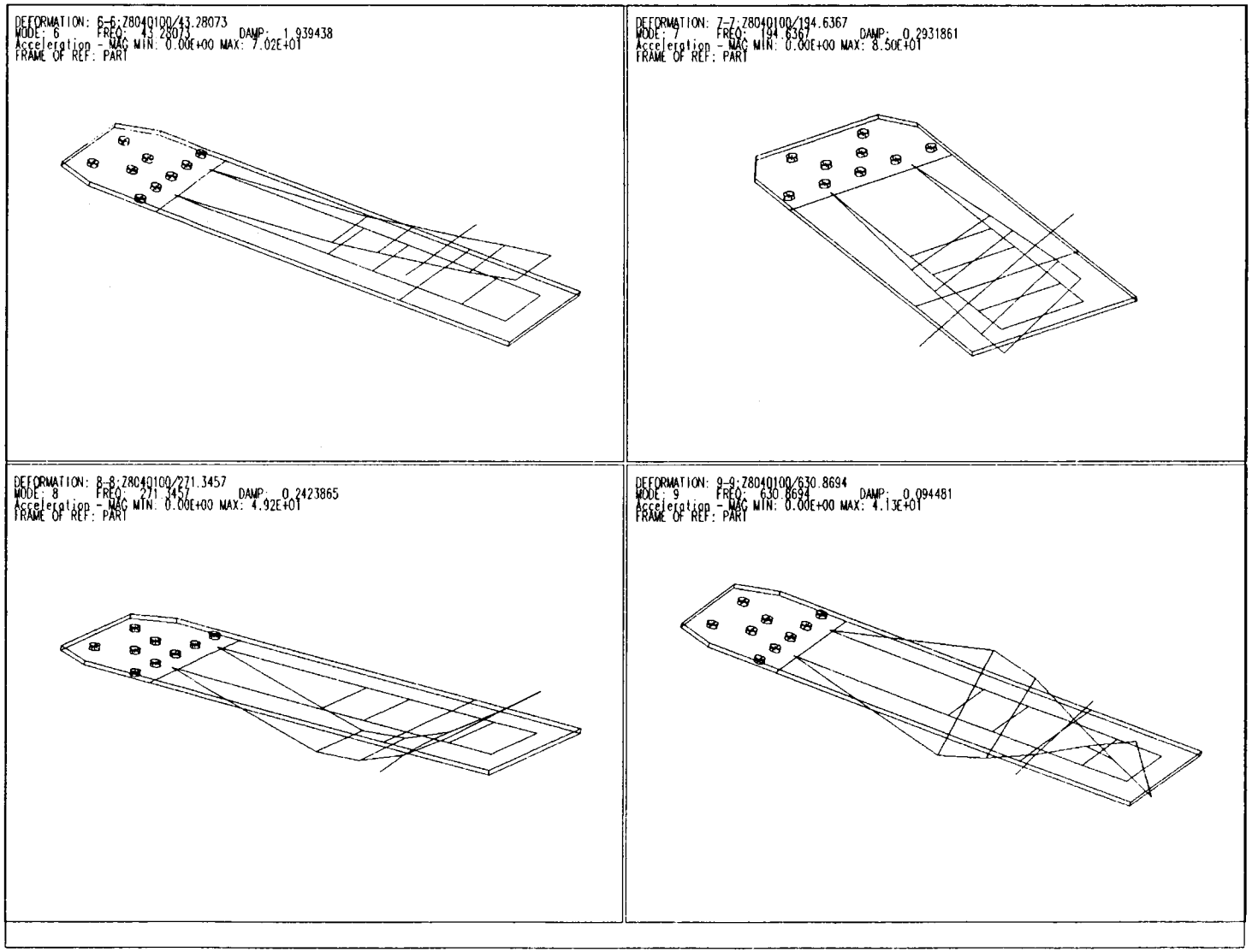


Figure A2-5, Mode Shapes for P8540100 as Generated From Test Data by the I-DEAS® Software

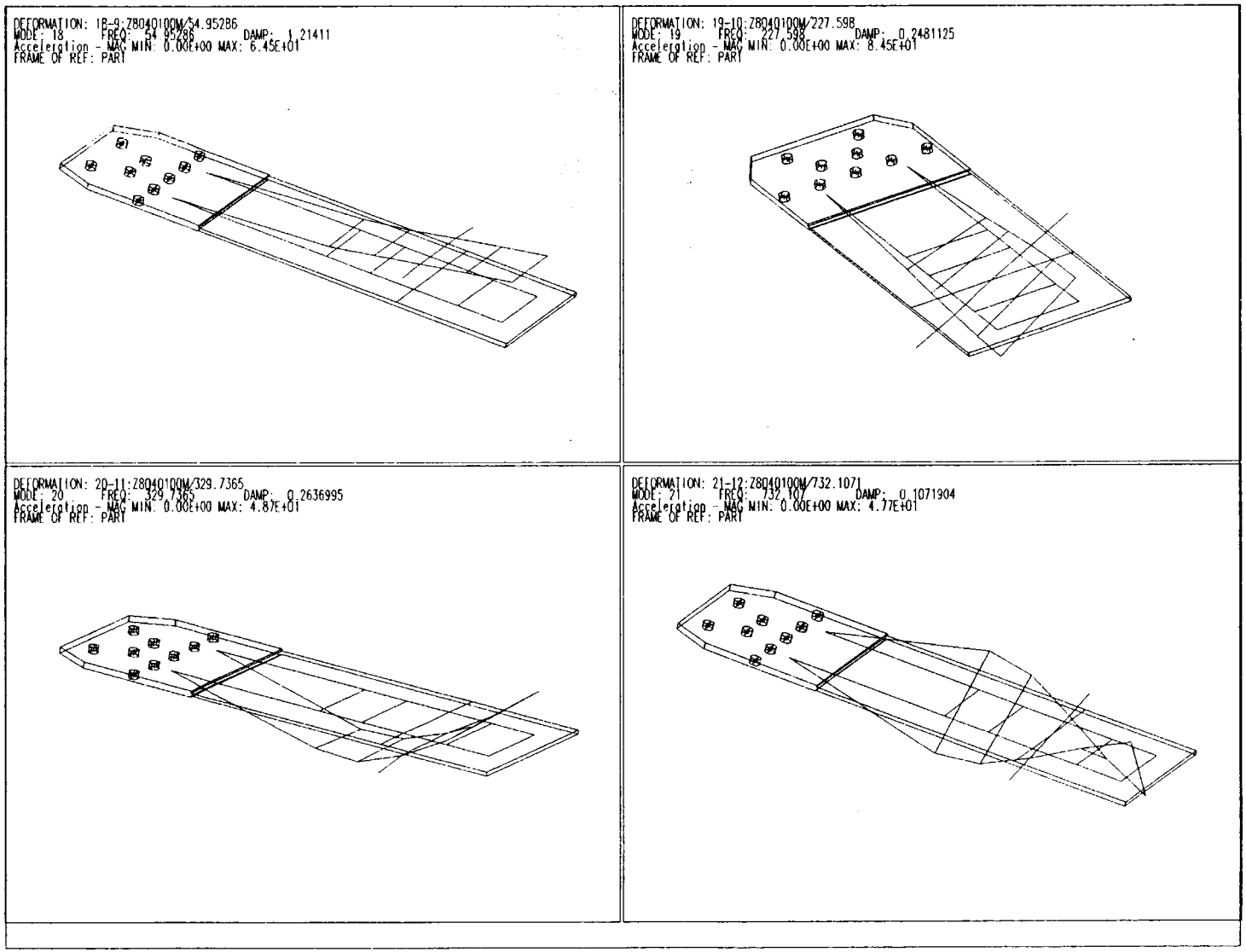


Figure A2-6, Mode Shapes for P8540100M as Generated From Test Data by the I-DEAS® Software

APPENDIX 3

IMPACT HAMMER CALIBRATION CERTIFICATE



THE MODAL SHOP INC.

Calibration Certificate

IMPULSE FORCE HAMMER

Model No.: 086C80 Serial No.: 9555

Calibrated by: LA Date: July 10, 1998.

HAMMER SENSITIVITY

	Tip	Steel	Red
Without Extender	mV/lbf	114.4	95.2
	mV/N	25.7	21.4
With Extender	mV/lbf	122.1	87.3
	mV/N	27.4	19.2

Standards used for this calibration

Manufacturer	Model Number	Serial Number	Due Date
PCB Piezotronics	309A	3242	September 27, 1998
Hewlett Packard	35670A	3245A00226	June 13, 1998
TMS	9961005A	826	August 19, 2002

Calibration procedure is in compliance with MIL-STD-45662A and traceable to NIST. The measurement standards used are traceable to the National Institute of Standards and Technology (NIST), fundamental or natural physical constants with values assigned or accepted by NIST, ratio type or self calibrating techniques, or comparison to consensus standards. This certificate may not be reproduced, except in full, without the approval of The Modal Shop Inc.

Notes:
Each specific hammer configuration has a different sensitivity. The difference is a constant percentage which depends on the mass of the cap and tip assembly relative to the total mass of the head. Calibrating the specific hammer structure being used automatically compensates for mass effects.

Helping you test, model and modify the behavior of structures.
1776 Mentor Avenue
Suite 170
Cincinnati, Ohio
45212-3521
U.S.A.
Ph 513-351-9919
FAX 513-458-2172
1-800-860-4867

APPENDIX 4

EIGENVECTORS CALCULATED FROM MEASURED DATA

Table A4-1, Raw Tabulated Eigenvectors as Calculated from Measured Data

	Test Article: P8540188				Test Article: P8540100				Test Article: P8540100M			
Mode No.	1	2	3	4	1	2	3	4	1	2	3	4
Frequency	89.20 hz	398.97 hz	547.72 hz	1265.45 hz	43.28 hz	194.64 hz	271.35 hz	630.87 hz	54.95 hz	227.60 hz	329.74 hz	732.11 hz
Data Point	dz	dz	dz	dz	dz	dz	dz	dz	dz	dz	dz	dz
5	13.54	18.07	-37.08	32.43	20.24	27.58	-48.95	39.12	17.40	24.95	-44.29	45.50
6	14.13	-18.59	-37.10	-32.49	20.14	-28.52	-49.24	-40.67	15.53	-26.11	-42.35	-44.04
7	20.47	22.99	-33.92	22.47	32.05	35.34	-44.54	28.09	26.61	35.40	-42.50	36.31
8	21.59	-25.22	-34.38	-23.90	31.35	-35.95	-45.98	-26.49	26.84	-37.67	-44.52	-37.06
9	29.84	28.49	-18.19	3.82	43.89	42.08	-24.09	3.95	40.20	42.16	-23.20	8.04
10	28.89	-0.15	-17.57	-0.40	43.11	0.61	-23.96	-1.12	40.01	1.11	-23.70	-1.44
11	28.76	-28.50	-18.07	-4.72	42.64	-42.72	-27.02	-6.07	39.18	-45.23	-24.73	-11.19
12	39.05	31.21	9.00	-18.38	56.86	47.47	9.77	-19.88	52.37	49.27	8.71	-23.61
13	38.29	-33.32	7.13	16.92	55.17	-49.03	6.54	18.81	52.28	-51.89	4.27	19.19
14	46.34	33.97	37.93	-35.92	68.18	49.59	48.07	-41.33	64.54	51.19	48.69	-47.65
15	46.18	-34.96	37.57	35.82	70.21	-51.49	46.13	40.41	63.09	-55.74	44.17	45.74
16	29.93	55.94	-21.65	7.84	42.50	80.94	-26.39	9.24	37.03	84.40	-28.10	18.86
17	29.06	-56.16	-21.36	-7.79	43.25	-85.01	-34.16	-12.92	36.99	-84.48	-33.16	-21.98

Note: After an initial assessment of the data quality, the responses at points 1,2,3, and 4 were discarded

Table A4-2 Processed Eigenvectors for P8540188

FE Node	Data Point	Mode 1 dz	Mode 2 dz	Mode 3 dz	Mode 4 dz
	5	13.84	18.33	-37.09	32.46
	6	13.84	-18.33	-37.09	-32.46
122	**7**	**21.03**	**24.11**	**-34.15**	**23.19**
124	**8**	**21.03**	**-24.11**	**-34.15**	**-23.19**
152	**9**	**29.30**	**28.50**	**-18.13**	**4.27**
154	**11**	**29.30**	**-28.50**	**-18.13**	**-4.27**
	12	38.67	-29.86	-13.53	-11.55
	13	38.67	29.86	-13.53	11.55
212	**14**	**46.26**	**-33.65**	**22.53**	**26.42**
214	**15**	**46.26**	**33.65**	**22.53**	**-26.42**

Table A4-3, Processed Eigenvectors for P8540100

FE Node	Data Point	Mode 1 dz	Mode 2 dz	Mode 3 dz	Mode 4 dz
92	**5**	**20.19**	**28.05**	**-49.10**	**39.90**
94	**6**	**20.19**	**-28.05**	**-49.10**	**-39.90**
122	**7**	**31.70**	**35.65**	**-45.26**	**27.29**
124	**8**	**31.70**	**-35.65**	**-45.26**	**-27.29**
	9	43.27	42.40	-25.56	5.01
	11	43.27	-42.40	-25.56	-5.01
	12	56.02	-45.10	-18.40	-12.97
	13	56.02	45.10	-18.40	12.97
212	**14**	**69.20**	**-49.31**	**27.31**	**30.07**
214	**15**	**69.20**	**49.31**	**27.31**	**-30.07**

Table A4-4, Processed Eigenvectors for P8540100M

FE Node	Data Point	Mode 1 dz	Mode 2 dz	Mode 3 dz	Mode 4 dz
92	**5**	**16.47**	**25.53**	**-43.32**	**44.77**
94	**6**	**16.47**	**-25.53**	**-43.32**	**-44.77**
122	**7**	**26.73**	**36.54**	**-43.51**	**36.69**
124	**8**	**26.73**	**-36.54**	**-43.51**	**-36.69**
	9	39.69	43.70	-23.97	9.62
	11	39.69	-43.70	-23.97	-9.62
	12	52.33	-47.25	-16.72	-17.40
	13	52.33	47.25	-16.72	17.40
212	**14**	**63.82**	**-51.54**	**26.48**	**33.42**
214	**15**	**63.82**	**51.54**	**26.48**	**-33.42**

VITA

Allen Fort Gwinn, Jr. was born in Nashville, Tennessee on April 12, 1953. His parents are Mary Frances Dowell Gwinn and the late Allen F. Gwinn, Sr. He grew up in Nashville where his educational career began at Dalewood Elementary School. After graduating from Isaac Litton High School in 1971, he attended Tennessee Technological University in Cookeville, Tennessee, where, in 1975, he received his Bachelor of Science degree in Engineering Science. He also received his Master of Science degree in Engineering Mechanics from Tennessee Technological University in 1979.

As an undergraduate, Fort was inducted into Tau Beta Pi Engineering Honor Society and Kappa Mu Epsilon Math Honor Society. While at Tennessee Tech, he also served as treasurer for Theta Tau Engineering Fraternity. Since 1976, he has been employed by Sverdrup Technology where he has served in a variety of roles.

Fort and his wife of twenty years, the former Elizabeth Frey Dorris, are long time residents of Tullahoma. They have two children, Allen Fort ("Trey") Gwinn, III (born February 13, 1984) and Susan Jaynes Gwinn (born October 7, 1986).